

Department of Physiology
Faculty II - Medicine: Theoretical Medicine and Biosciences
Saarland University, Homburg/Saar, Germany

**Electrical fusion pore measurements: a high-
resolution technique to study the molecular
mechanism of exocytosis**

Thesis

A dissertation submitted in partial fulfillment of the requirements
for the degree of Doctor of natural science at
SAARLAND UNIVERSITY

2011

Submitted by: Paanteha Kamalimoghadam
Born on: 07 May 1977, in Tehran

Aus dem Bereich: Physiology
Theoretische Medizin und Biowissenschaften der Medizinischen Fakultät II
der Universität des Saarlandes, Homburg/Saar, Deutschland

**Elektrische Fusionspore Messungen: eine
hochauflösende Technik um die molekularen
Mechanismen der Exocytose zu untersuchen**

Dissertation zur Erlangung des Grades eines
Doktors der Naturwissenschaften
der Medizinischen Fakultät
der UNIVERSITÄT DES SAARLANDES

2011

vorgelegt von: Paanteha Kamalimoghadam
geb. am: 07 Mai 1977, in Teheran

Acknowledgments

I am fully indebted to my supervisor Prof. Dr. Dieter Bruns for teaching me the patch-clamp technique and the basics of scientific thinking. For his incredible patience, help, support and having enough confidence in me to have me work on this special project.

I would like to thank Prof. Dr. Jens Rettig and all members of his lab for creating friendly atmosphere between our labs to discuss science.

I would like to express my gratitude to Dr. Maria Borisovska for teaching me from the beginning to the end. She taught me details in all aspects of my work and I am really grateful for the precious time she spent on my thesis correction. I hope that she will continue to advise me on my future ventures.

I am thankful to Dr. Chad Grabner, Dr. Ute Becherer, Dr. David Stevens, Dr. Detlef Hof, Dr. Ulf Matti and Dr. Claudia Schirra, for their support in various situations and for being open to discuss my results and ideas. I am very thankful to Barbara Lang that she spent some times to improve my German summery.

I would like to thank all members of my lab and all people who helped me in this project specially Yvonne Schwarz, Judith Wolf, Marina Wirth and Katja Klingler.

Last but not the least; I thank my husband Farhad for his extreme patience and support, my father for putting me on the highway to science, my mother for absorbing all my stress.

This dissertation is dedicated to love of my life, my Son.

Contents

Abbreviations	I
1. Abstracts	1
1.1 Zusammenfassung	1
1.2 Summary	3
2. Introduction	5
2.1 Exocytosis and neurotransmitter release	5
2.1.1 The exocytotic fusion pore	7
2.1.2 Full and transient mode of fusion	9
2.1.3 Swelling a consequence of fusion	10
2.2 The molecular mechanism of neurosecretion	10
2.2.1 SNARE protein family	10
2.2.2 SNARE interacting partner (complexin)	13
2.3 Time resolved admittance measurements	14
2.4 Experimental model: mouse chromaffin cell	17
2.5 Aim of the study	18
3. Materials and methods	20
3.1 Materials	20
3.2 Knock out mice	20
3.2.1 Synaptobrevin II and cellubrevin double knock-out mice ...	20
3.2.2 Complexin II knock-out mice	22
3.3 Chromaffin cell culture	23
3.3.1 Western blot	24
3.3.2 Viral constructs and transfection	24
3.4 Electrophysiological recording	24

3.4.1	Phase adjustment and calibration of capacitance measurements	24
3.4.2	Analyzing the filter setting.....	31
3.4.3	Noise analysis of the setup.....	33
3.4.4	Simulation of the exocytotic event for a given change in fusion pore conductance.....	35
3.4.5	Setting of the admittance measurements.....	37
3.4.6	Customized analysis.....	39
4.	Results	40
4.1	Simultaneous detection of single and global exocytotic events.....	40
4.1.1	Detailed analysis of single fusion event.....	42
4.2	Vesicle radius obtained from membrane capacitance measurements agrees well with electron microscopy data	44
4.3	Modes of vesicle fusion.....	46
4.3.1	‘Kiss-and-run’ mode of exocytosis	47
4.3.2	Abrupt opening of the fusion pore	48
4.3.3	Slowly expanding fusion pore.....	49
4.4	Comparison of amperometric spike and the conductance trace.....	51
4.5	Gradual decrease in capacitance trace, technical error or a phenotype?.....	53
4.6	Observed upward steps are v-SNARE dependent exocytosis.....	56
4.7	Extending the juxtamembrane region of synaptobrevin II attenuates exocytotic activity	60
4.1	Complexin II is required to control the size of narrow fusion pore.....	63
5.	Discussion	68
5.1	Discrete changes in capacitance indeed correspond to exocytosis of the single vesicle	68
5.2	Fusion pore modulatory effects.....	69

5.3	Molecular determinants of exocytosis can be studied with the developed technique	70
5.4	Fusion pore: a proteinaceous structure	71
5.5	Success rate of simultaneous cell-attached and whole-cell recordings	73
5.6	Possible implications of electrical measurements of the fusion pore	74
5.7	Future aims	75
	References	76
	Publications	86

Abbreviations

α SNAP	α -Soluble NSF Attachment Protein
Φ	Phase
ω	Angular frequency
Ω	Ohm
Ach	Acetylcholine
ATP	Adenosine triphosphate
Ca^{2+}	Calcium
$[\text{Ca}^{2+}]$	Calcium concentration
CpxII	Complexin II
bp	Base pair
Ceb	Cellubrevin
C_m	Membrane capacitance
DNA	Deoxyribonucleotide
DMEM	Dulbecco's Modified Eagle's Medium
dATP	Deoxyriboadenosine Triphosphate
Dko	Double knock out
EDTA	Ethylene Diamine Tetra-Acetic Acid
EGFP	Enhanced green fluorescent protein
EDTA	Ethylenbis-(oxyethylenitrilo)-tetraacetic acid
EM	Electron microscopy
fF	Femto farad
FCS	Fetal Calf Serum
Fig	Figure
GTP	Guanidinetriphosphate
G_A	Access conductance
G_m	Membrane conductance
HEPES	4-(2-hydroxyethyl)-1-piperazineethanesulfonic acid
H_2O	Water
Hz	Hertz
I	Current

Abbreviations

Im	Imaginary component of the admittance
kDa	Kilo Dalton
kHz	Kilo Hertz
LDCV	Large dense-core vesicle
mOsm	Milliosmol
N	Number of measured cells
n	Number of recorded events
nS	Nano Siemens
P	P-value from student's t-test
PCR	Polymerase Chain reaction
pH	Potentia hydrogenii
PSD	Phase sensitive detector
Re	Real component of the admittance
rms	Root mean square
SD	Standard deviation
SE	Standard error
SFV	Semiliki forest virus
Snap25	Synaptosome associated protein of 25 kDa
SNARE	Soluble NSF attachment protein receptor
SSV	Small synaptic vesicle
SybII	Synaptobrevin II
Syx	Syntaxin
TMD	Transmembrane domain
VAMP	Vesicle Associated Membrane Protein
wt	Wild type

1. Abstracts

1.1 Zusammenfassung

Die Exozytose geht mit einer Zunahme der Plasmamembranfläche einher, welche mit Hilfe der Patch-Clamp-Technik auf Einzelzellebene in Form einer Membrankapazitätserhöhung gemessen werden kann (Neher und Marty, 1982). Die Membrankapazität und deren Änderungen können im Voltage-Clamp-Verfahren ermittelt werden, indem Ströme als Reaktion auf kleine Spannungsstufen gemessen werden bzw. durch Applikation einer Sinusspannung und Analyse der resultierenden Ströme mithilfe eines Phasendetektors oder eines Lock-in-Verstärkers (für weitere Informationen siehe bitte Gillis, 1995; Lindau, 1991). Die Kapazitätsmessung in der hier verwendeten ‚cell-attached‘ Konfiguration erlaubt die Detektion exozytischer Ereignisse einzelner Vesikel mit einem Durchmesser von nur 40 nm, wodurch sich die Mehrheit von Fusionsereignissen in chromaffinen Zellen erfassen lässt.

Dabei beginnt die Freisetzung von Neurotransmittern und Hormonen mit der Bildung einer engen Fusionspore, die das vesikuläre Lumen mit dem Extrazellularraum verbindet (Breckenridge und Almers, 1987; Lindau und Alvarez de Toledo, 2003). Durch die Anwendung der cell-attached Patch-Clamp-Technik können sowohl Größe und dynamische Eigenschaften der Fusionspore untersucht werden (Lollike et al., 1995). Die vorliegende Studie, zeigt eine Weiterentwicklung der Membrankapazitätsmessung durch unmittelbare Kombination der cell-attached-Methode mit der whole-cell-Konfiguration. Somit können einzelne Fusionsereignisse direkt und unter kontrollierten Bedingungen, wie z. B. definierten intrazellulären Ionenkonzentrationen, gemessen werden.

Diese Methode wurde für chromaffine Mauszellen systematisch optimiert und kann routinemäßig zur Messung der Exozytose verwendet werden. Obwohl die Erfolgsquote dieser Methode gering ist und eine Untersuchung einer großen Zahl von Zellen erfordert, sind die sich daraus ergebenden Vorteile auch beträchtlich und von Bedeutung.

Frühere Arbeiten haben gezeigt, dass die Mitglieder der SNARE-Proteinfamilien (soluble *N*-ethylmaleimide-sensitive Fusionsprotein attachment protein receptors) für die Membranfusion während der Exozytose benötigt werden. Mehrere

SNARE Proteine lagern sich dabei zusammen und bilden so den SNARE-Komplex (Sollner et al., 1993), der als Kern der hochkonservierten Fusionsmaschinerie eine entscheidende Rolle bei der Membranfusion aller Sekretionswege spielt (Jahn und Sudhof, 1999). Die neuronalen SNARE-Proteine Syntaxin, SNAP-25 und das vesikuläre Membranprotein Synaptobrevin II, die bei der regulierten Exozytose in Neuronen und neuroendokrinen Zellen mitwirken, sind im Detail untersucht worden (Chen und Scheller, 2001; Sutton et al., 1998) dennoch ist ihre genaue Wirkweise nicht verstanden. Unter Anwendung der ‚cell-attached‘ Messkonfiguration wurde die Funktion des SNARE-Proteins Synaptobrevin II während der Exozytose embryonaler Chromaffinzellen der Maus analysiert. Dabei haben wir mit der funktionellen Analyse eines v-SNARE-Doppelknock-outs in chromaffinen Mauszellen begonnen und konnten anhand beider Patch-Clamp-Konfigurationen zeigen, dass die Exozytose chromaffiner Granulen in Abwesenheit von Synaptobrevin II und Cellubrevin verhindert wird. Durch akute virale Expression von Synaptobrevin II in Doppel-knock-out Chromaffinzellen konnten die Exozytose wieder hergestellt und eine Exozytoserate auf dem Niveau von Wildtypzellen erreicht werden. Die Einführung eines 12 Aminosäure (aa)-Linkers zwischen der Transmembrandomaine und der juxtamembran-Region von Synaptobrevin II verringert die Frequenz exozytotischer Ereignisse,

Die Ergebnisse legen darüber hinaus nahe, dass die Linkermutante die Initiierung der Exozytose verzögert und die Expansion der exozytotischen Fusionspore beeinträchtigt. Zusammengefasst unterstützen die Untersuchungen die Schlussfolgerung, dass eine ungestörte Kraftübertragung zwischen Transmembrandomaine und juxtamembranärer Region von SybII für die Exozytose von Bedeutung ist.

Darüber hinaus haben wir die funktionelle Bedeutung von Complexin II während der Exozytose in chromaffinen Maus-Zellen untersucht und konnten Hinweise erarbeiten, dass die Expansion der Fusionspore auch in ComplexinII-defizienten Zellen im Vergleich zu Wildtyp-Zellen stark beeinträchtigt wird, woraus auf eine wichtige Rolle von Complexin II in der Kontrolle der Porenöffnung geschlossen werden kann.

1.2 Summary

Exocytosis is associated with an increase in area of the plasma membrane. This can be measured on single cells with the patch clamp technique as an increase in membrane capacitance (Neher and Marty, 1982). The membrane capacitance and its changes can be obtained in voltage clamp experiments, measuring the currents in response to small voltage steps or by applying a sine wave voltage and analyzing the resulting currents with a phase sensitive detector or lock-in amplifier (for review see Gillis, 1995; Lindau, 1991). The cell-attached patch capacitance technique, we used here, allows investigation of single exocytotic events for vesicles as small as 40 nm. Thus most of the large dense core vesicles exocytosis may be studied with this technique.

Release of neurotransmitters and hormones begins with the formation of a narrow fusion pore, which connects the vesicular lumen with the extracellular space (Breckenridge and Almers, 1987; Lindau and Alvarez de Toledo, 2003). Using cell-attached patch clamp technique, fusion pore formation and expansion can be studied (Lollike et al., 1995). Our study described here shows the improvement of cell-attached membrane capacitance measurement by the combination of cell-attached and whole-cell patch configuration. Use of the double patch-clamp approach leads to the observation of unitary fusion events and has allowed us to determine the kinetics of fusion pore under precisely controlled conditions in mouse chromaffin cells. This method is now well established in mouse chromaffin cells and may be employed routinely for measurement of exocytosis. Although the success rate of the procedure is quite low, necessitating the testing of large numbers of cells, the advantages conferred by this configuration are substantial.

Membrane fusion during exocytosis and throughout the cell is believed to involve members of the SNARE (soluble *N*-ethylmaleimide-sensitive fusion protein attachment protein receptors) family proteins. The proteins associate to form a SNARE complex (Sollner et al., 1993) that has a crucial role in membrane fusion throughout the secretory pathway as the core of highly conserved fusion machinery (Jahn and Sudhof, 1999). The SNARE proteins syntaxin, SNAP-25, and vesicle-associated membrane protein (synaptobrevin II), involved in regulated exocytosis in neurons and neuroendocrine cells, have been studied in most detail (Chen and Scheller, 2001; Sutton

et al., 1998). The SNARE proteins are thought to be central components of the exocytotic mechanism but their precise functions remain unclear. Using the described technique, we analyzed the structure-function of SNARE protein synaptobrevin II in exocytosis of embryonic mouse chromaffin cells. We started by analysis of the functional impact of double v-SNARE deficiency in mouse chromaffin cells. We show that in the absence of both, synaptobrevin II and cellubrevin chromaffin granule exocytosis is abolished as recorded in cell-attached and in the whole-cell configuration. Acute, viral-driven expression of synaptobrevin II in double knock out chromaffin cells restored exocytosis to wild type level. The insertion of 12aa linker between transmembrane and juxtamembrane region of synaptobrevin II attenuate exocytosis, leading to the conclusion that the force transduction between transmembrane and juxtamembrane region is required for rapid evoked exocytosis.

In addition, the fusion pore dynamics were analyzed in linker inserted cells. Our results show that this linker mutation inhibits fusion efficiency, delays exocytosis initiation and alters the fusion pore expansion. From this we can conclude that the tight coupling between SNARE motif and the vesicle membrane is crucial for membrane merger and fusion pore widening. Furthermore we have analyzed the functional impact of complexin II in exocytosis of mouse chromaffin cells and show that the kinetics of the fusion pore expansion is different in the absence of complexin II. These data suggest that complexin II regulates the closure of the fusion pore during regulated vesicle exocytosis consistent with previous reports (Archer et al., 2002).

2. Introduction

2.1 Exocytosis and neurotransmitter release

Exocytosis is an essential step in neuronal transmission from the presynaptic to the postsynaptic cell. It represents fusion of membrane-bound vesicles with the cell's plasma membrane and is used by many cell types to transfer vesicle-contained substances, such as neurotransmitters (Katz et al., 1969), hormones (Trifaro, et al., 1977) or enzymes (Case et al., 1978). Eukaryotic cells possess at least two different pathways for the delivery of secretory products by exocytosis to the extracellular space. They are referred to as constitutive and regulated pathways (Burgess et al., 1987). The constitutive pathway is a basic feature of all cells and serves trafficking of proteins and lipids to the plasma membrane of the cell. It operates by a constant flow of small vesicles from the trans-Golgi network. These vesicles move to the cell surface and undergo exocytosis without intermediate packaging or storage of the secretory material. Many cells have a regulated pathway, primarily, specialized for the secretion of neurotransmitters, neuropeptides and proteins. It involves concentration and packaging of the exported material in secretory vesicles, the storage of these granules in proximity to the release site, and finally exocytosis of the vesicles in response to an appropriate stimulus.

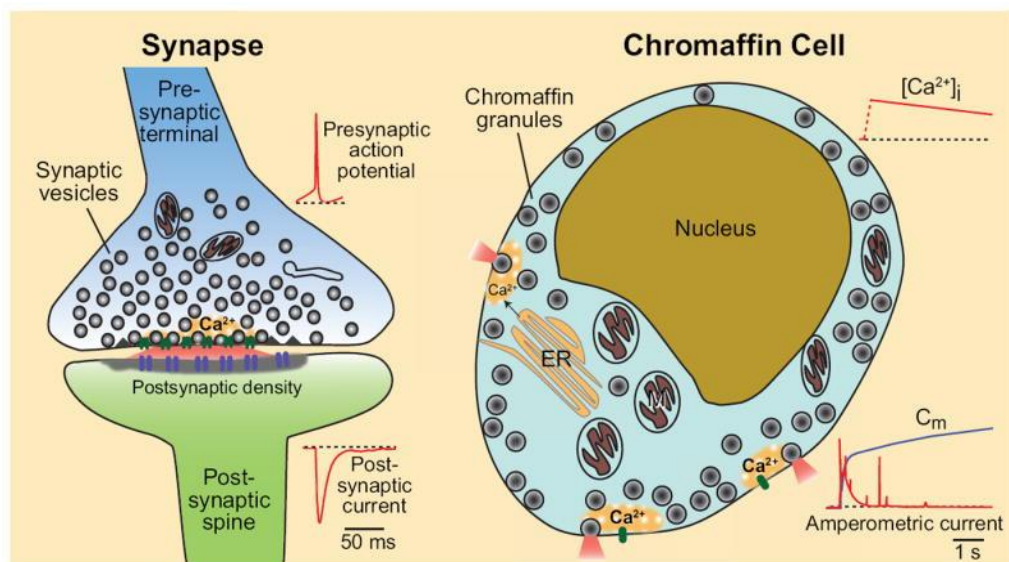


Figure 1. Synaptic and endocrine Ca²⁺ triggered exocytosis (Zhiping and Südhof, 2010)

Signalling between neurons occurs at specialized contact zones, the synapses. Within nerve terminals the transmitter molecules are stored in small membranous organelles, the synaptic vesicles (Fig. 1). Some vesicles are positioned so close to the plasma membrane that they touch the membrane, a phenomenon that is referred to as docking (Becherer and Retting, 2006; Parsons et al., 1995). Neurons maintain a resting intracellular Ca^{2+} concentration in the range of 40-100 nM (Sabatini et al., 2002). Upon arrival of an action potential, the synaptic plasma membrane depolarizes causing an opening of presynaptic calcium channels. This can lead to changes in Ca^{2+} concentration ranging from highly localized and transient Ca^{2+} elevations to longer lasting and global changes throughout the neuron (Augustine et al., 2003). The resulting rise in intracellular calcium triggers vesicular fusion. Released neurotransmitter molecules diffuse across the synaptic cleft and bind to specific receptors in the membrane of the postsynaptic cell which causes an immediate (ionotropic) or delayed (metabotropic) change in postsynaptic cell activity (Kandel, 2000). The regulated fusion pathway in neurons shows two striking features: it is strictly regulated by Ca^{2+} and it occurs with faster kinetics than any other known membrane fusion event (Sabatini et al., 1996). These properties are crucial for the rapid point-to-point communication that underlies neuronal function. Several different assays are used to monitor exocytosis. This work describes the refinements of patch-clamp technique to study kinetics of exocytosis by monitoring membrane merger at a very high time resolution.

The vesicles that package neurotransmitters fall into two distinct classes, large dense-core vesicles (LDCVs) and small synaptic vesicles (SSVs), the coexistence of which is widespread in nerve terminals. Small Synaptic vesicles represent a distinctive feature of nerve endings. SSVs typically contain neurotransmitters and mediate fast synaptic transmission, while neuropeptides and monoamines are typically secreted via larger vesicles with a dense core, the so-called large dense-core vesicles (LDCV) (Coulter, 1988; Hokfelt et al., 1986), which usually produce slower modulatory effects. Hormonal exocytosis of endocrine cells operates via large dense-core vesicles (LDCVs) that are probably similar to neuropeptide LDCVs in neurons. LDCV exocytosis has been studied mostly in adrenal chromaffin cells and in pancreatic β -cells (Voets et al., 1999; Braun et al., 2009). Exocytosis of LDCVs has been well described in chromaffin cells, and also appears to be regulated by Ca^{2+} (Fig. 1, Lefkowitz et al., 2009). In this

work, we have studied exocytosis of LDCVs in adrenal mouse chromaffin cells, with great interest in the dynamics of the fusion pore.

2.1.1 The exocytotic fusion pore

Ultrastructural techniques have shown that an early event in the exocytotic fusion of a secretory granule is the formation of a narrow, water-filled pore spanning both the granule and plasma membranes and connecting the lumen of the secretory granule to the extracellular environment (Chandler and Heuser, 1980). The formation of the fusion pore marks a well-defined stage in the fusion process that can be studied experimentally. Electron microscopy provided the first images of fusion pores with diameters of ≈ 50 nm, but it was pointed out that these pores could have grown from something smaller (Fig. 2). The preparations examined include posterior pituitary cells (Dreifuss, 1980), mast cells (Chandler et al., 1980), the neuromuscular junction (Heuser et al., 1981), adrenal chromaffin cells (Schmidt, 1983), and *Paramecium* (Momayezi, 1987). After formation, the fusion pore rapidly enlarges to a size that is sufficiently large to allow the hydrated proteoglycan matrix of the granule to be expelled into the extracellular space. In the extreme case of exocytotic fusion pores in beige mouse mast cells, the fusion pores must enlarge to a diameter of several micrometres so that the abnormally large matrix can be released (Breckenridge and Almers, 1987).

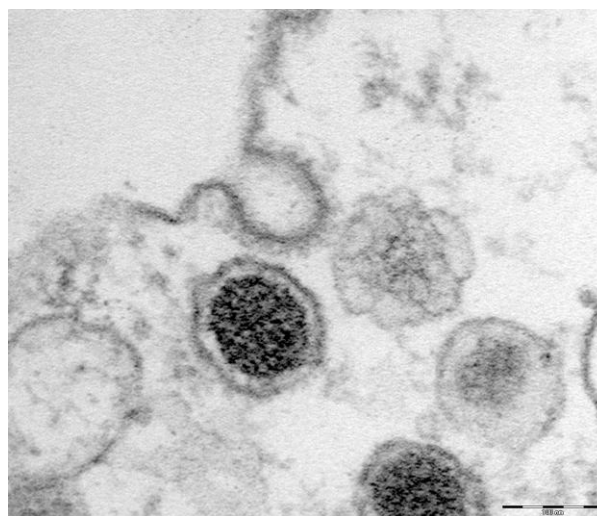


Figure 2. Electron micrograph of a cultured mouse chromaffin cell (2 days in culture, taken from Borisovska M., unpublished). Omega-shaped structure likely representing fusing granule. Scale, 100 nm.

The fusion pore has become a major focus of research in exocytosis. Sensitive biophysical measurements have provided information of what it looks like and how it behaves. The nature of fusion pore itself, which forms in the first moment of exocytosis, is presently controversial. It could consist of a proteinaceous pore, similar to ion channel (Lindau and Almers, 1995), or the involved proteins could lead to hemifusion and a subsequently forming lipid pore (Monck and Fernandez, 1994). Because of these properties, the opening of the fusion pore has been compared to the opening of an ion channel (Breckenridge and Almers, 1987a; Almers, 1990; Spruce et al., 1990) and the fusion pore is believed to control the release in the early stages of exocytosis (Alvarez de Toledo et al., 1993).

The secretory vesicles of mast and chromaffin cells actively accumulate biogenic amines, and this active uptake is powered by a pH gradient across the vesicle membrane (Johnson and Scarpa, 1984). An electrogenic H⁺ pump maintains the gradient that generates a lumen-positive potential across the vesicle membrane (Breckenridge and Almers, 1987b; Salama et al., 1980). As soon as the pore opens, the plasma and vesicle membrane become electrically connected. The difference between plasma and vesicle membrane potentials then drives an electric discharge through the fusion pore that adjusts the charge on the vesicle membrane capacitance until the two membranes have the same potential. Measurements of changes in the admittance of a cell membrane make it possible to obtain time-resolved measurements of the fusion pore conductance from the instant of its formation and throughout its growth (Breckenridge and Almers, 1987; Alvarez and Fernandez, 1988; Spruce et al., 1990). The time course of the fusion pore conductance can be measured by modelling a granule fusing with the cell membrane as a conductance (the fusion pore) in series with a capacitor (the granule membrane) (Zimmerberg et al., 1987; Breckenridge and Almers, 1987). When many experiments of this type are analyzed, it is suggested that the first electrically observable event in exocytotic membrane fusion is the formation of an aqueous pore with a conductance G_p values ranging from 20 to 330 pS, and from these values one can estimate a fusion pore diameter of on the order of ≈ 1 nm (Almers and Neher, 1987; Breckenridge and Almers, 1987; Alvarez and Fernandez, 1988; Spruce et al., 1990) which is significantly smaller compared to the fusion pores seen in electron micrographs (Chandler and Heuser, 1980; Ornberg and Reese, 1981; Chandler

et al., 1983, 1989).

2.1.2 Full and transient mode of fusion

Admittance measurements have shown that fusion pore opening is a reversible process (Klyachko and Jackson, 2002; Alvarez et al., 1993; Neher et al., 1982; Fernandez et al., 1984; Lollike et al., 1995; He et al., 2006) and amperometry has confirmed these observations (Alvarez et al., 1993; Ales et al., 1999; Wang et al., 2003; Wang et al., 2006). These studies define the fusion pore as a metastable intermediate that can evolve in two distinct ways. Upon formation, a fusion pore is not absolutely committed to growth, and the vesicle is not absolutely committed to collapse into the plasma membrane. Vesicles can take an alternative route, pulling back from the plasma membrane intact, possibly with some neurotransmitter remaining inside. The idea that vesicles can engage in a transient exocytotic contact with the plasma membrane while preserving their integrity had an early incarnation as a mechanism of efficient membrane recycling at synapses (Meldolesi et al., 1981). Thus, we can envision two distinct modes of release (Valtorta et al., 2001), ‘full fusion’ and ‘kiss-and-run’, with the fusion pore as the most likely bifurcation point. This gives the fusion pore a critical role as the structure that dictates the nature of the release process. Transient fusion (“kiss-and-run”) is accepted as a mode of transmitter release both in central neurons and neuroendocrine cells, but the prevalence of this mechanism compared with full fusion is still in doubt.

A consideration of how a small fusion pore would limit neurotransmitter release prompted the speculation that kiss-and-run could serve as an inhibitory signal in which low levels of neurotransmitter desensitize receptors and make synapses less responsive to an ensuing full-fusion event (Klyachko and Jackson, 2002; Wang et al., 2003; Taraska and Almers, 2004). This suggests that a new class of electrophysiological experiments will be needed to test the impact of a previous kiss-and-run event on a subsequent full-fusion event. Since the fusion pore emerges as a structure of molecular dimensions within a specialized contact between two fusing membranes, studying the structure and dynamics of the fusion pore reveals the process of exocytosis at a fundamental level.

2.1.3 Swelling a consequence of fusion

Many experimental approaches have been used to induce fusion, including the use of osmotic forces, divalent cations, electromechanical stress, and bilayer "depletion" (Cohen et al., 1982, 1989; Finkelstein et al., 1986). These strategies all increase the bilayer tension so that increased exposure of hydrocarbon at the membrane surface causes a reduction in the repulsive hydration forces. Consequently, swelling of the secretory granule matrix due to water entry through the fusion pore is thought to play an important role in dispersal of secretory granule contents (Holz et al., 1986; Lucy et al., 1986). Secretory vesicles often swell as cells secrete, which suggests that swelling stretches the vesicle membrane and thereby cause membrane fusion [for a review of this hypothesis see (Finkelstein et al., 1986)]. Two independent studies on mast cells (Almers and Breckenridge, 1988; Breckenridge and Almers, 1987a; Zimmerberg, 1987; Zimmerberg et al., 1987) have shown that the dilation of the fusion pore and release of the granule contents is associated with a rapid swelling of the granule matrix. In contrast, during transient fusion events or during periods of reversible fluctuations in the fusion pore conductance that occur before irreversible pore dilation, no swelling is observed (Breckenridge and Almers, 1987b; Zimmerberg et al., 1987). These observations have led to the proposition that swelling of the granule matrix provides the force necessary to drive the irreversible expansion of the fusion pore and subsequent release of secretory products (Zimmerberg et al., 1987; Breckenridge and Almers, 1987b; Merkle and Chandler, 1989; Chandler et al., 1989). Since our recording provides simultaneous information about the vesicle size and the kinetics of its fusion pore, we have related some of our data to the swelling phenomenon.

2.2 The molecular mechanism of neurosecretion

2.2.1 SNARE protein family

Membrane fusion in cells requires protein machines to overcome energy barriers and regulatory mechanisms to ensure that fusion occurs at the correct time and place (Rothman, 1994). In recent years it has become clear that most, and perhaps all, intracellular membrane fusion events are mediated by sets of evolutionarily conserved

membrane proteins. Among these, the SNARE proteins are the best candidates for catalyzing the fusion reaction. SNARE (soluble N-ethylmaleimide-sensitive factor attachment protein receptor) proteins are abundant on intracellular membranes and readily form stable complexes (Martens et al., 2008; Jahn et al., 2006). It is currently thought that these proteins operate as "nanomachines" which force the membranes together and thus initiate membrane fusion. SNARE proteins interact with a long and still growing list of other proteins that regulate their conformation and control their availability for the fusion reaction.

SNARE proteins comprise a superfamily of small membrane-bound proteins. They all share a common motif of approximately 60 amino acids, the SNARE motif that is located adjacent to the membrane anchor domain. SNARE motifs are unstructured as monomers but readily assemble into tight "core" complexes. These complexes can be reversibly dissociated by the chaperone-like ATPase NSF and cofactors termed SNAPs. SNARE complexes are represented by elongated four-helix bundles in which each SNARE motif contributes one α -helix, with the membrane anchor domains protruding at one end (Fig. 3). SNAREs are classified into Q-SNAREs and R-SNAREs based on the type of side chain in a centrally conserved part of the complex. The current model implies that appropriate sets of SNAREs assemble into "trans"-complexes that forms a connection between the fusing membranes (Figure 3; Sutton et al., 1998).

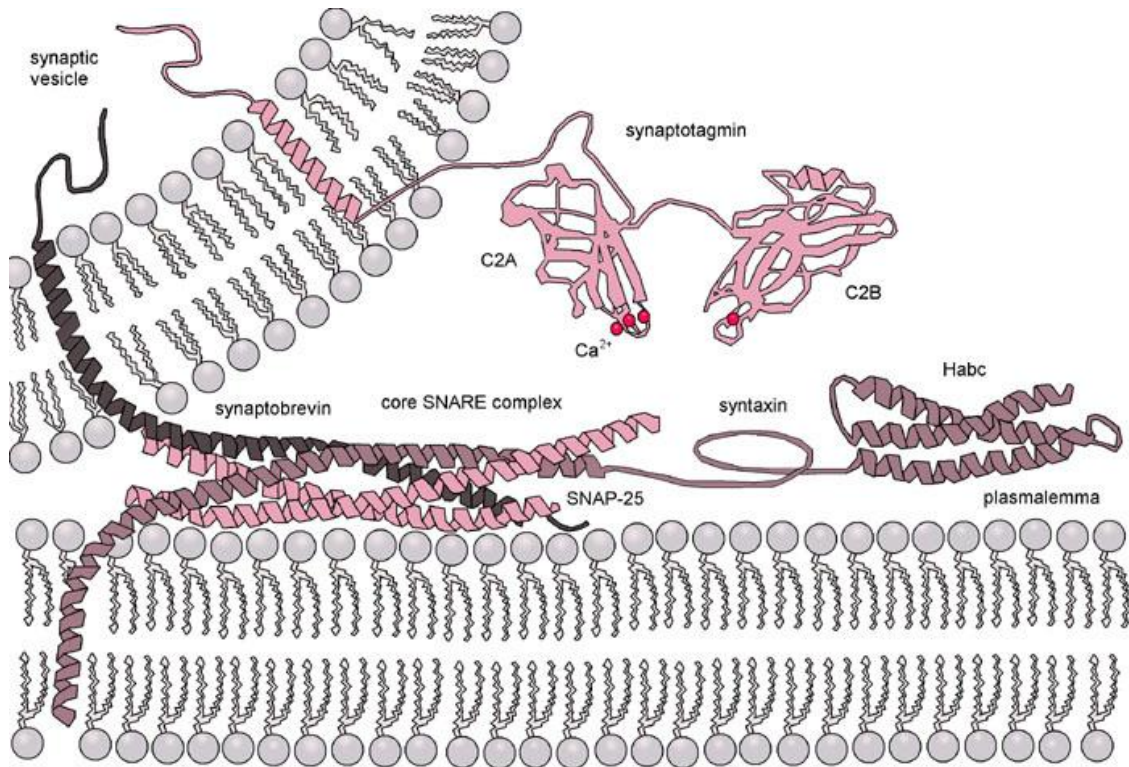


Figure 3. Vesicular and plasma membrane SNARE proteins assemble into the trimeric SNARE complex. Assembly of this complex is thought to drive the membrane fusion reaction (Littleton et al., 2001).

SNAREs are localized to the various intracellular organelles. Based on their localization, SNAREs can be classified into vesicle-associated v-SNAREs and target-membrane associated t-SNAREs. Fusion of SSVs and LDCVs are mediated by three SNARE core complex component proteins: Syntaxin and SNAP-25 (synaptosome-associated protein of 25 kDa) on the presynaptic plasma membrane, and Synaptobrevin (also called vesicle associated membrane protein; VAMP) on the vesicle membrane (Sutton et al., 1998; Chen et al., 2001). The energy released upon assembly would be utilized to overcome the energy barrier separating the membranes and preventing fusion. There are still debates whether association of these proteins or something else is driving fusion. From *in vitro* studies, the neuronal SNAREs are sufficient for membrane fusion when reconstituted in liposomes (Weber et al., 1998), but this occurs in a Ca²⁺ independent manner and with kinetics that are many orders of magnitude slower than exocytosis at the synapse suggesting an essential requirement for other proteins. After fusion, the trimeric complex binds to a complex of the ATPase N-ethylmaleimide sensitive factor (NSF) and soluble NSF attachment proteins (SNAPs),

which disassemble the SNARE complex and make the individual components available for subsequent reuse. Although the function of the SNAREs in membrane fusion is not fully understood, it must be fundamental because in the absence of both vesicle-associated SNARE proteins (v-SNARE) on a chromaffin granule, synaptobrevin II and cellubrevin, secretion is abolished without affecting biogenesis of docking of granules indicating that v-SNARE are absolutely required for granule exocytosis (Borisovska et al., 2006). Furthermore, it was shown by Kesavan et al. that increasing the physical distance between the SNARE domain and the TMD of sybII reduces the granule exocytosis. Thus exocytosis demands a tight molecular link between SNARE Domain and TMD Anchor of sybII (Kesavan et al., 2007). In following this strategy, we studied the functional impact of linker mutation on fusion pore kinetics at the resolution level of single vesicle release.

2.2.2 SNARE interacting partner (complexin)

Regulated exocytosis in neurons and endocrine cell are specialized to be fast and Ca^{2+} dependent suggesting the involvement of other regulatory proteins than SNAREs specific for regulated exocytosis. Among these are complexins. In mammals, complexins form a family of four small (134–160 residues), highly charged proteins (Reim et al., 2005). The first complexin isoforms, complexin I and complexin II, were identified and cloned by virtue of their ability to bind SNARE complexes (Mc Mahon et al., 1995; Ishizuka et al., 1995; 1997) as well as in a screen for cDNAs with repetitive sequences (Takahashi et al., 1995). In mammals, complexin I is expressed specifically in the central nervous system, while complexin II messenger RNA (mRNA) and protein are also detected in non-neuronal tissues (Mc mahon et al., 1995). They operate by binding to trimeric SNARE complexes consisting of the vesicle protein synaptobrevin and the plasma membrane proteins syntaxin and SNAP-25 (Ishizuka et al., 1997). Despite simple structure and binding mode of complexin, physiological studies have suggested diverse functions. Knockout of either one of the two complexin isoforms, I and II, produces a mild (II) or moderate (I) phenotype (Reim et al., 2001). In contrast, the double complexin I/II knockout mouse dies shortly after birth and shows a marked impairment of Ca^{2+} evoked neurotransmission. The exact contribution of complexin to SNARE complex assembly is controversial (Pabst et al.,

2002; Tokumaro et al., 2001), but structural data suggest binding of a single complexin to each independent SNARE complex via association of the complexin C-terminal. In this work, we have studied the dynamics of the fusion pore in the absence of complexin II proteins in chromaffin cells.

2.3 Time resolved admittance measurements

Patch-clamp method constitutes a very sensitive way to record membrane currents (Hamill et al., 1981), which, with appropriate voltage command signals, can be used to determine membrane capacitance at high resolution (Neher and Marty, 1982). The initial patch-clamp methods applied a voltage step and analyzed the exponential current decay in the time domain. Today the most popular methods are the Lindau–Neher (Lindau and Neher, 1988) and phase-tracking techniques (Fidler and Fernandez, 1989), which both use sinusoidal voltage stimulation and rely on the use of phase-sensitive lock-in amplifier measurements. This change was made largely to take advantage of the high time resolution and sensitivity provided by the sinusoidal stimulation techniques (Neher and Marty, 1982; Lindau and Neher, 1988; Chen and Gillis, 2000).

In high-resolution measurements, the PSD (phase sensitive detector) is implemented in hardware with a lock-in amplifier (Neher and Marty, 1982; Lindau and Neher, 1988). Membrane capacitance is measured in the frequency domain, in which a sinusoidal voltage command charges and discharges the membrane capacitance. The lock-in amplifier generates the sinusoidal voltage used to stimulate the membrane and detect the response of the same reference frequency. The amplitude of the resulting sinusoidal current and its phase shift relative to the sinusoidal voltage input are then determined with a phase sensitive detector. The lock-in amplifier then resolves the response into two components, ‘in-phase’ and ‘out-of-phase’ signal in comparison with the applied voltage.

The time resolved patch-clamp admittance measurements allows monitoring exocytosis at the level of single cells and even single secretory vesicles. Capacitance measurements assay relies on the fact that each exocytotic event is accompanied by an increase membrane surface area. The plasma membrane of cells appears electrically as a thin insulator separating the cytosol from the exterior bathing solution. It is therefore

appropriately modelled as a parallel plate capacitor, with the property that the capacitance is proportional to the membrane area. A simple capacitor consists of two-parallel conducting plates separated by an insulator. The capacitance of such a capacitor is directly proportional to its surface area (A), the dielectric constant (k), the permittivity of free space (ϵ_0) and the distance between the plates (d).

$$C = \frac{k\epsilon_0 A}{d} \quad \text{Eq. 1}$$

In case of biological membranes the two plates are formed by the electrically conducting cytosol and extracellular fluid, separated by insulator, the phospholipid bilayers. All biological membranes have a similar bilayer composition and the membrane capacitance (C) is directly proportional to the membrane area (A) as well as the specific capacitance (C_s) with unit $\text{fF}/\mu\text{m}^2$.

$$C = C_s A \quad \text{Eq. 2}$$

By measuring the cell's membrane capacitance and correlating this with the membrane area, the specific capacitance was found to be above $10 \text{ fF}/\mu\text{m}^2$ (Cole, 1968). Later refinements proposed a value of $9 \text{ fF}/\mu\text{m}^2$ (Albillos et al., 1977). When secretion is sufficiently slow (no more than a few vesicles per second), the membrane capacitance can be seen to increase or decrease in small steps, each reporting the exo- or endocytosis of a single secretory vesicle, respectively. Such capacitance steps have been seen in adrenal chromaffin cells (Neher and Marty, 1982), mast cells (Fernandez et al., 1984), pancreatic acinar cells (Maruyama, 1986), neutrophils (Nusse and Lindau, 1989), and pituitary lactotrophs (Mason et al., 1988). By virtue of relationship between capacitance and surface area the size of granule, which undergoes exo- or endocytosis, can be estimated. Thus, membrane capacitance measurements allow a direct detection of changes in membrane area as occurring during the fundamental cellular processes of exocytosis and endocytosis (Neher and Marty, 1982; Fernandez et al., 1984) and it has proved powerful in elucidating details of the membrane fusion process in exocytosis (Breckenridge and Almers, 1987).

Time resolved patch-clamp admittance measurements provide a tool for studying the fusion pore that forms during the initial contact of vesicle with the plasma membrane. Most of the fusion pore studies were performed on cells with very large granule like mast cells or eosinophils, because the unavoidable noise of the RC circuit

formed by access resistance and membrane capacitance in whole-cell patch clamp technique (Neher and Marty, 1982; Gillis, 1995). Current recordings from a small membrane patch in the cell-attached configuration show considerably lower noise level than whole-cell measurements (Hamill et al., 1981) because of the much smaller capacitance of the membrane patch (Neher and Marty, 1982; Lollike et al., 1995; Albillos et al., 1997). An equivalent circuit of a cell-attached patch is shown in Fig. 4.

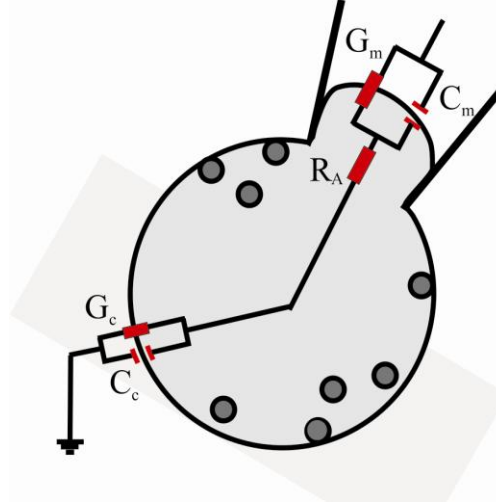


Figure 4. Equivalent circuit for the cell-attached patch configuration. C_c and C_m are the capacitance of the patch and the whole cell membrane, respectively. Since $C_m \ll C_c$ the total capacitance can be approximated by C_m . G_m and G_c are the conductance of the patch and the whole cell membrane, respectively. R_A is the access resistance of the pipette tip.

The admittance of the equivalent circuit in Fig. 4 can be expressed in complex notations

$$Y(\omega) = \frac{1}{R_A + \frac{-j}{\omega C_m} + \frac{1}{G_m}} = \frac{G_m + j\omega C_m}{(1 + R_A G_m) + j\omega R_A C_m} = \frac{G_m + R_A G_m^2 + \omega^2 C_m^2 R_A + j\omega C_m}{(1 + R_A G_m)^2 + (\omega C_m R_A)^2} \quad \text{Eq. 3}$$

with the real part

$$\text{Re } Y(\omega) = \frac{G_m + R_A G_m^2 + \omega^2 C_m^2 R_A}{(1 + R_A G_m)^2 + (\omega C_m R_A)^2} \quad \text{Eq. 4}$$

and the imaginary part

$$\text{Im } Y(\omega) = \frac{\omega C_m}{(1 + R_A G_m)^2 + (\omega C_m R_A)^2} \quad \text{Eq. 5}$$

With an appropriate adjustment the outputs of the lock-in amplifier are proportional to the real and imaginary parts of the pipette current and therefore to the complex admittance Y of the cell for cell-attached configuration.

The work presented here combines high-resolution low-noise cell-attached admittance measurements with whole-cell membrane capacitance measurements (Fig. 7). By having access to the lumen of the cell, one can, beside recording the whole cell membrane capacitance, use also different stimulation paradigms to increase calcium concentration and thereby exocytosis. The exocytosis of a single vesicle can thus be correlated with the exocytosis that occurs over the entire cell membrane. In the recording configuration capacitance noise levels as low as 40 aF (rms) have been obtained and the fusion pore conductance of vesicles as small as 0.6 fF could be resolved. The well-defined experimental setup allows new insight into the time course of single exocytotic events in embryonic mouse chromaffin cells.

2.4 Experimental model: mouse chromaffin cell

Chromaffin cells of the adrenal medulla are a primary neuroendocrine output of the sympathetic nervous system. When stimulated, they secrete a host of transmitter molecules, including catecholamine and neuropeptides, through the fusion of dense core secretory granules with the cell surface (De Robertis et al., 1960; Baker et al., 1981), followed by retrieval of membrane from the surface into intracellular vesicles (Baker et al., 1981; Abrahams et al., 1973; Winkler et al., 1972). LDCV secretion has been best characterized in adrenal chromaffin cells. These cells are part of the adrenal medulla, which contains three types of chromaffin cells, comprising adrenaline- (60%), noradrenaline- (40%), and dopamine-containing cells (<1%). All three types of hormone are synthesized from tyrosine in the adrenal medulla. A single chromaffin cell contains about 30,000 vesicles or chromaffin granules, which contain a mixture of hormones and neuropeptides.

Due to their spherical shape, chromaffin cells are well suited for electrophysiological recordings of membrane capacitance. By combining patch-clamp recordings of membrane capacitance and amperometric recordings of released catecholamine, chromaffin cells can be used to study the exocytosis of a single chromaffin granule with very high temporal resolution and with high signal to noise

ratio. Granules in chromaffin cells fuse all over the cell surface and therefore are suitable for the cell-attached patch recordings. This experimental accessibility together with the fact that in chromaffin cells LDCVs undergo regulated exocytosis and chromaffin cells express the same set of exocytotic proteins as neurons, have led to the widespread use of chromaffin cells as a model system for the analysis of regulated transmitter release.

2.5 Aim of the study

High-resolution capacitance recordings can reveal unitary steps that are proportional to size of the fusing vesicle. Measurements of capacitance steps during LDCV and secretory granule fusion in endocrine cells have thereby provided important insights into the mode of exocytosis (Neher, 1982; Fernandez et al., 1984; Lollike et al., 1995). However, extending these measurements to small embryonic chromaffin cells has been proven difficult.

As a model system we used embryonic mouse chromaffin cells in order to take advantages of genetically deficient mice strains, like synaptobrevin II knock-out, which die at birth. We established a technique to record single vesicle capacitance steps in embryonic mouse chromaffin cells in response to intracellular perfusion with high Ca^{2+} -containing solution. With the use of electrochemical techniques, like carbon fiber amperometry (Bruns, 2004), the release of oxidisable materials from granules through the narrow fusion pore can be analysed, but does not provide direct information about the dimensions or the kinetics of the pore opening and closure. However monitoring how fusion pore forms and initially expands is critical for understanding of the molecular mechanisms of exocytosis. In this work, we characterize the kinetics of the fusion pore (the first connection between vesicular lumen and extracellular solution) in embryonic mouse chromaffin cells and study the role of vesicular SNARE proteins in fusion of single chromaffin granules. Using this method, we are able to study the effects of the synaptobrevin II linker mutant on a zero genetic background providing new insight into mechanism of force transduction from SNARE complex to vesicular membranes. The results provide new insight into the role of v-SNARE in neurosecretion.

Furthermore, complexins may operate at a post-priming step in synaptic vesicle

exocytosis, either by stabilizing SNARE complexes in a highly fusogenic state (Reim et al., 2001; Xue et al., 2007) or by acting as a prefusion clamp that arrests SNARE complexes to prevent fusion (Huntwork et al., 2007; Giraudo et al., 2006; Tang et al., 2006). Despite this effort, the actual role of complexins in the vesicle fusion process has remained a focus of significant controversy. Using our technique can provide new insight into the role of complexins in vesicle fusion.

3. Materials and methods

3.1 Materials

All reagents and chemicals were ordered from Sigma, unless otherwise mentioned here.

Reagent

Product	Company
Papain	Worthington.Lakewood, NJ
DMEM	Cat. N31966-021 Invitrogen, San Diego, CA
Trypsin inhibitor	Sigma, St. Louis, MO
Insulin-transferring-selenium-X	Gibco
Penicillin-streptomycin	Gibco
pSFV1	Invitrogen, San Diego, CA

3.2 Knock out mice

3.2.1 Synaptobrevin II and cellubrevin double knock-out mice

The synaptobrevin II and cellubrevin double knock out deficient mice used in this study were generated in our lab and have been described previously (Borisovska et al., 2005). Chromaffin cells used in this study were cultured on embryonic day 18 (E 18). For each experiment wild type (wt) or heterozygous littermates (Heterozygous for sybII and homozygous-ko for cellubrevin) were used as controls. The protocol for PCR genotyping is described here.

PCR Genotyping for synaptobrevin II wild type reaction

Forward Primer: Syn_WT1 5'-GCC CAC GCC GCA GTA CCC GGA TG -3'
Reverse Primer: Syn_WT2 5'-GCG AGA AGG CCA CCC GAT GGG AG -3'
SybII wt allele: 500 bp

Reaction Mixture		PCR Program	
5X Buffer	5 µl	95°C for 5 min	- 1 cycle
dNTPs 25mM	0.5 µl	95°C for 50 sec	┌
DMSO	2 µl	55°C for 45 sec	35 cycle
Primer Syn_WT1	0.5 µl	65°C for 90 min	└
Primer Syn_WT2	0.5 µl	95°C for 10 min	- 1 cycle
Amersham Taq	0.5 µl		
dH ₂ O	18.5 µl		
Template DNA	4 µl		

PCR Genotyping for Synaptobrevin II mutant reaction

Forward Primer: 1910 5'-CAC CCT CAT GAT GTC CAC CAC -3'

Reverse Primer: 1911 5'-CAG CAG ACC CAG GCC CAG CG -3'

SybII mutant allele: 550 bp

Reaction Mixture		PCR Program	
10X Buffer	3 µl	95°C for 4 min	- 1 cycle
dNTPs 25mM	0.5 µl	95°C for 30 sec	┌
Mg ₂ Cl 25mM	0.5 µl	60°C for 30 sec	40 cycle
Primer 1910	0.5 µl	72°C for 2 min	└
Primer 1911	0.5 µl	72°C for 10 min	- 1 cycle
Red taq polymerase	1 µl		
dH ₂ O	24 µl		
Template DNA	2 µl		

PCR Genotyping for Cellubrevin wild type and mutant reaction

Forward (wt): VAMP3_WT_Fw 5'-CAG ACT CAC TGA ACC TAT GAG AG -3'

Forward (mutant): VAMP3_WT_mut 5'- CAG CGC ATC GCC TTC TAT CGC-3'

Reverse primer: VAMP3_WT_Rev 5'-CTC ACC TGA TAC ATG CAG CAC -3'

Ceb wt allele: 500 bp

Ceb mutant allele: 350 bp

Reaction Mixture		PCR Program	
10X Buffer	3 µl	95°C for 4 min	- 1 cycle
dNTPs 25mM	0.5 µl	95°C for 30 sec	┌
VAMP3_WT_Fw	0.5 µl	60°C for 30 sec	40 cycle
VAMP3_WT_mutant	0.5 µl	72°C for 2 min	└
VAMP3_WT_Rev	1 µl	72°C for 10 min	- 1 cycle
Red taq polymerase	1 µl		
dH ₂ O	19.5 µl		
Template DNA	4 µl		

3.2.2 Complexin II knock-out mice

Complexin II deletion mutant heterozygous mouse strain was kindly provided by Kerstin Reim (Max-Planck-Institute for Experimental Medicine, Neurogenetic, Gottingen, Germany) and has been described previously (Reim et al., 2001). CpxII homozygous knock-out mice were obtained by cross breeding of heterozygous mice. Chromaffin cells from complexin knock-out mice were cultured from P1 pups and wt or heterozygous littermates were used as controls. The PCR genotyping protocol is described here.

PCR Genotyping for cpxII wild type reaction

Forward Primer: CPX WT_FW 5'-CGG CAG CAG ATC CGA GAC -3'
 Reverse Primer: CPX WT_Rev 5'- GAG AGG GGC ATG AAG TCA AGT CAG-3'
 CpxII wt allele: 400 bp

Reaction Mixture		PCR Program	
10X Buffer	2.5 µl	94°C for 5 min	- 1 cycle
dNTPs 25mM	2 µl	94°C for 30 sec	┌
CPX WT_FW	1 µl	64.5°C for 45 sec	41 cycle
CPX WT_Rev	1 µl	72°C for 1 min	└
Red taq polymerase	1 µl	72°C for 7 min	- 1 cycle
dH ₂ O	17.5 µl		
Template DNA			

PCR Genotyping for cpxII mutant reaction

Forward Primer: 1111 5'-CGC GGC GGA GTT GTT GAC CTC G -3'
 Reverse Primer: 1128 5'-CAG GCA CAC TAC ATC CCA CAA ACA-3'
 CpxII mutant allele 350 bp

Reaction Mixture		PCR Program	
10X Buffer	2.5 µl	94°C for 5 min	- 1 cycle
dNTPs 25mM	2 µl	94°C for 45 sec	┌
DMSO	0.7 µl	59.1°C for 30 sec	41 cycle
Primer 1111	0.5 µl	72°C for 1 min	└
Primer 1128	0.5 µl	72°C for 7 min	- 1 cycle
Red taq polymerase	1 µl		
dH ₂ O	16.8 µl		
Template DNA	2 µl		

3.3 Chromaffin cell culture

Embryonic and newborn mouse chromaffin cell culture was prepared as previously described (Sorensen et al., 2003). Briefly, embryos (removed via caesarean section from mother) or newborn mice were decapitated. Adrenal glands were dissected and transferred into Locke's solution (containing in mM: 154 NaCl, 5.6 KCl, 3.6 NaHCO₃, 5.6 Glucose, 5 Hepes, pH 7.3) to trim away excess fatty tissues. The cleaned glands were incubated with enzyme solution (containing DMEM supplemented with 0.2 mg/ml L- cystein, 1 mM CaCl₂, 0.5 mM EDTA and 10-20 unit/ml papain) at 37°C for 20 minutes in a shaker bath. The enzyme solution was replaced by inactivating solution (containing DMEM supplemented with 10% heat activated fetal calf serum, 2.5 mg/ml albumin, 2.5 mg/ml trypsin inhibitor) and incubated for 3 minutes in 37°C bath shaker. The solution was then replaced with enriched DMEM (Containing DMEM supplemented with 1% insulin-transferrin-selenium-X and 0.4% penicillin-streptomycin) and the glands were triturated gently with a 200µl pipette tip until cells were suspended. The cell suspension was plated on sterile coverslips in 6 well plates and incubated at 37°C, 9% CO₂ for 20 minutes to settle. Then 2ml of enriched DMEM

was added to the coverslips. The chromaffin cells were kept at 37°C, 9% CO₂ and were used in day 2-4.

3.3.1 Western blot

Western blotting experiments were performed according to standard procedure (Towbin et al., 1979).

3.3.2 Viral constructs and transfection

cDNA encoding for sybII and its mutants were subcloned into the viral plasmid pSFV1 (Invitrogen, San Diego, CA) upstream of an independent open reading frame that encodes for enhanced green fluorescent protein (EGFP). EGFP labelling was used to identify infected cells. GFP expression was checked using an excitation light at 470nm wavelength. Mutant construct carrying 14 amino acids were constructed using the overlapping primer method as described (Higuchi, 1988). Virus particles were produced as described (Ashery et al., 1999). 400 µl of virus solution was activated by 100µl chymotrypsin (2 mg/ml; Sigma, St. Louis, MO). After 4 hours activation, 110µl aprotinin (6 mg/ml; Sigma, St. Louis, MO) was added to inactivate chymotrypsin. To stabilize enzyme activity 100 µl BSA (6.5 %; Sigma, St. Louis, MO) was added to the virus solution. Virus solutions were kept in room temperate and were used for 3 days. Infected cells were used for electrophysiological recording 5-7 hours after infection.

3.4 Electrophysiological recording

3.4.1 Phase adjustment and calibration of capacitance measurements

For high-resolution measurements of membrane capacitance and conductance, it is important to know the phase relation between incremental current changes resulting from small changes in the three circuit elements R_A , G_m and C_m . To determine the phase setting for the correct separation of capacitance and conductance changes, the piecewise linear technique, originally developed by Neher and Marty in 1980, was used. The variations of admittance (Y) with perturbations in the circuit elements are given by

$$\Delta Y = \frac{\partial Y}{\partial C_m} \Delta C_m + \frac{\partial Y}{\partial R_A} \Delta R_A + \frac{\partial Y}{\partial G_m} \Delta G_m = T^2(\omega)(\Delta G_m + j\omega\Delta C_m - (G_m + j\omega C_m)^2 \Delta R_A) \quad \text{Eq. 6}$$

where $T^2(\omega)$ is a complex phase and attenuation factor:

$$T^2(\omega) = |T(\omega)|^2 e^{-j\varphi} = \frac{(1 + R_A G_m) - j\omega R_A C_m}{((1 + R_A G_m)^2 + (\omega R_A C_m)^2)} \quad \text{Eq. 7}$$

The phase is then calculated (Lindau, 1991):

$$\varphi = -2 \arctan\left(\frac{\omega C_m R_A}{1 + G_m R_A}\right) = -2 \arctan(\omega t_{\text{slow}}) \quad \text{Eq. 8}$$

Where $\omega=2\pi\nu$, and ν is the frequency of the applied sinusoidal voltage in Hz (Neher and Marty, 1982). The piecewise linear is based upon the approximation that small deviations in C_m lead to linear changes in the admittance of the equivalent circuit, which are orthogonal to changes in admittance introduced by small deviations in G_m or R_A . From these considerations, it is clear that capacitive changes can be well separated from fluctuations in G_m (e.g., the opening and closing of ionic channels) and from fluctuations in R_A (the cytoplasm inside the pipette tips), provided the argument of the quantity $T^2(\omega)$ has been found.

In our recordings two important technical aspects have been considered: the determination of the correct phase where changes in capacitance and conductance are well separated (Neher and Marty, 1982; Fidler and Fernandez, 1989; Lindau and Neher, 1988; Debus et al., 1995; Gillis, 1995) and the choice of the sine wave frequency where the best signal to noise ratio is obtained (Neher and Marty, 1982; Lindau and Neher, 1988; Gillis, 1995). For practical phase adjustment and calibration of the set up the EPC-7 amplifier was equipped with a capacitance dither switch adding a resistor in series with the C_{slow} potentiometer. The C_{slow} potentiometer was set to the smallest possible value, and the series conductance was set to 0.2 nS. With the sine wave voltage switched on, the pipette current was nulled, using C_{fast} and τ_{fast} . The switch produced a defined capacitance compensation change of 20 fF, allowing for coarse phase adjustment and providing an approximate calibration step. When the phase was

adjusted to the phase of calibration, steps are restricted to the capacitance (C) trace and flickers to the conductance (G) trace, indicating that the phase was properly adjusted.

A change in the slow capacitance compensation “capacitance dithering” produces an admittance change leading to a change in the sine wave current (Debus et al., 2000). In the case of a correct adjusted phase the change in rms current amplitude, measured at the capacitance phase, is

$$\Delta I_{pipette} = V_0 \Delta C \omega |T(\omega)|^2 \quad \text{Eq. 9}$$

where V_0 is the rms sine wave voltage, ΔC is the amplitude of capacitance dithering step, ω is angular frequency of the lock in amplifier and the calibration factor $|T(\omega)|^2$ is

$$|T(\omega)|^2 = \frac{1}{1 + (\omega\tau)^2} \quad \text{Eq. 10}$$

where τ is the time constant of amplifier compensation network. The resulting change at the lock-in output V_{out} is

$$\Delta V_{out} = G t(f) \Delta I_{pipette} \quad \text{Eq. 11}$$

where G is the gain of the patch-clamp amplifier (the voltage divider (1/10) and the lock-in amplifier output (*10) compensate each other), and $t(f)$ is the frequency dependent transmission of the setup (see Fig. 5). It is dominated by the patch-clamp amplifier and depends on the settings of the internal filters. $t(f)$ was measured by applying different sine wave frequency from the lock-in to the headstage, using the “Test” mode of the patch-clamp amplifiers, and reading the rms value of the output signal from the lock-in display. The lock-in was operating in the r , theta mode (Debus et al., 2000).

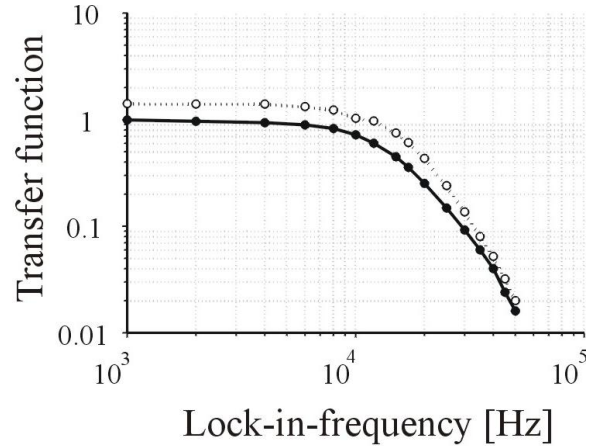


Figure 5. Frequency dependent transmission $t(f)$ of the setup. The plot shows the frequency response of all instruments in the signal pathway. The $t(f)$ was determined separately for EPC7 (filled circle) and EPC9 (empty circle) patch-clamp amplifier.

To determine the time constant (τ_{slow}) of the amplifier compensation network, the responses (ΔV_{out}) to dithering step were measured at different frequencies. The changes of ΔV_{out} were normalized with respect to the dithering step size, gain, frequency dependent transmission, and rms sine wave amplitude. The plot of the normalized ΔV_{out} as a function of frequency (Fig. 6) was used to find the τ_{slow} .

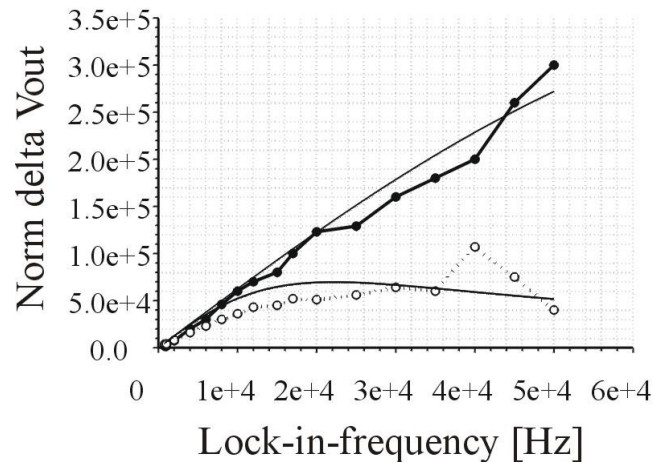


Figure 6. Determination of the time constant τ_{slow} of the EPC7 (filled circles) and the EPC9 (empty circles) compensation network. The changes of the ΔV_{out} were normalized to dithering step size, gain, frequency response, and sine wave amplitude and plotted as a function of frequency. The plots then were fitted with Eq. 12, giving τ_{slow} of $1.2\mu\text{s}$ and $7.17\mu\text{s}$ for EPC7 and EPC9 amplifier, respectively.

$$\frac{DV_{out}}{DCGt(f)V_0} = \frac{2pn}{1 + (2pnt_{slow})^2} = w|T(w)|^2 \quad \text{Eq. 12}$$

The data in Fig. 6 were fitted with Eq. 12, revealing a τ_{slow} of 1.2 μ s and of 7.17 μ s for the EPC7 and EPC9 amplifier, respectively.

A correct phase setting is of particular importance for the determination of vesicle capacitance and the fusion pore conductance. When a large granule fuses with the plasma membrane, the admittance of the membrane is changing therefore the vesicle capacitance and non-zero conductance of the fusion pore must be considered. The equivalent circuit of a granule just fusing with the plasma membrane is shown in Fig. 7. Here C_v denotes the capacitance of the fusing granule and G_p the variable conductance of the fusion pore.

It should be noticed that for the fusion event we now consider the case where all equivalent circuit parameters except G_p are constant. Using Eq. 6 with $C_v \ll C_m$ and $\omega C_v \ll 1/R_A$, conditions which are usually fulfilled, the admittance changes between state before vesicle fusion (Fig. 4) and when fusion pore is formed as shown on Fig. 7 can be approximated by (Breckenridge and Almers, 1987a):

$$\Delta Y = T^2(\omega) \left[\frac{(\omega C_v)^2 / G_p}{1 + \left(\frac{\omega C_v}{G_p} \right)^2} + i \frac{\omega C_v}{1 + \left(\frac{\omega C_v}{G_p} \right)^2} \right] \quad \text{Eq. 13}$$

If the phase is set correctly, the real and imaginary part of the pipette current can be measured at the two outputs of lock-in amplifier. In this case:

$$\text{Re} = \frac{(\omega C_v)^2 / G_p}{1 + \left(\frac{\omega C_v}{G_p} \right)^2}; \quad \text{Im} = \frac{\omega C_v}{1 + \left(\frac{\omega C_v}{G_p} \right)^2} \quad \text{Eq. 14}$$

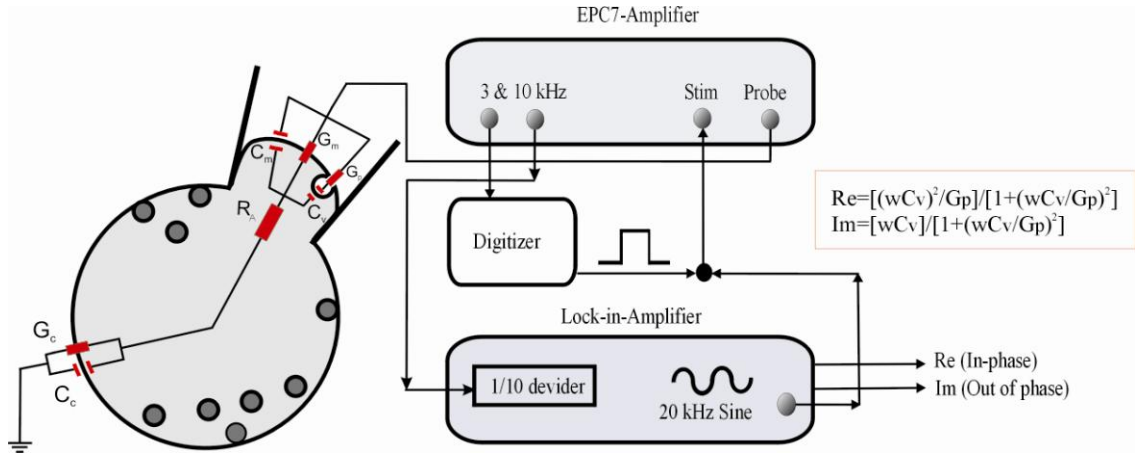


Figure 7. Block diagram of the instruments and the equivalent circuit for cell-attached membrane capacitance measurements during secretion of a single chromaffin granule. An SR830 two-phase lock-in amplifier is used in combination with an EPC-7 patch clamp amplifier. Time-resolved patch clamp capacitance measurements were made under voltage clamp condition in conjunction with a phase sensitive detector. Cell was stimulated using sinusoid voltage and the lock-in amplifier resolved the response in two components, in phase (Re) and out of phase (Im) signal in comparison with applied voltage. The output of the lock-in amplifier is displayed on the oscilloscope and clampex software. The Real (Re) part of the admittance is proportional to the patch conductance while the imaginary (Im) part is proportional to the patched membrane capacitance.

Fusion pore conductance and the vesicle capacitance can be calculated from these traces according to the following formula (Lindau, 1991; Lollike et al., 1995):

$$C_v = \frac{\text{Im}^2 + \text{Re}^2}{\omega \text{Im}} ; G_p = \frac{\text{Im}^2 + \text{Re}^2}{\text{Re}} \quad \text{Eq. 15}$$

After the experiment, the recorded file was analyzed using the data processing software Igor Pro. A dithering step for phase correction is usually not perfect and when capacitance step occurred in Im trace, small projections are visible in Re trace.

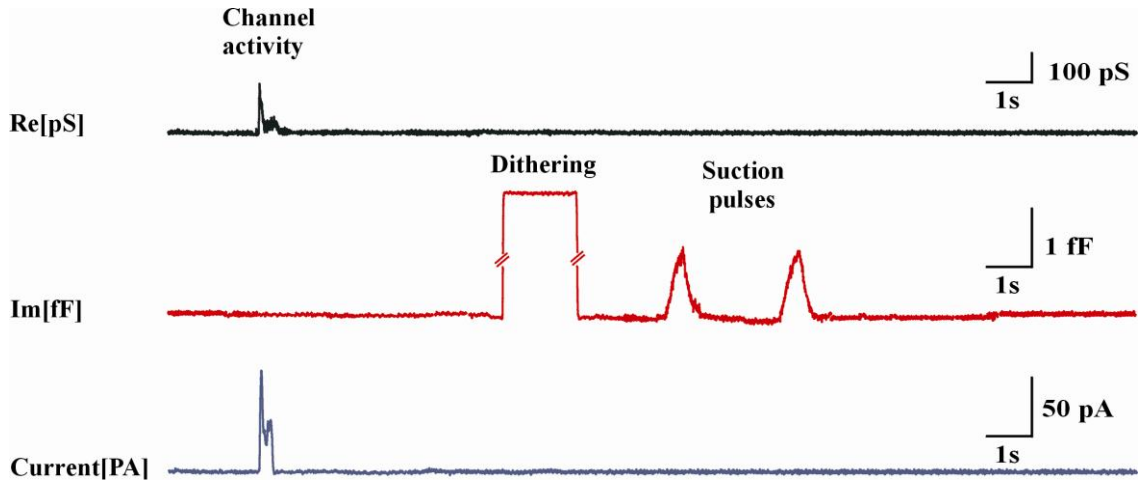


Figure 8. Exemplary parameters considered in offline phase correction. A channel activity (flickers on current trace which should reflect only on the conductance trace), a dithering step (a 20 fF capacitive step made by slow capacitance compensation should reflect on Im trace) and the suction pulses (slow transient capacitance changes applied by gentle suction which should reflect only on Im trace).

Another way of adjusting the phase is to apply gentle suction to the pipette during the actual recording. This manipulation causes transient capacitance changes as the patch is sucked reversibly up into the pipette (Fig. 8). With the correct offline-phase setting projections, which can occur in the conductance trace, should be eliminated. Another control over phase correction was to monitor spontaneous single channel activity or temporary seal instability. Such events should not cause fluctuations in the capacitance trace, and the best phase adjustment should be the one that minimizes noise reflection in such a capacitance segment (Fig. 8). With an appropriate phase setting the changes in the capacitance trace should be eliminated. The phase shift then can be calculated from the changes in Im and Re trace produced by suction pulse or channel fluctuation as

$$\Delta\Phi = -\tan^{-1}\left(\frac{\Delta\text{Re}}{\Delta\text{Im}}\right) \quad \text{Eq. 16}$$

The correct phase of the patch Φ_{patch} is obtained by subtracting the phase shift $\Delta\Phi$ from the phase corresponding to τ_{slow} .

$$\Phi_{\text{patch}} = -2 \tan^{-1}(\omega\tau_{\text{slow}}) - \Delta\Phi \quad \text{Eq. 17}$$

The time constant τ_{patch} is then obtained as

$$\tau_{patch} = -\frac{1}{\omega} \tan\left(\frac{\Phi_{patch}}{2}\right) \quad \text{Eq. 18}$$

Therefore the phase needed to be corrected by few degrees. To correct these small phase $\Delta\varphi$ error off-line, the capacitance and conductance traces are computed from the recorded Re and Im traces with an additional small phase shift $\Delta\varphi$ according to the following formulas:

$$\Delta \text{Re}_{corr} = \Delta \text{Re} \cdot \cos \Delta\varphi + \Delta \text{Im} \cdot \sin \Delta\varphi \quad \text{Eq. 19}$$

$$\Delta \text{Im}_{corr} = \Delta \text{Im} \cdot \cos \Delta\varphi - \Delta \text{Re} \cdot \sin \Delta\varphi \quad \text{Eq. 20}$$

The correlation usually changes the phase setting by 0 - 20° from the value set online during an experiment. In our actual recording average $\Delta\Phi$ was ~ 10 degrees and by using τ_{slow} of 1.2 μs for EPC7 amplifier, $|T(\omega)|^2$ is larger than 0.9 for 20 kHz sine wave frequency. For our measurement the capacitance trace was converted from Volt to fF using Eq. 21 and the scale of the conductance was calculated according to $\Delta G = \omega \Delta C$:

$$\Delta C = \frac{\Delta V_{out}}{V_0 \omega |T(\omega)|^2 G t(f)} \quad ; \quad \Delta G = \frac{\Delta V_{out}}{V_0 |T(\omega)|^2 G t(f)} \quad \text{Eq. 21}$$

For our usual setting ($V_0 = 50$ mV (rms); $v = 20$ kHz; $G = 50$ mV/pA; $t(f) = 0.252$; $|T(\omega)|^2 = 0.96$) the conversion factor for capacitance trace were obtained as $\frac{\Delta C}{\Delta V_{out}} = 13.4$ aF/mV. Using this conversion factor the size of our dithering step was confirmed to be 20 fF thus provides a proper calibration value and recalibrating using τ_{patch} is not necessary.

3.4.2 Analyzing the filter setting

In order to record signals with a reasonable signal-to-noise ratio, the outputs of the lock-in-amplifiers must be filtered. This raises the question to what extent the filter

influences amplitude and kinetics of the response. In particular the transient nature of the Re signal may produce responses that are so short that the full (real) amplitude of the response cannot be detected.

To characterize the rise time of our filter setting, a rectangular step input (Fig. 9 black traces) with different duration can be induced by dithering switch. The output is then filtered as the real signal.

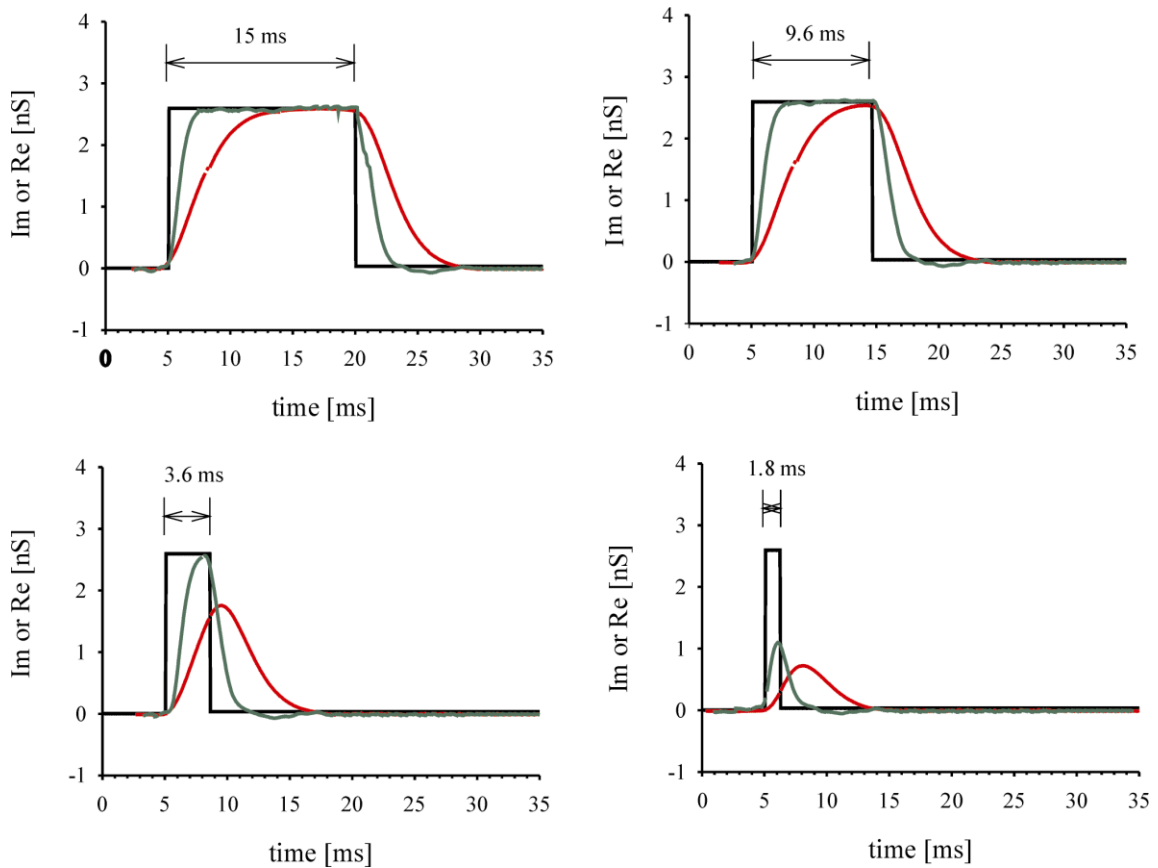


Figure 9. Illustration of the expected responses in admittance (Re or Im) to step-wise increase using different filter settings. The black lines show deflections in admittance of different length produced by dithering. The green and red lines display the response of the lock-in amplifier filter set to an RC-time constant of 300 μ s (24dB) and 1ms (24dB), respectively. The estimated 10-90% rise time of the filter settings are about 1.8 ms and 4.8 ms, respectively.

In the case of long event the effect of the filtering is merely to roll off the square corner of the transition. But a large variety of other patterns can be produced when short events occur. Some examples are shown in Fig. 9. The lock-in amplifier output filter was set to two different time constants, 300 μ s and 1ms with 24dB roll off. Each filter setting was analyzed for its 10-90% rise time as illustrated in Fig. 9. Green

and red traces represent the signal time course for an RC-time constant of 300 μ s and 1ms, respectively. Note that with shorter duration of the input signal, the effect of the filter setting is more pronounced.

We found that the 10 - 90% rise time of the filter settings was 4.8 ms and 1.8 ms, for a RC time constant of 1ms and 300 μ s, respectively. As shown in Fig. 9, only signals with duration longer than twice the 10 - 90% rise time reach the maximum amplitude. With further shortening of the signal time course ($< 2t_r$) the amplitude of the recorded response is progressively attenuated.

Given these properties, in majority of recordings, we have set the filter to 300 μ s. This allowed us to measure full amplitude of the Re responses with duration as short as 7ms. Shorter events were excluded from analysis which covers about 2 percent of the events. The output filter setting of the lock-in amplifier was selected as a compromise between better time resolutions and lowering the noise.

3.4.3 Noise analysis of the setup

Exocytosis of small vesicles can be measured at improved resolution in the cell-attached configuration (Neher and Marty, 1982; Lollike et al., 1995; Albillos et al., 1997; Kreft and Zorec, 1997). In the cell-attached configuration, several noise sources must be considered. These include noise generated within the amplifier, the noise of the seal conductance and patch as well as noise picked up by recording pipette. The instrumental noise was determined by making admittance measurements with open head stage input. Admittance measurements were analyzed for the rms deviation, either online (using the oscilloscope) or offline. For the offline analysis, segments of admittance measurements were selected and the rms deviations of the fitted residuals gave the noise level of V_{out} , which was then converted into capacitance or conductance noise, using Eq. 21. The Fig. 10 shows the instrumental capacitance noise level measured with the EPC-7 and the EPC-9, respectively. The resulting capacitance noise (Fig. 10) decreases with increasing frequency up to 10 kHz and then again increases toward 80 kHz. The rms noise of EPC7 amplifier was lower in comparison with EPC-9 that was a good reason to choose EPC7 for our recordings.

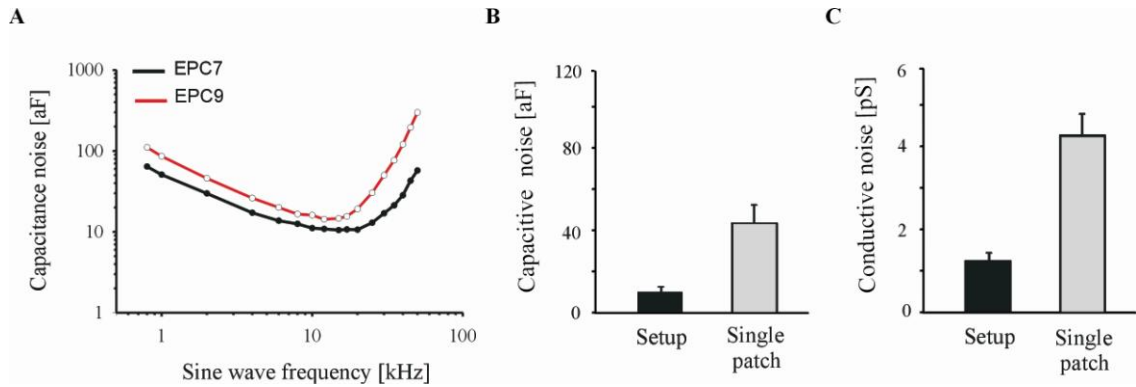


Figure 10. Determination of instrumental noise. (A) Amplifier noise (open head-stage) calibrated in capacitance unit for the EPC-7 and EPC-9 as a function of frequency. (B, C) In parallel, capacitance noise measurements were carried out in cell-attached single patch configuration, using mouse chromaffin cells. The capacitance and conductance noise was measured when 20 kHz, 50 mV(rms) amplitude sine wave stimulus was applied, using 1ms filter setting.

The noise of the actual recording in cell- attached configuration was ~ 4 times the noise of the setup (Fig. 10). However, adding the second patch pipette, using double patch configuration, did not increase the noise much in comparison with single patch configuration. In double patch configuration the rms noise level of 60 aF could be routinely obtained at 25 kHz using a 300 μ s output filter setting of Lock-in amplifier (Table 1). This allows us to detect exocytosis and endocytosis of vesicles with as low as 120-aF capacitance or a 64-nm diameter (Using specific membrane capacitance of 9fF/ μ m²). To further decrease, the equipment noise bandwidth a strong filtering of the lock-in outputs could be applied.

Table1: The rms noise in actual recordings (double patch configuration)

Filter time constant: $\tau_{\text{Lock-in}}$	Sine wave frequency: ν_{sine}	rms noise [aF]	rms noise [pS]
1ms	20kHz	27	3.4
300 μ s	20kHz	103	13.6
300 μ s	25kHz	59	9.4

Low noise capacitance measurements are not only important for the reliable measurements but are similarly essential for measuring the fusion pore conductance over a wide range of conductance value. To resolve the fusion pore, G_p has to be on the order of ωC_v (Curran et al., 1993). The detection limits in pore conductance

measurements can be estimated according to the following formulas (Klyachko et al., 2007):

$$G_p^{lower} = A\omega\Delta C ; G_p^{upper} = \frac{1}{A} \cdot \frac{\omega C_v^2}{\Delta C} \quad \text{Eq. 22}$$

Where C_v is the vesicle capacitance, A is the signal to noise ratio (3:1), ΔC is the capacitance noise (rms), and $\omega=2\pi\nu$, and ν is the frequency setting of the lock-in amplifier in Hertz. The low noise of patch recording makes it possible to measure fusion pore conductance in comparatively small vesicles because of the high signal to noise ratio. For chromaffin cells a frequency of 25 kHz ($\omega=157,000 \text{ s}^{-1}$) is used so that a fusion pore conductance of as $G_p^{lower} \sim 20 \text{ pS}$ and $G_p^{upper} \sim 200 - 2000 \text{ pS}$ is resolved for a 0.25 - 3 fF vesicle which is sufficient for chromaffin cells.

3.4.4 Simulation of the exocytotic event for a given change in fusion pore conductance

Using cell-attached admittance measurements it is possible to study the kinetics of the fusion pore during the first milliseconds of its existence and its subsequent expansion. As explained above, direct information about the kinetics of the fusion pore can be derived from the calculated conductance trace (G_p) using Re (and Im) output of the lock in amplifier. To understand the behaviour of the Im and Re component in the case of a fusing granule in more detail, we have simulated exocytotic events with different fusion pore dynamics (Fig. 11). For a given conductance behaviour the corresponding Re and Im components were calculated using Eq. 14 with assuming a vesicle capacitance of 1 fF and sine wave frequency of 20 kHz.

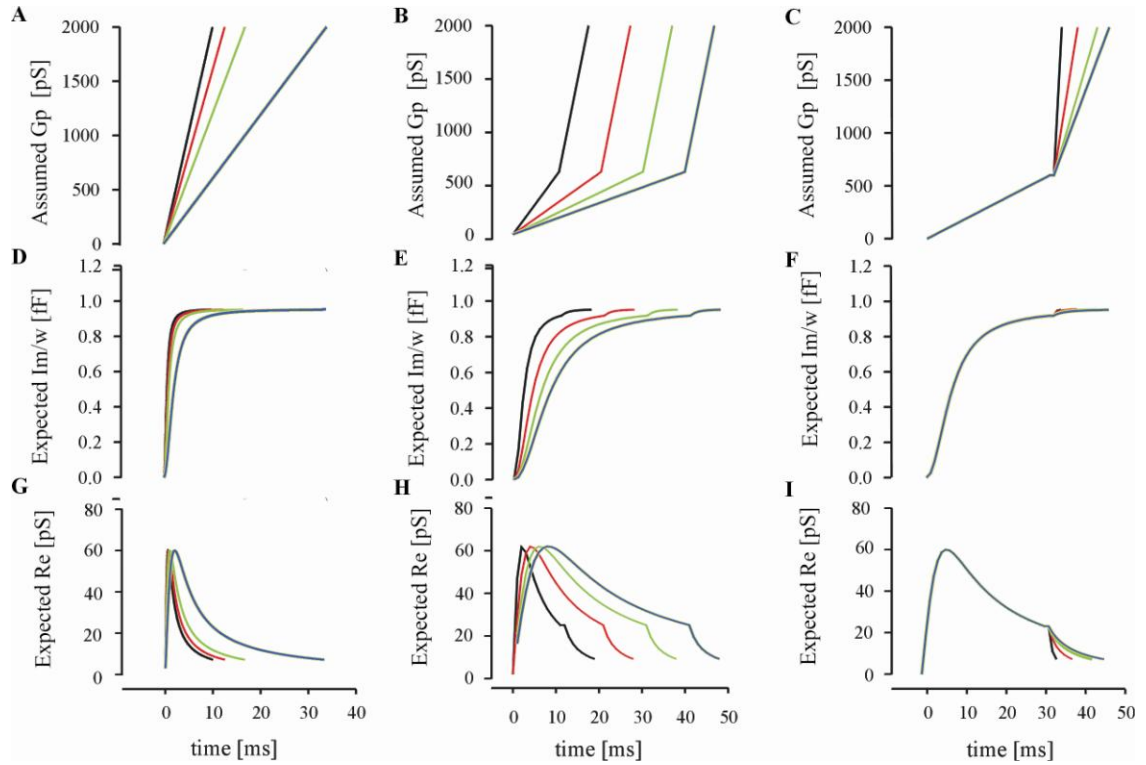


Figure 11. Mathematical calculation of expected Re and Im traces from given fusion pore kinetics. Fusion pore conductance (upper panel, A-C) was used to calculate corresponding Im/ω (middle panel, D, E, F) and Re (lower panels, G, H, I) components. A) Linear and monotonic increase in fusion pore conductance at 4 different rates (colored traces). B) Pore conductance develops in two phases, an initial slow increase of conductance with different rates is followed by a more rapid increase of conductance. C) Pore conductance develops in two phases, with an initial slow increase followed by a rapid increase at different rates. D, E, F and G, H, I show calculated Im/ω and Re trace for scenarios described under A, B and C respectively.

First, we assume a fast and linear opening of the fusion pore at 4 different rates (Fig. 11 A). Such a scenario is often seen in amperometric recordings and coincides with the spike of the amperometric event, reflecting bulk transmitter release from the fusing granule (Chow et al., 1992, Bruns and Jahn et al., 1995, Albillos et al., 1997). The computed imaginary (Im/ω) and real (Re) component for such a conductance is shown in fig 11D and 11G, respectively. As the imaginary part increases, the real part increases steeply and reaches its maximum when $\omega C_v = G_p$ (where the first derivative of the Re as a function of G_p turns to zero). For 20 kHz sine wave frequency and 1fF vesicle capacitance, maximum Re is calculated to be 62.8 pS. After that the real part returns to the baseline, as the imaginary part (Im/ω) reaches the actual vesicle capacitance (C_v). From Fig. 11G we can conclude that very fast and linear opening of

the pore have a very short-lived changes in Re. Using our filter setting, events with shorter life time than 7ms have reduced amplitude and cannot be used for analysis.

In the second scenario, we assume a biphasic behaviour with an initial slow opening of the pore that restricts initial transmitter efflux from the vesicle (generating a 'foot' signal in amperometry) followed by a more rapid expansion of the pore coinciding with bulk release of neurotransmitters (Fig. 11B). The calculated imaginary (Im/ω) and real (Re) component are shown in Fig 11 E and H, respectively. Im and Re components behave similar to the first scenario except for longer duration of Re and the formation of the tail at the end of this component. As it is illustrated in Fig. 11H, the duration of transient changes in Re correlates with the rate of slow conductance increase, the slower the pore opens the longer the duration of transient Re is. From Fig. 11H we can conclude that if any factors limit the initial slow opening of the pore, we can observe this phenotype in our conductance measurements. Fusion events, recorded in *sybII ko* cells by Borisovska et al., exhibit a much longer amperometric 'foot' duration leading to an increase in charge and in maximum current amplitude of the 'foot' signal as expected for prolonged fusion pore expansion. This kind of phenotype should be detectable in our technique.

Third, we assume biphasic behaviour with different rate of rapid expansion. The second phase may accelerate the exocytosis so that at the end the fusion pore conductance goes to infinity (Fig. 11C). The calculated imaginary (Im/ω) and real (Re) component is shown in Fig 11 F and I, respectively. From the computed Re we can conclude that the changes in the rate of rapid pore expansion are shown only in the tail of Re trace. As it was explained in section 2.4.4 due on the noise level of the recording and the vesicle size it may be that the tail of Re component is covered in the noise or could not be clearly identified. Therefore it could be hard to judge the rate of rapid fusion pore expansion preceded by fusion pore dilation at low rate. That may also be the case for our results regarding the linker insertion. Even though clear differences in rate of the rapid expansion were observed in amperometry, we could not observe it with our set of data obtained using this technique.

3.4.5 Setting of the admittance measurements

Cell-attached capacitance measurements were performed with an SR830 two-

phase lock-in amplifier (Stanford Research Systems, Sunnyvale, CA) coupled to a low noise EPC-7 patch-clamp amplifier (HEKA electronics, Lambrecht, Germany). The optimized sine wave frequency of 25 kHz (50mV rms) from lock-in amplifier was superimposed on the command potential of 0 mV. Experiments were done with ≤ 1 M Ω resistance patch pipette (science products, Borosilicate cat No. GB 150F-8p) heavily coated with sylgard. The evoked current at the patch was filtered at 10KHz by EPC7 amplifier and driven back to the Lock-in amplifier input, through a 1 k Ω : 10 k Ω voltage divider. The in-phase (Real) and out-of-phase (Imaginary) output current of the lock-in amplifier was low pass filtered at 300 μ s (24 dB). Data acquisition and analysis were done with a 16-bit A/D converter and stored at 5 kHz sampling rate in a personal computer.

Whole-cell recording were performed with an EPC10 patch-clamp amplifier with the pulse software (v 8.65), both from Heka Electronics (Heka, Lambrecht, Germany). Experiments were done with 4-6 M Ω resistance patch pipette (science products, Borosilicate cat No. GB 150F-8p) coated with honey wax. Passive cell parameters (membrane capacitance, C_m ; access resistance: R_A ; membranes conductance: G_m) were estimated with the 'sine wave + DC' technique (Lindau and Neher, 1988) and computed using the virtual lock-in amplifier of pulse. A 1 kHz, 35 mV peak-to-peak sinusoid voltage stimulus was superimposed onto a DC-holding potential of -70 mV. Current signal were digitized at 12.5 kHz and filtered at 3 kHz. Data were acquired through X-Chart plug-in module of the pulse software.

Double patch-clamp configuration was used to control the intracellular milieu with a whole-cell pipette while simultaneously recording single capacitance events in a cell-attached patch configuration (Fig. 7). During dialysis of intracellular solution, capacitance measurements noise was sufficiently low (40 aF) that fusion of single LDCVs can be resolved.

The bathing solution contained (in mM): 142 NaCl, 4 KCl, 2 CaCl₂, 1MgCl₂, 10 Hepes, 20 Glucose, and PH 7.3 with NaOH. For cell-attached recording, the pipette contained (in mM): 117 NaCl, 4 KCl, 2 CaCl₂, 1MgCl₂, 20 Hepes, 20 Glucose, 20 tetraethylammoniumCl (TEA), PH 7.3 with NaOH. For Ca²⁺ Infusion experiments, the pipette solution contained (in mM): 110 Cs-Glutamate, 8 NaCl, 20 DPTA, 5 CaCl₂, 0.2 Fura-2, 0.3 Furaptra, 2 MgATP, 0.3 Na₂GTP, 40 HEPES, pH 7.3, (19 μ M free calcium). All measurements were performed at room temperature.

3.4.6 Customized analysis

The recorded file (pclamp wave) was imported and analyzed offline using the data processing software Igor Pro 5.01 (Wavemetrics, Lake Oswego, OR, USA). A software procedure was self-written to display Re, Im and pipette current in one window. The procedures include self-programmed tools to determine step size by subtracting line fits to portion of the recording before stepwise events, algorithm for off line phase correction, and calculating the vesicle capacitance as well as fusion pore conductance. All these features were implemented in a graphical user interface in Igor, along with functions to browse through long traces. The most prominent features of the capacitance trace are the slow upward drift. It was gradual, not observed in all recording showing that plasma membrane slowly moving into the pipette as an expanding bulge. To account for drifts or slow variations in the capacitance recording, segments of capacitance traces were fitted by an appropriate polynomial, and the fitted line was subtracted from the measured data points.

4. Results

4.1 Simultaneous detection of single and global exocytotic events

Exocytosis triggered by Ca^{2+} entry can be tracked by measuring membrane capacitance. Using the cell-attached admittance measurements one can observe unitary fusion events in mouse chromaffin cells (Albillos et al., 1977). In order to measure Ca^{2+} triggered exocytosis, it was required to find an appropriate stimulation protocol. It has been shown that depolarisation of chromaffin cells by application of Ringer's solution containing high concentration of KCl increased the fusion rate of LDCVs (Liming He, et al., 2006). Yet, perfusion results in an increase of the bath solution volume, which in turn increases the noise level due to the capacitance of the pipette. In addition, it has been shown that depolarization with KCl was unable to stimulate unitary exocytotic step in cell- attached configuration in 55% of the patched pituitary cells (Klyachko et al., 2007). I used 5-10 μM ionomycin solutions, to increase the internal calcium concentration. On other hand stimulating the cell by patching it in whole-cell configuration has several advantages. It allows monitoring the cell health and applying a persistent steady stimulus without increasing the bath volume.

In our experiments, exocytosis was stimulated by intracellular perfusion with high Ca^{2+} -containing solution (20 μM free calcium) and monitored simultaneously with cell-attached and whole-cell membrane capacitance measurements. It is a reliable method to stimulate and study Ca^{2+} dependent exocytosis. Such a strong stimulus allowed us to gather a large number of single events in cell-attached configuration. Fig. 12A shows the schematic drawing of experimental set-up consisting of cell-attached and whole-cell patch-clamp configurations. The cell-attached configuration (as shown on the left) allowed us to detect single exocytotic events that happen underneath the pipette tip. Fusion of single vesicles produced stepwise changes in membrane capacitance. The whole-cell configuration (shown on the right) gave us the information about exocytosis over the entire cell membrane. This combination has the advantage of gaining access to the cell interior to control the intracellular milieu and to stimulate exocytosis by intracellular perfusion with high Ca^{2+} containing solution.

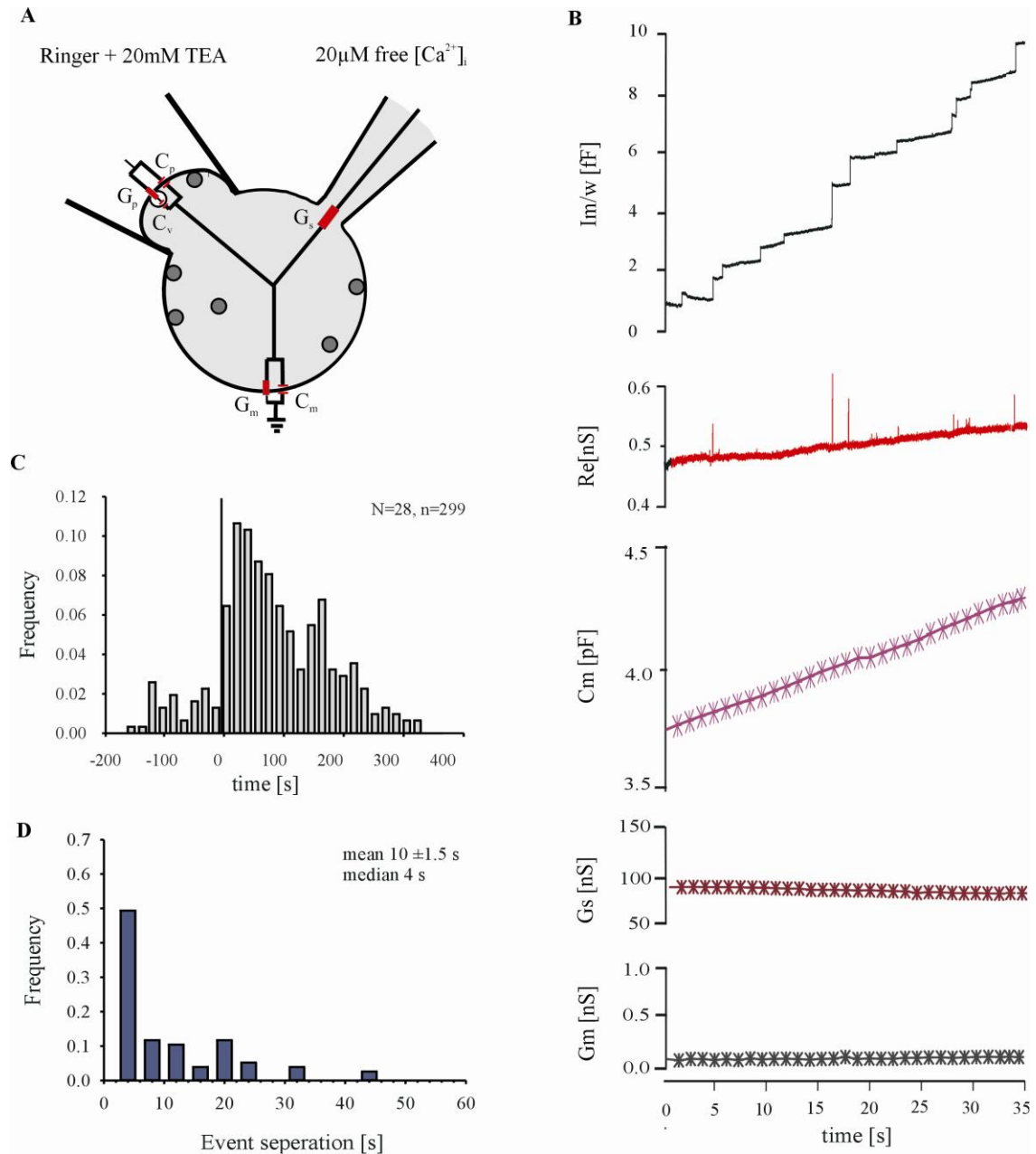


Figure 12. A combination of on-cell and whole-cell configuration is a tightly controlled method to monitor single exocytotic events. (A) Schematic presentation of the electronic circuit of double patch configuration. (B) Representative recording of a newborn mouse chromaffin cell. Capacitance trace (Im/w) and rapid changes in conductance trace (Re) are detected via cell-attached recording. Changes in whole-cell membrane capacitance (C_m), access conductance (G_s) and membrane conductance (G_m) can be recorded via whole-cell configuration (software lock-in amplifier implemented in pulse program). (C) Intracellular perfusion with high Ca^{2+} containing solution causes a robust increase in the number of exocytotic events measured with cell-attach configuration. (D) Distribution of the time intervals between subsequent exocytotic events recorded in 28 cells for the time period of the first 50 s after stimulation.

Upon the start of intracellular Ca^{2+} perfusion, cells (N=28) respond with a strong increase in the frequency of unitary capacitance steps (on average 9.6 ± 1.6 upward steps in 100s) as well as with whole cell membrane capacitance increase (567 ± 184 fF/60s) (Fig 12B). The close correspondence between the two independent measurements shows that the unitary capacitance signals are due to granule exocytosis. The whole-cell recording allows monitoring access resistance (G_s) and the membrane resistance (G_m) showing the efficiency of calcium perfusion and the healthiness of the cell, respectively.

In the single patch configuration (cell-attached) without stimulation only 12 from 44 cells showed little exocytotic activity. In the double patch configuration, instead, the likelihood for recording exocytotic activity was significantly improved (86%). From 30 cells recorded in double patch configuration, 26 cells had multiple exocytotic steps, 2 cells showed only a single exocytotic step and only 2 cells showed no responses to Ca^{2+} . On average 20s after the start of the intracellular Ca^{2+} perfusion, chromaffin cells respond with a strong increase in the frequency of single exocytotic events (Fig. 12C). The frequency distribution of the time intervals between two subsequent fusions events is shown in Fig 12D. In 28 cells recorded for duration of 100s, the average time interval between full fusion steps was 10s (0.1 Hz) while the time interval between events in resting chromaffin cells was 23.7 s. Given this result, it is clear that exocytosis stimulated with high Ca^{2+} proceeded at a higher rate in comparison to non-stimulated cells. The whole-cell capacitance also increased immediately following the Ca^{2+} entry an overall stimulation of exocytosis.

Still, a direct correlation between the number of exocytotic steps and the increase in whole cell membrane capacitance was not observed (data not shown). Often increases in membrane capacitance (C_m) were not accompanied with occurrence of single fusion events or vice versa. This may be due to inhomogeneities in the subcellular distribution of vesicles or to endocytosis, which can mask the exocytotic response measured in the whole-cell configuration.

4.1.1 Detailed analysis of single fusion event

An exemplary recording of an embryonic mouse chromaffin cell is illustrated in Figure 13. Steps in the capacitance trace (Im/ω) represent fusion of individual granules.

Some fusion events are accompanied with rapid changes of the real (Re) component. The Re trace represents the real part of the admittance from which the conductance of the pore (G_p) was calculated. The relation between Re and Im allows to calculate vesicle capacitance (C_v) and fusion pore conductance (G_p). The size of the step in C_v presents the size of the vesicle. The conductance changes (G_p) represents the appearance of an electrical conductance connecting the vesicle lumen to the outside, namely the conductance of the fusion pore while it has not dilated fully. ΔRe vanishes when the pore conductance becomes too large to support a significant voltage difference under sinusoidal excitation.

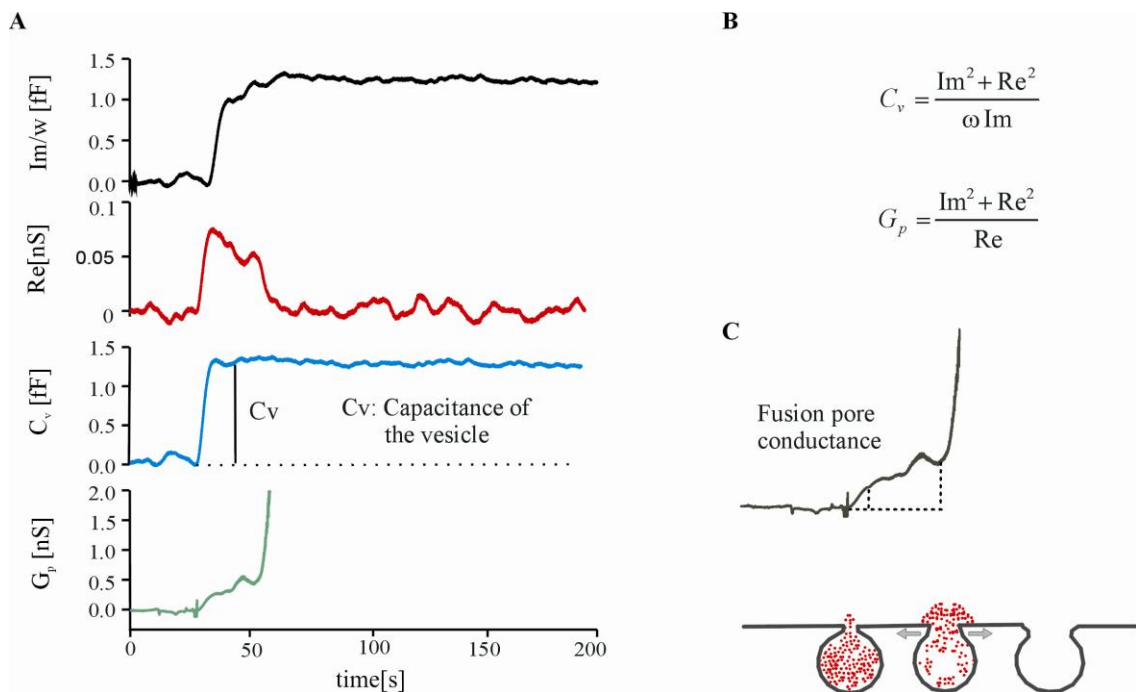


Figure 13. (A) An exemplary recording of a single exocytotic event. Sometimes upward step in imaginary trace is followed by transient changes in Re component. (B) The relation between Re and Im leads to the calculation of vesicle capacitance (C_v) and the fusion pore conductance (G_p). (C) The conductance of fusion pore mostly showed biphasic behaviour. Initial increase may present the release of catecholamine through a narrow fusion pore followed by rapid increase in conductance, which occurs upon bulk secretion of materials from the granule.

Theoretical analysis of a single exemplary step was made using the equations written in Figure 13. The size of the step in C_v corresponds to the size of the vesicle. The conductance of the fusion pore (G_p) shows roughly biphasic behaviour, initial slow expansion followed by rapid expansion. The initial expansion of the pore may allow

release of catecholamine from the vesicle through a narrow fusion pore followed by a rapid increase in conductance that coincides with bulk secretion from the granule.

Besides exocytotic upward steps in membrane capacitance, also downward steps in the capacitance trace (Im), representing endocytosis of chromaffin granule, were occasionally detected. When a vesicle buds from the cell surface or when it constricts an initially wide connection with the external space, the result is a downward Im step accompanied sometimes by a ΔRe increase. The conductance trace (Re) represents the resistance of the aqueous connection called the fission pore. ΔRe vanishes when the fission pore has closed completely. In our recording the vesicle capacitance of the chromaffin cells for endocytotic events in mouse chromaffin cells was 0.52 ± 0.04 fF ($N=27$, $n=17$). Assuming a specific membrane capacitance of $9\text{fF}/\mu\text{m}^2$, we could directly calculate from the capacitance value the size of the vesicle (67 ± 3.1 nm) (mean \pm SE). It should be mentioned that exocytosis was much more abundant than endocytosis, likely because exocytosis was heavily stimulated and also possibly because mechanical effects of the cell-attached pipette favour exocytosis over endocytosis which is in consistent with others finding (Klyachko et al., 2007).

4.2 Vesicle radius obtained from membrane capacitance measurements agrees well with electron microscopy data

To test whether the steps in imaginary trace are representing the exocytosis of the chromaffin granules, we comparatively analysed capacitance measurements and electron microscopy data in wt mouse chromaffin cells. The distribution of capacitance steps obtained from capacitance measurements in nonstimulated cells are shown in Fig. 14A. The average membrane capacitance of a single granule was 0.81 ± 0.45 fF. Assuming a spherical vesicle and a specific membrane capacitance of $9\text{fF}/\mu\text{m}^2$, we could directly calculate from the capacitance value the size of the vesicle (82.2 ± 21.5 nm).

This value comes close to the morphological radius of chromaffin granules determined from EM micrographs (65 ± 18 nm, Borisovska et al., 2005). Furthermore, the coefficient of variation ($CV=SD/\text{mean}$) is similar for the electrical ($CV=0.25$) and the morphological measurements ($CV=0.27$) of the vesicle size, indicating a similar scatter of the parameters. Differences in the mean radius may result from granule

shrinkage during chemical fixation and could be also explained by an underestimate of the granule diameter due to sectioning the organelle at non-equatorial planes.

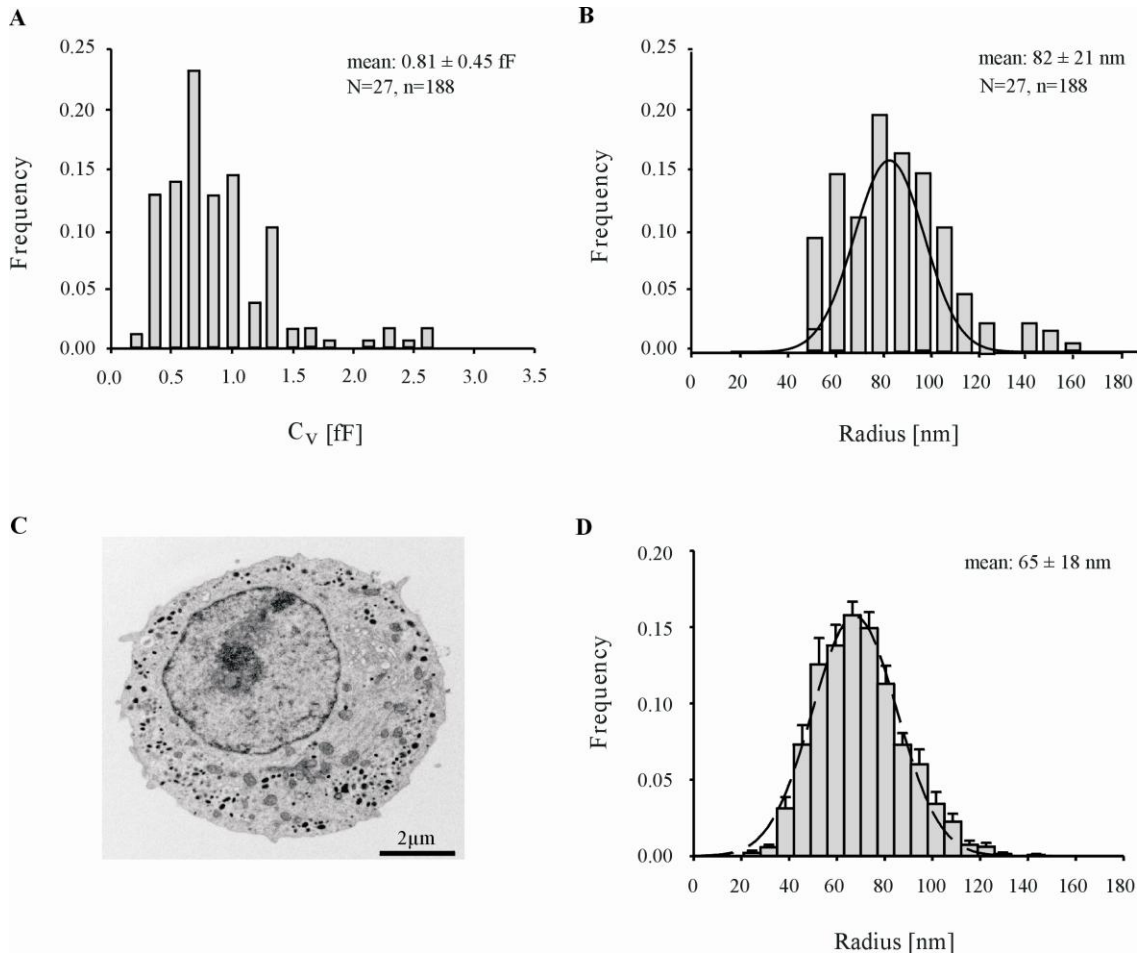


Figure 14. Frequency distribution of the vesicle radius obtained from membrane capacitance measurements, agrees well with electron microscopy data. (A) Frequency distribution of the capacitance steps obtained in newborn wt mouse chromaffin cells. (B) Vesicle radii were obtained from membrane capacitance measurements using a conversion factor of $9\text{fF}/\mu\text{m}^2$. The plot was fitted using Gaussian fit (mean \pm SD). (C) Exemplary electron microscopy picture of a mouse chromaffin cell (2 days in culture). (D) Frequency distribution of the vesicle radius, measured in EM micrographs taken from Borisovska et al., 2005.

Taken together, we found a reasonable agreement between the membrane capacitance step size and the vesicle's morphological dimensions, suggesting that the exocytotic response measured in the cell-attached configuration indeed reflects exocytosis of single vesicles.

4.3 Modes of vesicle fusion

Exocytosis begins with the formation of narrow water filled pore connecting the lumen of the secretory granule with the extracellular space. The initial fusion pore (the first connection between vesicular lumen and extracellular solution) can either collapse causing transient fusion events and leaving an intact granule inside the cell, or expand to a much larger pore size, that allows release of the granule contents into the extracellular medium. The molecular nature of the exocytotic fusion pore remains obscure, the main difficulty has been an inability to directly monitor opening of the fusion pores (Sulzer and Pothos, 2000).

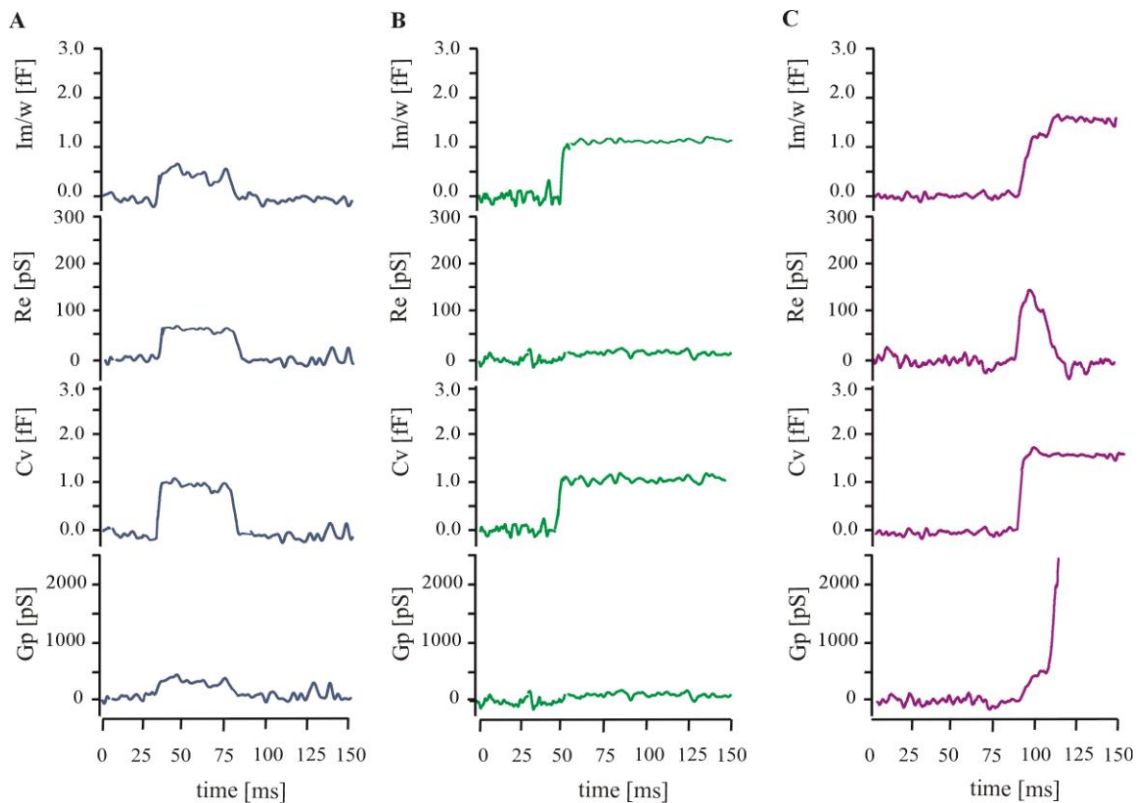


Figure 15. Three modes of fusion pore activity in mouse chromaffin cell. (A) Sequential up- and down-steps referred to as transient fusion (kiss-and-run). Repeated events with similar amplitudes counted as a similar vesicle, which repeatedly fuse with the plasma membrane. (B) Instant upward steps in capacitance (Im/ω) corresponding to the full fusion of single vesicle and abrupt opening of the pore. (C) Slow upward steps referred to as a full fusion event with slower and detectable fusion pore dynamics.

Here, I established a technique to study directly the properties of exocytotic fusion pores in embryonic mouse chromaffin cells. Electrical admittance measurements

allow directly monitoring the kinetics of fusion pore formation, dilations and widening, even if there is no neurotransmitter discharge from the vesicle. This method is advantageous over amperometry, which gives information about the fusion pore only by means of neurotransmitter discharge kinetics from a vesicle. Here we investigate the dynamics of fusion pores of Ca^{2+} dependent exocytosis in mouse chromaffin cells, we show that the cell-attached admittance measurements revealed three different modes of fusion pore activity (Fig. 15).

4.3.1 ‘Kiss-and-run’ mode of exocytosis

Upward capacitance steps were occasionally followed in a few seconds by downward steps (Fig. 15A). These capacitance flickers also referred to as transient events may reflect ‘kiss-and-run’ exocytosis, as they indicate a reversal of the opening of a fusion pore. It means that the vesicle membrane was added to the plasma membrane and the fusion pore opens but then the fusion pore closes again such that the vesicle retains its integrity. Kiss-and-run may be accompanied with partial release of neurotransmitter due to premature closure of the fusion pore. In wt mouse chromaffin cells stimulated with high Ca^{2+} , only 2% of the events were found to be kiss-and-run events ($N=27$, $n=269$). The low frequency of flickers is also similar to that reported for mast cells (Spruce et al., 1990), posterior pituitary nerve terminals (Klyachko and Jackson, 2002) and fibroblasts (Spruce et al., 1991).

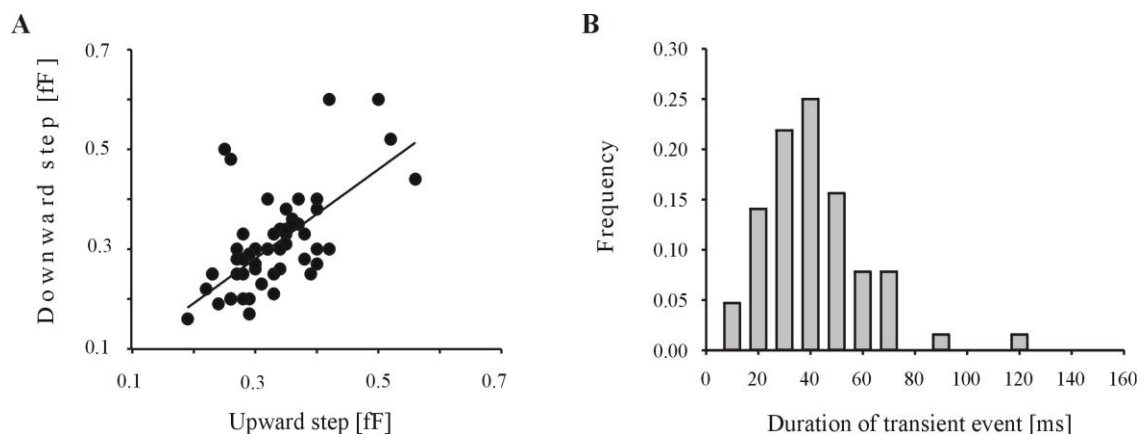


Figure 16. Detailed analyses of kiss-and-run fusion events. (A) Comparison of upward and following downward step amplitudes in capacitance trace for kiss-and-run fusion events shows high correlation and slopes near one (continues line, linear regression: $y = 0.89x + 0.01$; $r^2 = 0.42$). (B) The duration of the transient events showed a wide distribution, giving the average duration of 37 ± 2.3 ms.

It is noteworthy to mention that more kiss-and-run events were observed in resting chromaffin cells. In 7 cells with spontaneous activity we observed 78 ‘kiss-and-run’ events.

The apparent similarity between up- and down-steps was confirmed by analysing the correlation in amplitudes for LDCVs (Fig. 16A). The amplitude of the up-step was tightly correlated with the amplitude of the paired down-step, indicating that the same vesicle fused with the plasma membrane was subsequently endocytosed (Fig. 16). The average C_v was 0.36 ± 0.04 fF giving the average radius of 56 ± 1.8 nm (mean \pm SE). These vesicles are smaller than the estimated average for a single dense core vesicle in chromaffin cells ($P < 0.01$; Fig.14). The differences may be appeared due to the limited number of events and unavoidable repeated transient event in non stimulated cells.

The time when large dense core vesicle stays open during kiss-and-run mode has a wide distribution showed in Fig. 16B. On average the duration of kiss-and-run exocytotic events for LDCVs was 37 ± 2.3 ms, consistent with others finding in nerve terminals (Klyachko et al., 2001). Taking together, we can conclude that ‘kiss-and-run’ is the mechanism of vesicle exocytosis under resting or moderate stimulation conditions. In our recordings kiss-and-run events were rarely accompanied by changes in Re component. Since we did not optimize the resolution of recording for non stimulated cells, it could be that small fusion pore conductance for partial release of neurotransmitter was covered by the noise therefore could not be detected.

4.3.2 Abrupt opening of the fusion pore

The second mode of fusion pore activity reflects a fast step-increase in capacitance (Fig. 15B) that is not accompanied by any discernible changes in the Re component. About 73% of exocytotic upward steps resemble such an event type, which may reflect a rapid opening of the fusion pore to large diameter (> 2 nm radius) (Fig. 15B).

14 % of these vesicles are too small (< 0.4 fF) to support a strong Re signal that is large enough to stand out of the noise. Furthermore, filtering reduces the amplitude of very fast signals (ΔRe) strongly, so that they hardly stand out of the noise. Therefore

most probably, the fusion pore of these secreted vesicles opens very fast to a very large value ($> 1\text{nS}$) which is beyond our detection limits.

The vesicle capacitance calculated for these types of events in mouse chromaffin cells range from 0.2 - 2.5 fF with an average capacitance of 0.74 ± 0.02 fF ($N=27$, $n=159$). Using specific membrane capacitance of $9\text{fF}/\mu\text{m}^2$, the average vesicle radius of 81 ± 1.3 nm (mean \pm SE) can be calculated. These vesicle sizes are in good agreement with the estimated average size of granules obtained from electron microscopy (section 4.2).

4.3.3 Slowly expanding fusion pore

In 23% of non-flicker up-steps, a transient ΔRe (real component of the admittance) was detected when a 20 kHz sine wave command was applied. The transient ΔRe change gave us an estimate of the fusion pore conductance. These events resulted from the slow expansion of an initial fusion pore (Fig. 15C). In these slow events the fluctuation in the Re and Im traces can be seen. Due to the detectable changes in Re component it makes it possible to study fusion pore properties, maybe due to the larger size of the vesicles and slow expansion of the fusion pore. After formation of the fusion pore, it expands to a large size (>2 nm radius) and the vesicle membrane becomes fully incorporated into the plasma membrane. The average vesicle capacitance of slow full fusion events in mouse chromaffin cells is 1.14 ± 0.02 fF ($N=27$, $n=79$). The vesicle radius is calculated to be 98 ± 1.4 nm (mean \pm SE). The average sizes of these vesicles are significantly bigger than those vesicles explained in section 4.3.2 ($p < 0.1$).

The detailed kinetic analysis revealed that the fusion pore opening has two kinetically defined phases. The fusion pore opens to a defined conductance and from this state they usually expand gradually until beyond the detection limit (Fig. 17). The conductance trace was analyzed with parameters such as: initial fusion pore conductance G_{p_i} (initial conductance amplitude when the trace reaches the steady state), duration of the slow expansion Δt (time period from the beginning of the event to the inflection point), the maximum conductance before rapid expansion ΔG_p (conductance amplitude of the inflection point) and the rate of rapid conductance RE (rate of rapidly expanding pore from inflection point to 2nS).

Results

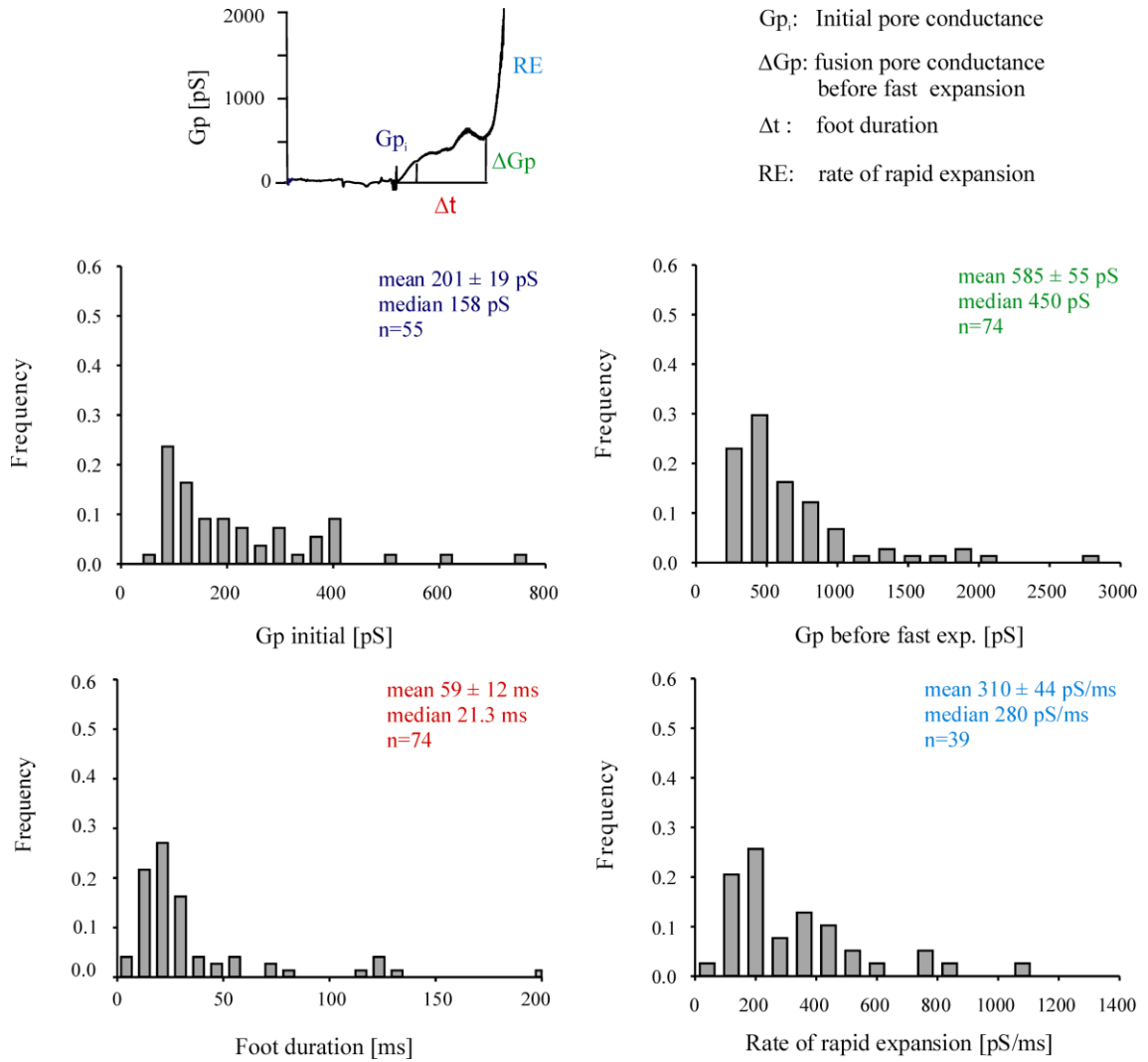


Figure 17. Fusion pore kinetics displays in two distinct phases in newborn mouse chromaffin cells. The frequency distributions and the mean values of initial conductance of the pore, the maximum conductance of the pore before rapid expansion, the duration of the first slow phase of expansion and the rate of very rapid increase in conductance are given.

Vesicles larger than 0.4 fF initiate fusion pores with average conductance of 201 ± 19 pS, which slowly increases for 59 ± 12 ms until reaches the maximum value of 585 ± 55 pS and then accelerates its expansion with the average rate of 310 ± 44 pS/ms. The diameter of the pore is given by Ohm's law. The resistance of a conducting structure R_{pore} is equal to the integral of the resistance along the path of current flow, which for a cylinder is:

$$R_{pore} = \rho \frac{\ell}{\pi r^2} \quad \text{Eq.25}$$

Where ρ is the resistivity of solution, ℓ and r are the length and radius of the pore respectively. The pore is approximately 10 nm long and is bathed in a solution with resistivity of $r=100W\cdot Cm$. The calculated pore diameter ranges from 1.58 to 2.6 nm before rapid expansion of the pore. These data agree well with data obtained from bovine chromaffin cells (Dernick et al., 2005).

In addition, it should be noted that these types of events were not detected in low calcium concentration (resting chromaffin cells). The exact reason of this phenotype is not clear. Given that these vesicles are most likely larger in size we can speculate that smaller vesicle fuse at lower calcium concentration, while big vesicles fuse in presence of high calcium stimulus.

Fulop et al., provided evidence that at low Ca^{2+} concentration fusion pores are narrower and often vesicles do not fuse fully. Or it can be that in high Ca^{2+} concentration a larger proportion of less mature and LDCVs exocytose.

Comparing the vesicle size and the mode of fusion pore activity we can conclude that the larger vesicles exhibit long lasting fusion pore and smaller vesicles produce shorter lived fusion pores as seen by Sombers et al., 2004.

4.4 Comparison of amperometric spike and the conductance trace

Much has been learned about the mechanisms of vesicular release through analysis of individual amperometric spikes. These transient oxidation events reveal the amount of secreted neurotransmitter and the time course of release from single vesicle by means of carbon fiber amperometry, which allows detection of oxidizable neurotransmitters producing a current (Bruns et al., 2004). On the other hand, admittance measurements provide information about electrical properties of the fusion pore. Transmitter that is not bound to the intra-vesicular matrix may leak through the fusion pore to create a feature in the amperometric trace known as the foot signal (Chow et al., 1992; Wightman et al., 1991). This ‘foot’ represents the flux of neurotransmitter through the narrow fusion pore. Fusion pore opening allows a small fraction of the vesicle’s content to escape during an early stage of exocytosis, before the vesicle membrane actually begins to fuse with the plasma membrane.

The amplitude of the foot current gives some indication of the fusion pore size and the duration tells us something about its stability. Upon expansion of the fusion pore, there is a rapid flux of transmitter out of the exposed intravesicular matrix (Fig. 18). This generally leads to a sharp amperometric current transient with a shape characterized by a fast but not instantaneous rise to peak amplitude and a more gradual decay to baseline (Robinson et al., 1996). Here we compare kinetics of release in mouse chromaffin cells monitored by amperometry (Kesavan et al., 2007) and capacitance measurements (Fig. 18).

Admittance measurements showed that the conductance of the fusion pores behave biphasic, initial slow opening followed by rapid expansion of the pore. The initial slow increase in conductance appears to be similar to the foot signal of the amperometric spike. The initial fusion pore conductance ranges from 50 pS to 800 pS. After formation the pore opens slowly with an average rate of 5 nS/s. It has shown by others (Albillos et al., 1997; Ale's et al., 1999) that in chromaffin cells the amperometric foot signal is associated with fusion pores with conductance around 400 pS.

The median duration of early fusion pore obtained from admittance measurements has a close correspondence to the average duration of the foot signal in amperometric signal (Kesavan et al., 2007) shown in Fig. 18 but the corresponding frequency distribution differ. The time period of slowly expanding fusion pore ranges from 7 – 530 ms. The rapid events < 7 ms are not detectable with conductance measurements most likely due to the strong filtering of the signal. In addition, the empty vesicles are not detectable by amperometry.

In second phase of fusion pore conductance, the more rapidly expanding fusion pore has rate of pore opening ranging from 800 pS to over 10 nS with an average value of 1000 nS/s. This may reflect the upstroke of the amperometric spike as proposed by others (Graham et al., 2002; Artalejo et al., 2002).

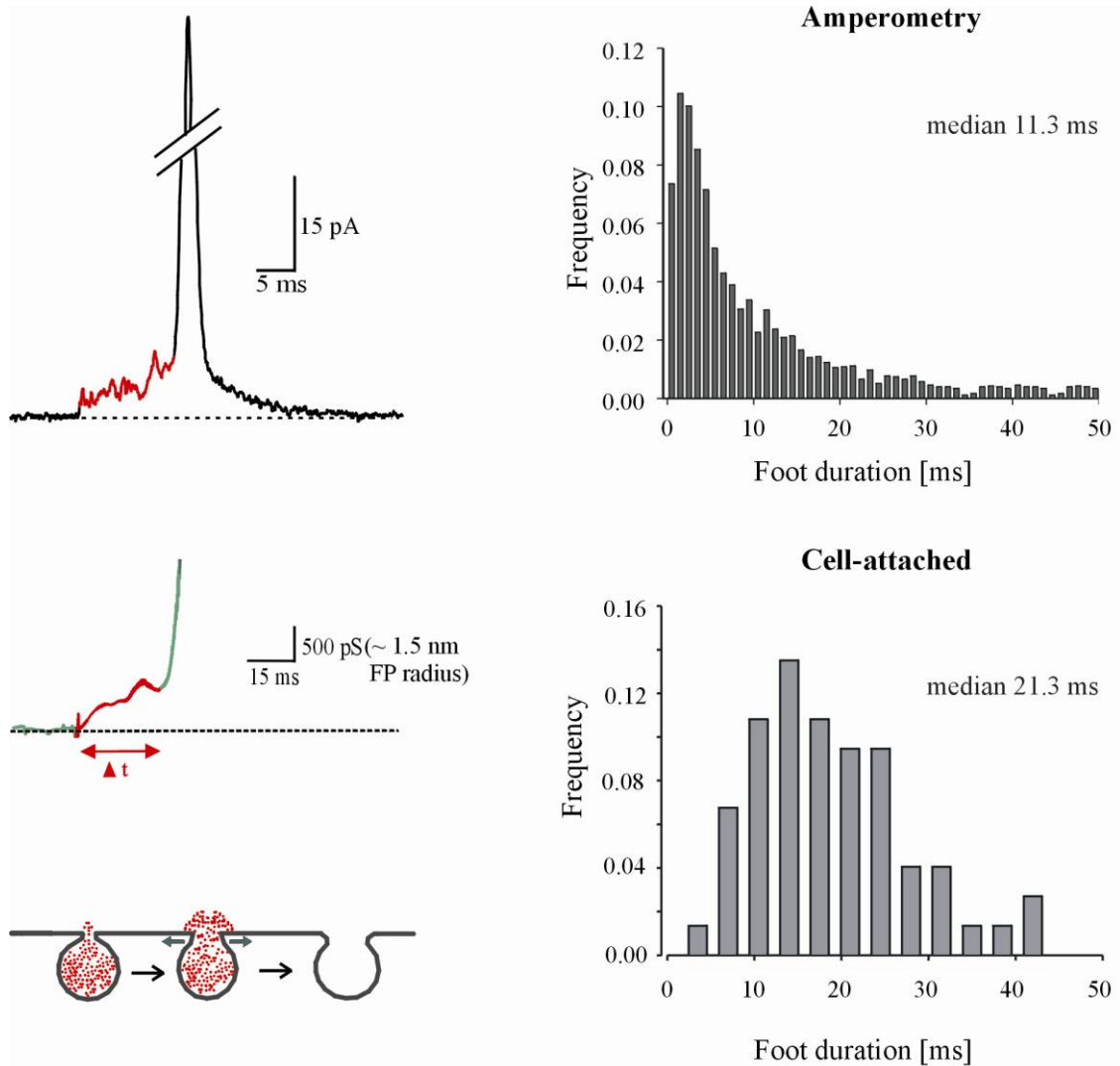


Figure 18. The basic properties of electrical fusion pore measurements agree well with that of amperometric recordings. Exemplary amperometric recording (upper panels) of single granule fusion is shown. Amperometric foot signal (red), which is thought to reflect neurotransmitter discharge through a narrow fusion pore, looks similar to initial rise of fusion pore conductance (lower panels) measured with cell-attached membrane capacitance measurements. (Amperometric data is taken from Kesavan et al., 2007).

4.5 Gradual decrease in capacitance trace, technical error or a phenotype?

In our set of data we have found interesting types of events. The capacitance step (C_{v1} : 1.3 ± 0.03 fF) was some times followed by a gradual decrease (not-stepwise) to a level higher than the baseline (C_{v2} : 0.72 ± 0.03 fF) (Fig. 19). These capacitance steps were mostly followed by a transient changes in Re component and the gradual decrease were preceded with expansion of the fusion pore. The extent and the time

course of this gradual decrease were very variable (not shown). Fig. 19A shows an exemplary event with a fast capacitance decrease.

Lollike and his co-workers also observed these types of fusion events when stimulating the human neutrophils cells by high concentration of ionomycin (Lollike et al., 1998). They conclude that the full incorporation of a vesicle into the plasma membrane leads to a changes in the overall geometry of the patch. In some cases, this could lead to increased attachment of membrane to the glass and a corresponding decrease of the free area contributing to the patch capacitance. This would be electrically detected as a decrease in capacitance, and could thus also explain these observations.

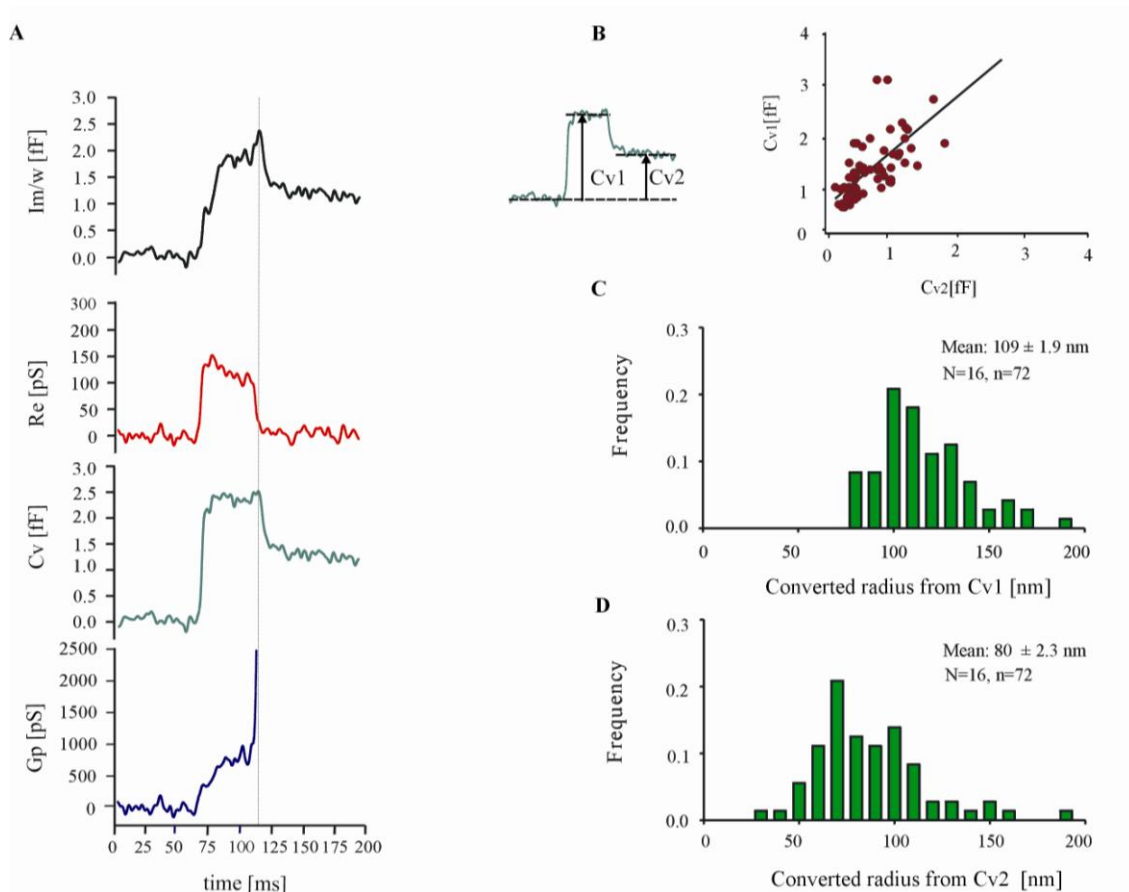


Figure 19. Some vesicles swelled during exocytosis before fully incorporate into the plasma membrane. (A) An exemplary fusion events with initial transient increase in capacitance following by a rapid decrease. (B) The distribution of the capacitance before and after decline (C_{v1} , C_{v2}) is shown. The comparison shows a high correlation between C_{v1} and C_{v2} (continues line, linear regression: $y = 1.1 x + 0.5$; $r^2 = 0.55$). (C, D) The distribution and average of the vesicles transformed from granule capacitance, C_{v1} and C_{v2} , respectively.

In addition our set of data showed a linear correlation between the initial step size C_{v1} and the step size after gradual decrease C_{v2} (Fig. 19B). The vesicle capacitance was reduced to about 26% of its initial size. On average the initial size of the vesicle (radius converted from C_{v1} : 109 ± 1.9 nm) is bigger than average size of the vesicle observed in chromaffin cells (82 ± 21 nm from section 4.2). Furthermore the size of the vesicle after gradual decrease (radius converted from C_{v2} : 80 ± 2.3 nm) is much similar to the mean vesicle size in chromaffin cells. Indicating that these vesicles may have swollen before secretion and upon widening of the pore they turn to their original size.

Plasma membrane is flaccid and its optimal membrane thickness depends on the lipid acyl chain length, the degree of saturation and the angle of tilt within the membrane. From these observations we can conclude that due to the high calcium stimulus some vesicle undergo swelling phenomenon, the angles of the lipid acyl chain may change to reach a thinner membrane. The transition from thicker to a thinner membrane generates some disorder that increases elastic energy. Following this the deformation of the lipid chains progressively should vanish upon exocytosis so that the bilayer recovers its unperturbed thickness (Dumas et al., 1999; Jensen and Mouritsen, 2004). This can be observed as a shrinking phenomenon and can be detected as a gradual decrease in membrane area. For minor perturbations, membrane area adjustments go unnoticed, but when swell–shrink perturbations engage large quantities of membrane, result in easily detected capacitance changes.

Surprisingly we observed that the frequencies of these types of event were increased in some cells recorded in a hot summer day (unavoidable high temperature $\sim 30^\circ$ C). In addition the size of their gradual decrease was bigger than those recorded in room temperature (23° C). With increasing temperature, molecules start vibrating with more kinetic energy, and at higher frequencies and amplitudes, which may lead to overcoming the Van der Waals forces between molecules. This may cause the phospholipid bilayer to move apart, and for the cholesterol molecules to bind weaker with the fatty acid chains of the phospholipids leading to phospholipid bilayers to become more fluid and allow more movement. This increased membrane fluidity at high temperature may be the reason that this swell-shrink phenomenon becomes more frequent.

Our set of data shows that upon widening of the pore the capacitance of the vesicle gradually decreases, this may also support the idea that when the pore is wide

open the core is separated from the vesicle and perturb the thickness of the membrane resulting in reduction in membrane capacitance.

In our experiments, we did not observe the gradual capacitance decrease in transient fusion events in agreement with other's observations (Breckenridge and Almers, 1987b; Zimmerberg et al., 1987). It shows that if the granules have already swollen, the fusion of secretory granules with the plasma membrane cannot be reversed and the swelling disappears only when the fusion pore rapidly expands, suggesting that granule swelling might be pushing exocytosis to completion.

4.6 Observed upward steps are v-SNARE dependent exocytosis

To study the functional impact of v-SNARE proteins in Ca^{2+} triggered exocytosis, we took advantage of a recently developed mouse strain, being deficient for two v-SNARE proteins: synaptobrevin II and cellubrevin (double v-SNARE knockout, Borisovska et al., 2005). The double v-SNARE knockout (dko) animals generated in Bruns's lab, turned out to be a perfect model to study the molecular mechanism of exocytosis with the ability to express any v-SNARE to restore secretion. The double knock-out animals were used in our experiments to validate our method and show that the exocytotic signals measured by cell-attached membrane capacitance measurements are indeed exocytotic events and not an artefact.

In these experiments, exocytosis was stimulated by intracellular perfusion with high Ca^{2+} - containing solution and monitored simultaneously with cell-attached and whole-cell membrane capacitance measurements. In the absence of v-SNARE proteins, cellubrevin and synaptobrevin II, no stepwise changes in capacitance trace (ΔIm) and no transient changes in conductive trace (ΔRe) were observed (Fig. 20) indicating that no exocytotic events other than SNARE-driven exocytosis is detected with this method. Furthermore in whole-cell membrane capacitance measurements no detectable increase in whole-cell membrane capacitance was observed, consistent with previous reports (Borisovska et al., 2005), indicating that these v-SNAREs are absolutely required for Ca^{2+} dependent exocytosis in mouse chromaffin cells.

It should be mentioned that even though no exocytotic steps were observed we have detected some endocytotic steps in cell-attached configuration (not shown).

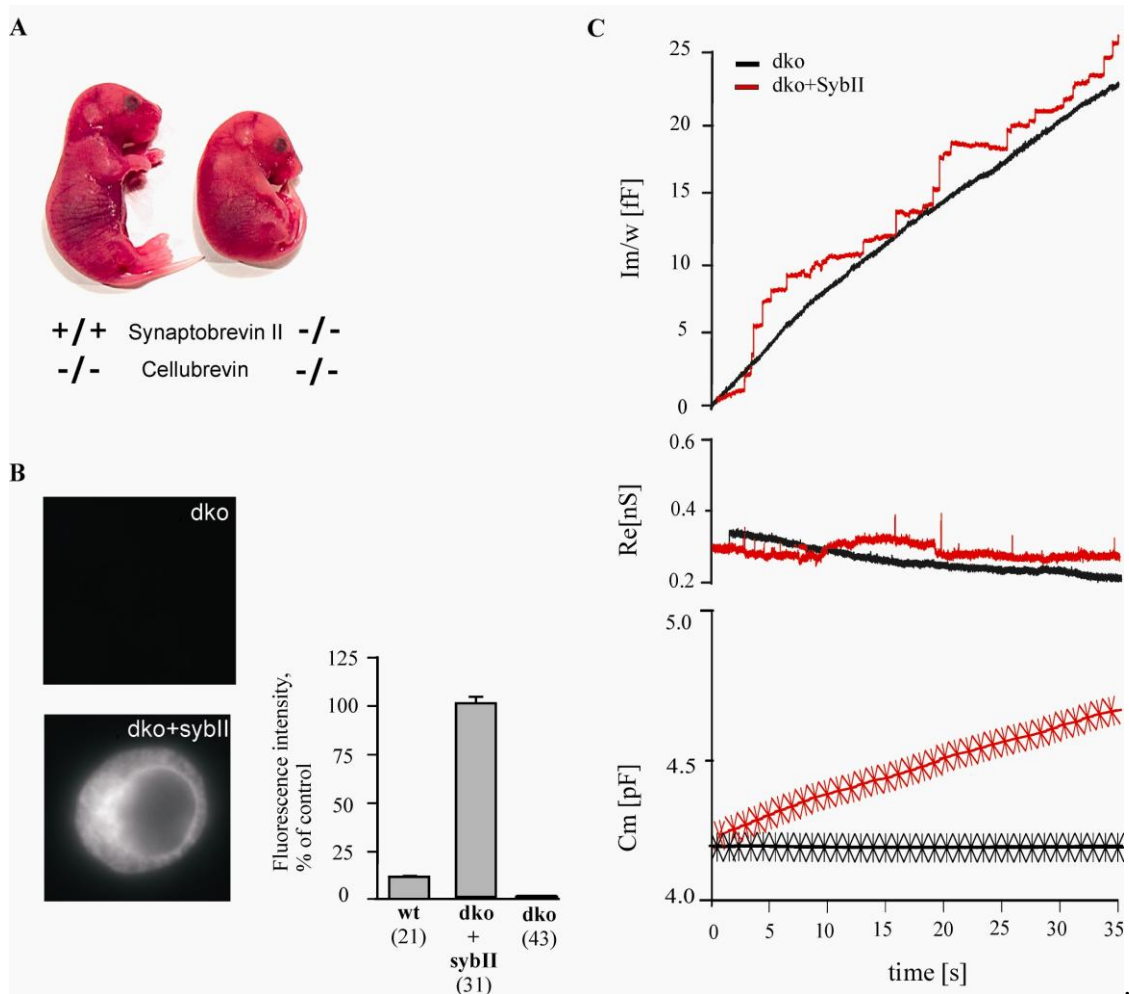


Figure 20. In the absence of both v-SNARE proteins secretion detected in the cell-attached or in the whole-cell configuration is abolished. (A) Appearance of double v-SNARE-deficient mutant mice at stage E18.5 compared with littermates (ceb ko). (B) Immunocytochemistry of cultured chromaffin cells with the indicated genotype stained for synaptobrevin II. Immunosignals for synaptobrevin II are abolished in the dko cells. The dotted appearance of the immunolabel seen in overexpressing cell, suggests that the v-SNAREs are sorted correctly and associate with secretory organelles. Mean intensity of the v-SNARE immunosignal determined for the indicated genotypes (taken from Borisovska et al., 2005). (C) An exemplary recording of dko cells (black) and dko cells expressing synaptobrevin II (red) showing that acute viral driven expression of synaptobrevin II in dko cells fully restores exocytosis with the frequency of exocytotic event similar to those of wt cells.

To confirm that the observed phenotype is due to the absence of the v-SNARE proteins, we acutely overexpressed the proteins in double knock-out cells using Semliki Forest virus system. Upon start of intracellular Ca^{2+} perfusion in double knock-out cells transfected with synaptobrevin II, chromaffin cells respond with a strong increase in the frequency of exocytotic events (on average 7 ± 1.6 upward steps per 100s) as well as an increase in whole-cell membrane capacitance of 459 ± 179 fF/60s (Fig 20C).

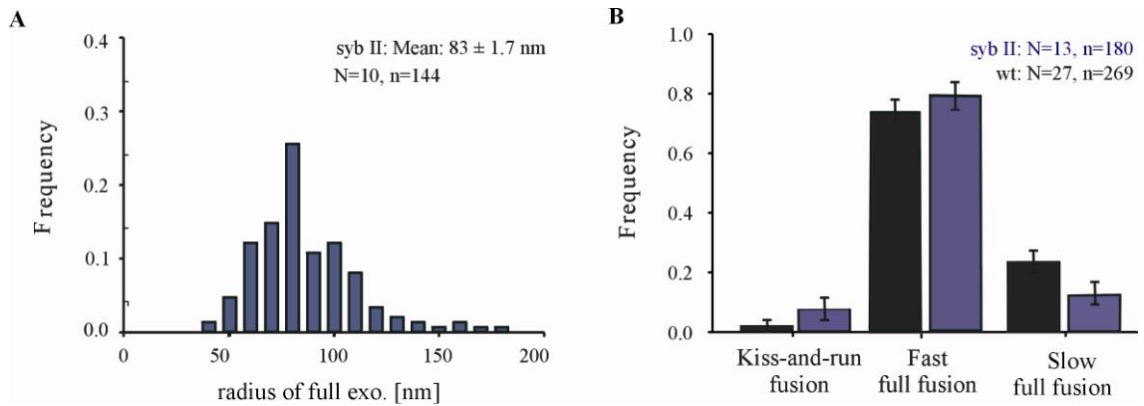


Figure 21. Detailed analysis of vesicle fusion in dko + sybII. (A) The frequency distribution of the full fusion events as well as mean vesicle radius in dko + sybII is similar to those in wt cells. (B) The frequency of three different modes of fusion observed in dko + sybII is shown. Comparative analysis shows no significant differences in comparison to wt cells.

Secretion from double v-SNARE deficient cells can be fully rescued within only 4.5 - 6 hours after start of virus-driven protein expression. This observation gives an estimate of the time required for the v-SNARE sorting to chromaffin granules. It was shown (Borisovska et al., 2005) that upon overexpression of synaptobrevin II in double knock-out cells the protein levels increase on average more than 14 fold compared with endogenous level in wt cells (Fig. 20B). But the exocytosis is restored leading to a capacitance increase to the level found in wt cells. The experiment above was telling us whether developmental defects or simply the loss of the protein is responsible for the absence of the secretory response. By acute overexpression with the Semliki Forest virus we could provide evidence that solely the loss of the protein can be held responsible.

Furthermore we have comparatively analyzed the properties of single exocytotic events in wt (N=27) cells and dko + sybII cells (N=13). Comparing the vesicle size we found that the mean vesicle radius in wt cells was indistinguishable from those in dko + sybII and step size distribution was very similar (Fig. 21A). We also comparatively analysed the occurrence of the mode of fusion in wt and dko + sybII cells. As it is shown in figure 21B, no significant differences were observed.

Results

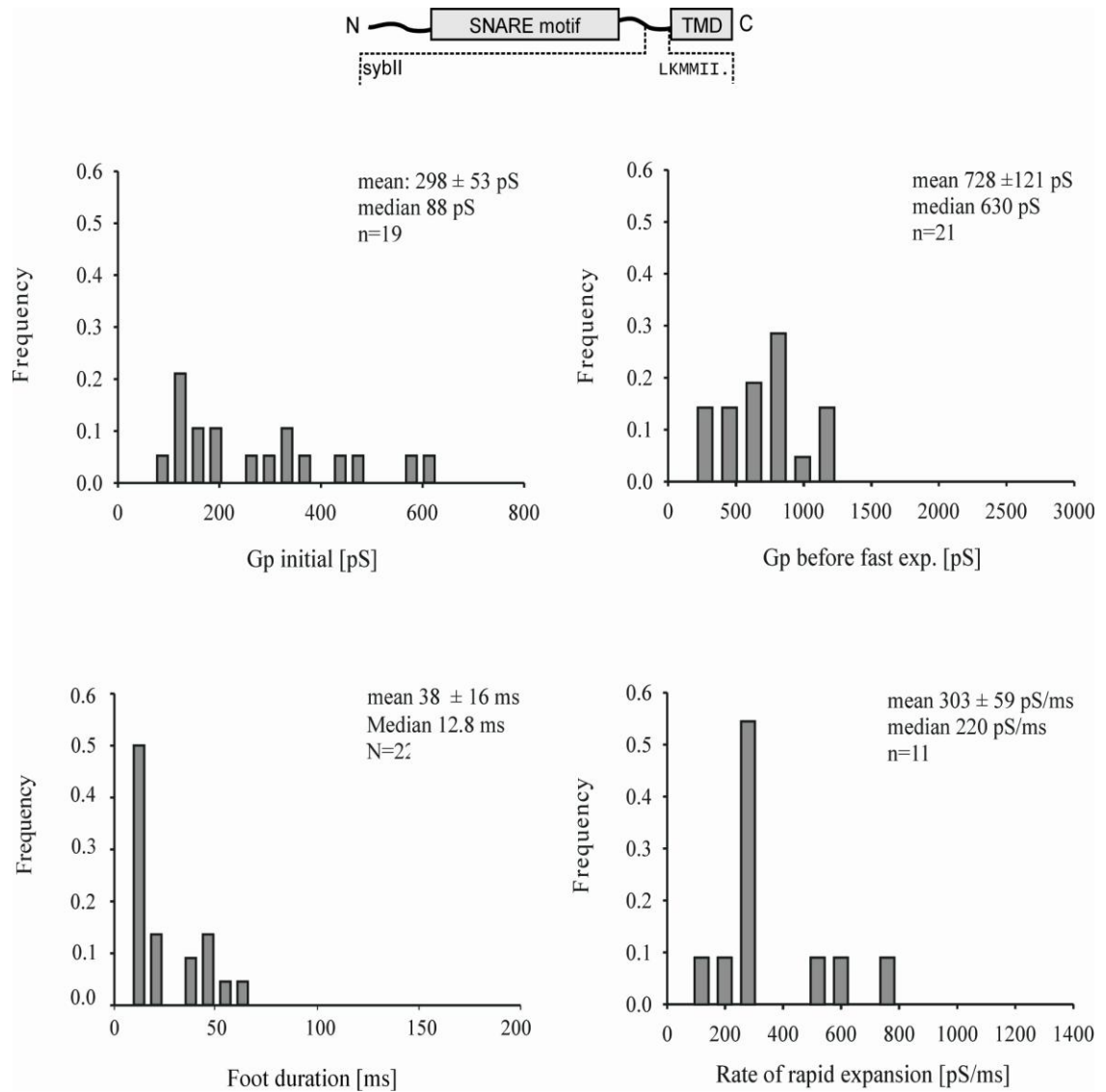


Figure 22. Detailed analysis of the kinetics of fusion pore conductance in dko cells transfected with synaptobrevin II. Schematic view of synaptobrevin II domains (top panel). SNARE motif and TMD are boxed. The frequency distribution and the mean value of initial conductance of the pore, the maximum conductance of the pore before rapid expansion, the duration of the first slow phase of expansion and the rate of very rapid increase in conductance is shown.

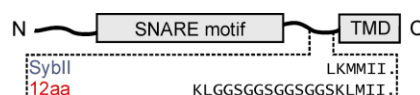
Furthermore, the detailed kinetic analysis of the fusion pore revealed that the fusion pore opening proceeds in two kinetically defined phases in dko + sybII cells as it was in wt cells (Fig. 22). The fusion pore conductance initiates on average with conductance of 298 ± 53 pS (wt: 201 ± 19 pS) and slowly increases for 38 ± 16 ms (wt: 59 ± 12 ms) until reaches the maximum conductance value of 728 ± 121 pS (wt: 585 ± 55 pS) and then rapidly increases with the average rate of 303 ± 59 pS/ms (wt: 310 ± 44 pS/ms). Small but non-significant differences in maximum conductance of fusion pore

before full expansion can be explained by higher number of sybII in comparison with endogenous condition. A higher number of sybII molecules may have access to the fusion pore and lead to the more force transduction and wider opening of the pore.

Taken together, we found that double knock-out cells transfected with synaptobrevin II have fusion pore properties (fusion pore expansion time, dimensions of initial fusion pore) similar to those of wild type cells and no significant differences were observed. These results show that expression of synaptobrevin II in double knock-out cells leads to a full recovery of the exocytotic properties and these results set a stage to study the functional impact of different mutants on fusion pore properties.

4.7 Extending the juxtamembrane region of synaptobrevin II attenuates exocytotic activity

To accomplish fusion, membrane must overcome large energy barriers created by local dehydration of polar phospholipids head groups and membrane deformation. The role of SNARE proteins in overcoming those energy barriers has been shown in various membrane trafficking pathways (Jackson and Chapman, 2006; Jahn and Scheller, 2006). It is widely accepted that prior to membrane fusion, SNARE proteins assemble in trans between the membranes as a bundle of four α -helices, the energy released during assembly being thought to drive fusion (Bruns and Jahn, 2002). Previous results from our laboratory have shown that exocytosis demands a tight molecular link between SNARE domain and transmembrane anchor of sybII (Kesavan et al., 2007). In following this strategy, we intended to increase the physical distance between the SNARE domain and the TMD and studied the functional impact of linker mutation at the resolution level of single vesicle release with cell-attached membrane capacitance measurement. As illustrated below a linker insertion of 12 extra amino acids (12aa) was introduced at the same position as described by McNew et al.



Upon start of intracellular Ca^{2+} perfusion, the linker mutant promotes a reduced secretory response with the longer delay (35 second) for single fusion events. Both, cell-attached recordings (12aa: 4 ± 2.6 upward steps in 100s; sybII: 7 ± 1.6 upward

steps in 100s) and whole-cell membrane capacitance measurements (12aa: 235 ± 72 fF/60s; sybII: 459 ± 179 fF/60s) showed a similar attenuation in the exocytotic activity measured for the 12aa linker insertion. The close correspondence between cell-attached and whole-cell capacitance measurements indicates that the observed changes in the capacitance signal are due to alterations in granule exocytosis. From these data we can conclude that due to the longer distance between TMD and juxtamembrane region of synaptobrevin II the connection between TMD and juxtamembrane region of sybII is weakened and it is likely that large number of vesicles cannot overcome the energy barrier required to fuse to the plasma membrane and therefore the number of exocytotic events is strongly reduced.

Furthermore, Comparing the vesicle size we found that the mean vesicle radius in cells expressing a 12aa linker mutant was indistinguishable from those in sybII-expressing dko cells and step size distribution was very similar (12aa: 89 ± 2.4 nm; sybII: 83 ± 1.7 nm) (Fig. 23A).

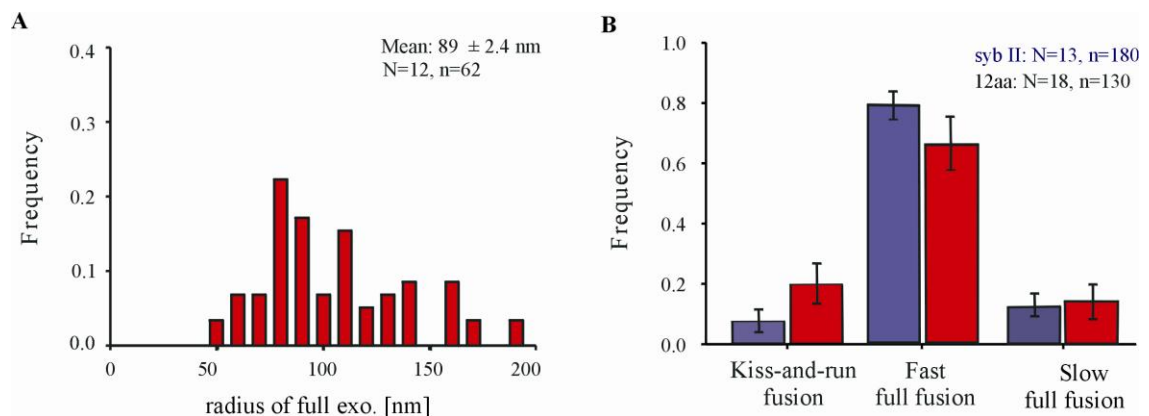


Figure 23. Detailed analysis of vesicle fusion in dko + 12aa. (A) The frequency distribution of the events as well as mean vesicle radius in dko + 12aa is shown. The mean vesicle size is similar to vesicle size in dko + sybII cells. (B) The frequency appearance of three different mode of fusion observed in 12aa is shown. Comparative analysis shows no significant differences.

Furthermore, the dko+12aa cells exhibited three different modes of fusion events as it was observed in dko+sybII cells (Fig. 23B). On average 20% of fusion events were kiss-and-run (sybII: 7% transient), 64% were abrupt fusion events (sybII: 79% fast full fusion fusion) and 15% slowly expanding fusion pore (sybII: 12% slowly expanding pore). Our results show higher (but not significant) frequency of transient

fusion events (kiss-and-run mode of exocytosis) and lower frequency of the abrupt fusion events in linker mutant expressing dko cells. The small but not significant differences in the number of transient events show that the fusion pore kinetics is affected. Maybe the low energy transfer between TMD and juxtamembrane region of sybII leads to the partial opening of the pore, suggesting that there is insufficient energy for a complete membrane merger.

In addition the detailed kinetic analysis of the fusion pore in sybII + 12aa cells shows that fusion pore conductance initiates on average with conductance of 190 ± 45 pS (sybII: 298 ± 53 pS) and slowly increases for 70 ± 32 ms (sybII: 38 ± 16 ms) until reaches the maximum conductance value of 452 ± 48 pS (sybII: 728 ± 121 pS) and then rapidly increases with the average rate of 357 ± 65 pS/ms (sybII: 303 ± 59 pS/ms). In comparison with sybII cells, the conductance of the fusion pore before rapid expansion significantly decreased in 12aa cells (sybII: 728 ± 121 pS; 12aa: 452 ± 48 pS; $p < 0.1$). Vesicles tend to fuse with the plasma membrane via a smaller pore size before expansion. It suggests that 'loosely-coupled' sybII cannot provide the same amount of energy for opening of the pore as the wild type protein.

Taken together this linker mutation inhibits fusion efficiency and reduces the size of the fusion pore without affecting the vesicle size. Our data suggest a confirmation of the fusion pore effect as it was observed by Kesavan et al. From this we can conclude that the tight coupling between SNARE motif and the vesicle membrane is crucial for membrane merger and fusion pore widening.

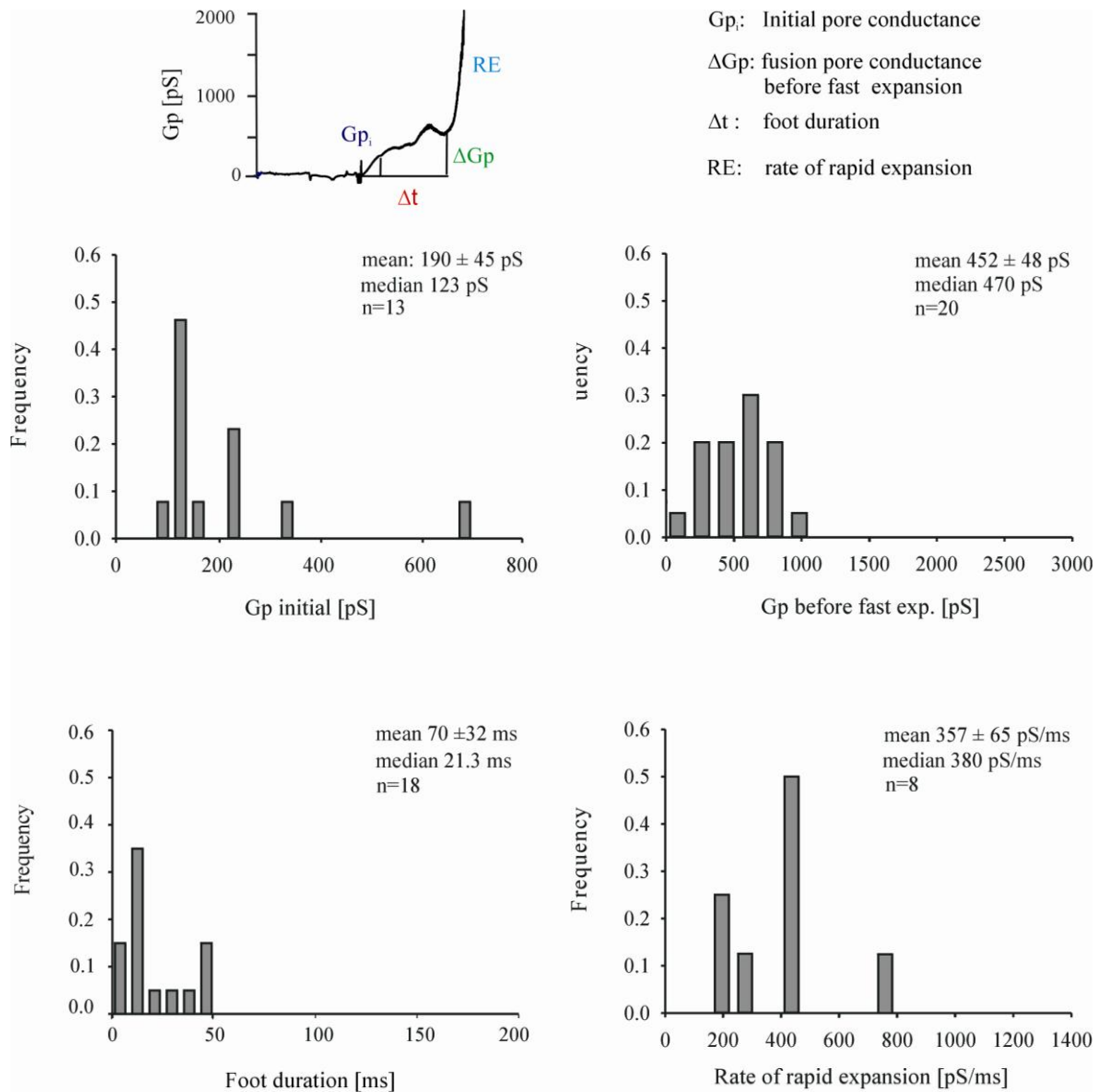


Figure 24. Detailed analysis of the kinetics of fusion pore conductance in 12aa mediated fusion events. The frequency distribution and the mean value of initial conductance of the pore, the maximum conductance of the pore before rapid expansion, the duration of the first slow phase of expansion and the rate of very rapid increase in conductance are shown.

4.1 Complexin II is required to control the size of narrow fusion pore

To explore the functional implication of complexin II, we investigated chromaffin granule exocytosis in the complexin II knock-out mice. We have used double patch membrane capacitance measurements to evaluate the influence of complexin II on single vesicle fusion and kinetics of fusion pores. We recorded capacitance in cell-attached and whole-cell configuration from complexin heterozygous (cpx hz) and knockout (cpx ko) chromaffin cells. Complexin II deficient chromaffin cells respond

with a strong increase in the frequency of exocytotic events (cpx hz: 17 ± 2 upward steps per 100s; cpx ko: 18 ± 4 upward steps per 100s) as well as with an increase in whole-cell membrane capacitance (cpx hz: 522 ± 84 fF/60s; cpx ko: 469 ± 71 fF/60s) in response to whole-cell perfusion with intracellular solution containing $20 \mu\text{M Ca}^{2+}$. These data shows no significant differences in rate of exocytotic activity in the absence of complexin II. Complexin II deficient cultured hippocampal neurons show no change in rate of asynchronous neurotransmission but do have reduced efficiency of a synchronous evoked neurotransmitter release. The latter phenotype can be overcome with elevating calcium concentrations to stimulate release (Reim et al., 2001; Xue et al., 2007). Our data is consistent with the neuronal phenotype. By applying a persistent and long-lasting stimulus we mainly focus on the asynchronous release. Moreover stimulation with $20 \mu\text{M}$ free calcium is probably high enough to overcome the effect of complexin II in fast calcium triggered exocytosis. Thus, we are analysing the same population of events in complexin-II ko and controls and we can solely focus on the role of complexin II in fusion pore kinetics.

The mean vesicle radius obtained from cell-attached capacitance measurements was not significantly different between complexin II heterozygous (81 ± 1.3 nm) and complexin II knock-out cells (79 ± 2.5 nm) (Fig. 25).

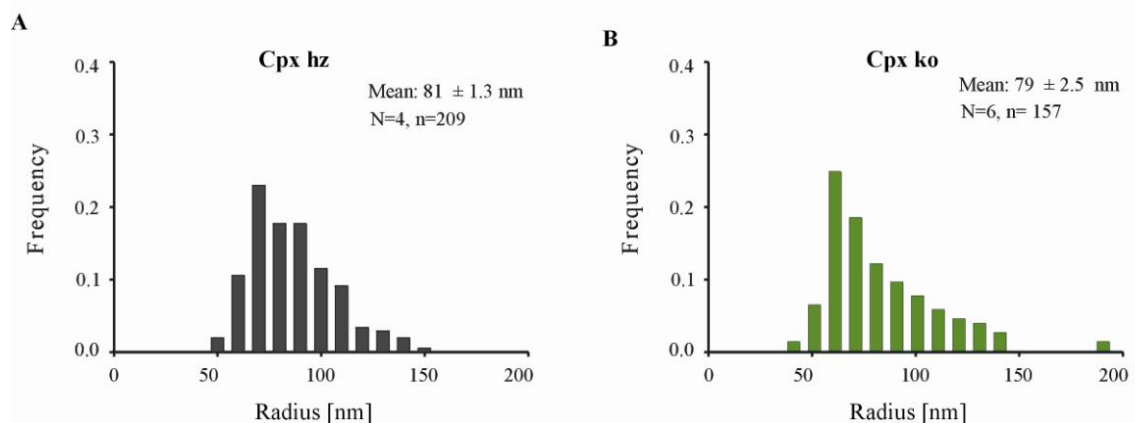


Figure 25. The frequency distribution of the full fusion events as well as mean vesicle radius in cpx hz (A) and cpx ko (B) cells are shown in grey and green, respectively.

We observed similar occurrence of three different types of fusion pore modes in cpx hz and cpx ko cells. The average frequency of transient fusion (cpx hz: 20%; cpx ko: 5%), fast full fusion (cpx hz: 55%; cpx ko: 66%) and slow full fusion events (cpx hz: 23%; cpx ko: 26%) are shown in figure 26. These results showed no significant

changes in distribution of different modes of the fusion pore activity in cpx ko cells compared to littermate heterozygous controls.

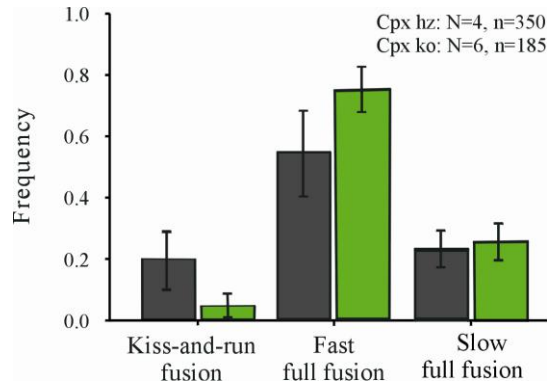


Figure 26. Detailed analysis of mode of vesicle fusion in cpx hz and cpx ko cells. The average frequency (over cell) for three different mode of fusion in cpx hz (shown in grey) and cpx ko (shown in green). Comparative analysis shows no significant differences.

Furthermore, the characteristics of the fusion pore conductance signal in cpx hz and cpx ko cells were examined. The detailed kinetic analysis (Fig. 27, 28) revealed that the mean initial pore conductance (cpx hz: 160 ± 13 pS; cpx ko: 283 ± 38 pS) as well as the mean conductance before rapid expansion (cpx hz: 443 ± 23 pS; cpx ko: 808 ± 101 pS) tend to increase in cpx ko cells while other properties remained similar. It means that the fusion pore size before fast expansion was bigger in cpx ko cells in comparison to events occurring in complexin II heterozygous chromaffin cells. This data suggests that complexin II is involved in regulating the size of the narrow fusion pore before its rapid expansion. Complexins bind SNARE complexes and it is likely that complexions are still functioning at the final stage of membrane merger by controlling the fusion pore. These data is consistent with previous reports suggesting that complexin II is involved in restricting the fusion pore dilation (Archer et al., 2002).

Results

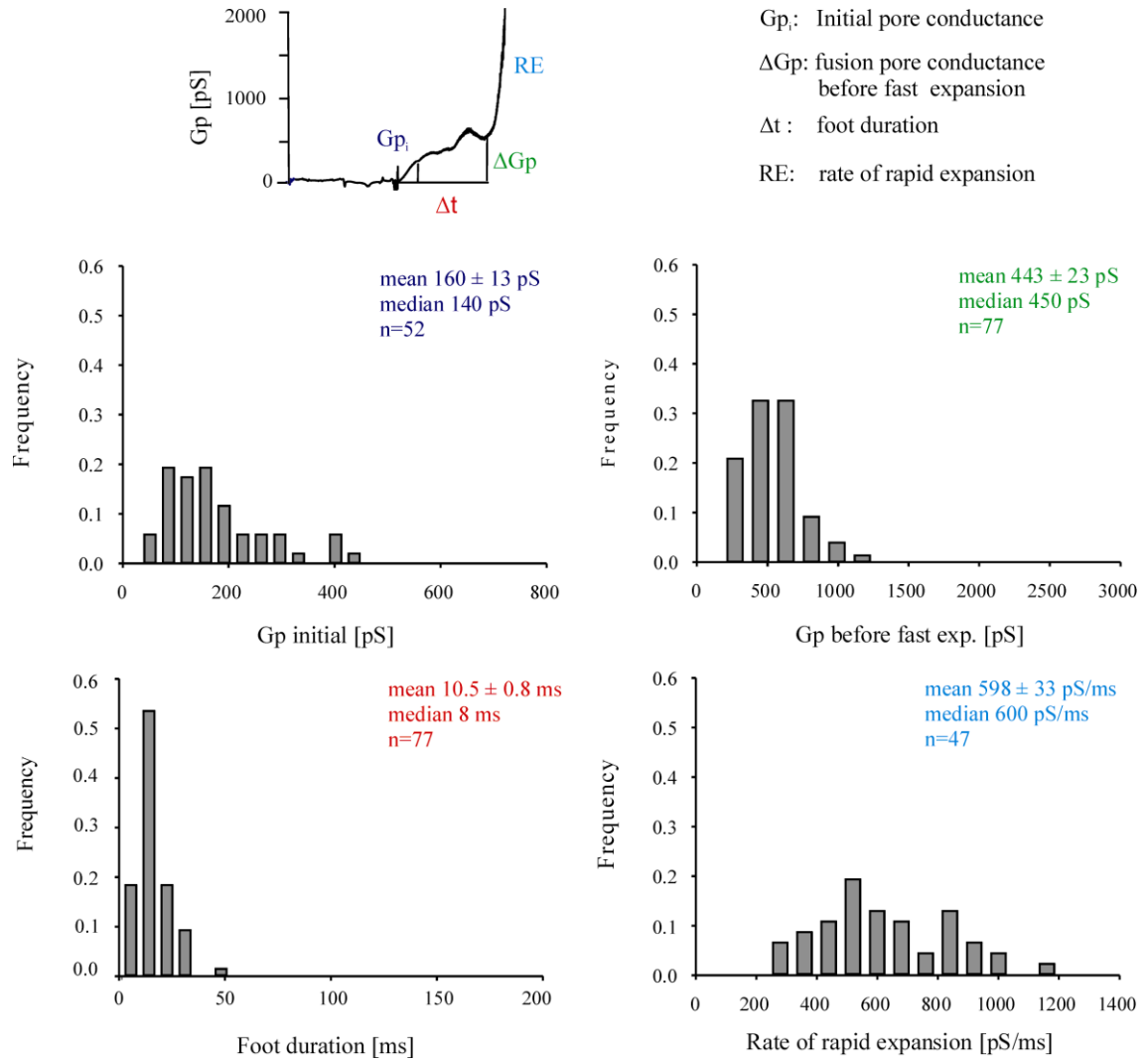


Figure 27. Detailed kinetic analysis of fusion pore conductance in cpx hz cells. The frequency distribution and the mean value of initial conductance of the pore, the maximum conductance of the pore before rapid expansion, the duration of the first slow phase of expansion and the rate of very rapid increase in conductance are shown.

Results

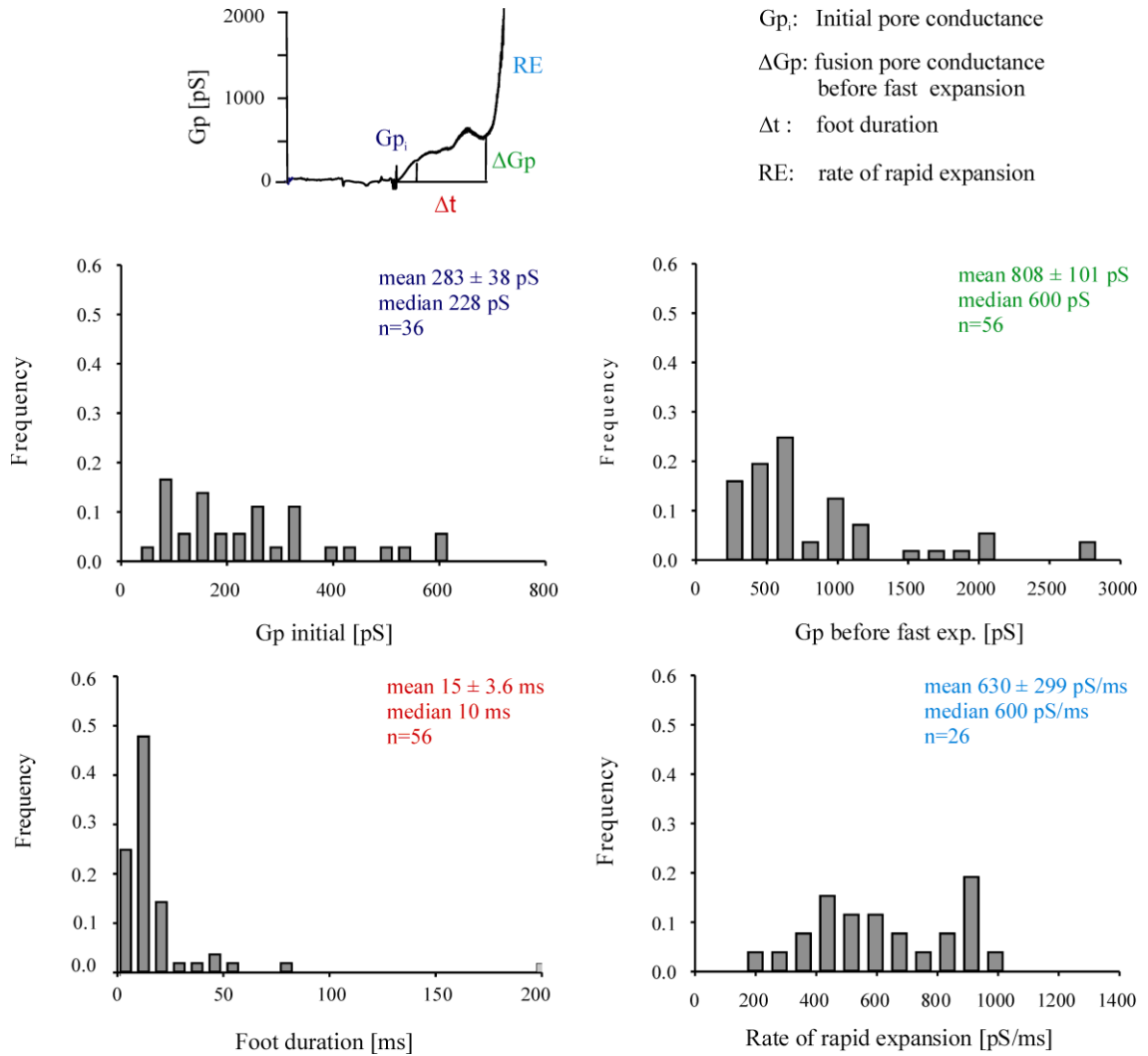


Figure 28. Detailed analysis of the kinetics of fusion pore conductance in *cpx ko* cells. The frequency distribution and the mean value of initial conductance of the pore, the maximum conductance of the pore before rapid expansion, the duration of the first slow phase of expansion and the rate of very rapid increase in conductance are shown.

5. Discussion

5.1 Discrete changes in capacitance indeed correspond to exocytosis of the single vesicle

Capacitance recording provides readout of membrane area that can be used to monitor exo- and endocytosis in neurons and secretory cells in real time. In this work, we developed a modified technique that combines high-resolution cell-attached capacitance measurements with simultaneous whole-cell capacitance measurements in double patch configuration. This method allows monitoring simultaneously the total cell response as well as single exocytotic events. The cell-attached patch-clamp technique makes it possible to separate exocytosis from endocytosis, to determine vesicular size with a resolution below 0.1 fF, to distinguish modes of fusion events, and to monitor individual fusion pore kinetics. On other hand, the whole-cell patch-clamp technique allows to control the composition of the cytoplasm, to dialyze the cell with the solution containing high calcium concentration or other modulators of fusion. This combination has provided enormous insight into the details of intracellular signaling and the fusion process itself.

Using this technique, we can propose that the discrete changes in capacitance described above correspond to exocytosis of the single vesicle. The evidence for that can be summarized as follows:

- (i) Frequency of upward capacitance steps strongly increases upon calcium stimulus.
- (ii) Single capacitance step were detected simultaneous with global increase in membrane capacitance.
- (iii) The distribution of vesicle radius determined from single capacitance steps is in good agreement with the distribution of the surface area of chromaffin granules as determined from electron microscopy data (Borisovska et al., 2005) when a unitary capacitance of $9 \text{ fF}/\mu\text{m}^2$ is assumed.
- (iv) Downward steps were found after upward steps, as expected from transient fusion process.

- (v) In the absence of both v-SNAREs synaptobrevin II and cellubrevin cell-attached membrane and whole-cell membrane capacitance recordings shows absolutely no activity as it is seen by others (Borisovska et al., 2005).
- (vi) Acute viral driven expression of synaptobrevin II in dko cells fully restores exocytosis with the frequency of exocytotic event similar to those of wt cells.

5.2 Fusion pore modulatory effects

The fusion pore has become a major focus of research in exocytosis. Experimentally, use of the double patch-clamp approach provides sensitive biophysical measurements to study how the fusion pore opens, closes or dilates. In this work we characterized the dynamics of fusion pore in mouse chromaffin cells which is in great agreement with other's findings (Klyachko and Jackson, 2002; Lindau and Almers, 1995).

It was suggested that a fusion pore could act as a gate to the release of different cargo molecules depending on its size. Moderate stimulation of chromaffin cells triggers the release of catecholamines only, but stronger stimulation triggers the release of larger neuropeptides as well (Fulop et al., 2005). My set of data supports the idea that this selectivity can be achieved by favoring kiss-and-run fusion mode at lower calcium concentrations (resting condition). While fusion pores stay narrow and open for a short amount of time to pass catecholamine, stronger stimulation shifts the mode of release to full fusion (98%) such that larger cargo molecules can also be secreted from widely open fusion pore (Elhamdani et al., 2006).

It was shown by Sombers et al. that the vesicle size affects the dynamic of the fusion pore. Our data shows that smaller vesicles (average radius: 84 ± 1.9 nm) undergo abrupt opening of the fusion pore producing a short-lived fusion pore, which are beyond our detection limits. While larger vesicles (average radius: 98 ± 1.4 nm) produce longer-lasting fusion pores and could be well characterized by our technique. The ability to monitor the fusion pore behavior is physiologically significant because changes in fusion pore dynamics have recently been proposed to play a role in synaptic plasticity (Choi et al., 2000).

Furthermore, our set of data suggests that when the pore is wide open, the core of the dense-core-vesicle leaves the vesicle through the pore. Upon removal, the inner formation of the lipid membrane is perturbed leading to the thicker membrane and lower membrane capacitance.

5.3 Molecular determinants of exocytosis can be studied with the developed technique

A large body of work on chromaffin cells, using amperometry and capacitance recording has addressed how various molecules function in different stages of exocytosis. Cell-attached capacitance recordings were previously done on either bovine chromaffin cells or other cell types, which are not ideal for studying neuronal exocytosis. However, genetic knock-outs of proteins are predominantly done in mice and deletion of proteins involved in exocytosis often results in lethal phenotype. So the recordings can be only made from cells prepared from embryos or newborn mice.

Here with our low noise double patch clamp technique, we provide insight into the exocytosis of embryonic mouse chromaffin granules by recording from v-SNARE dko, v-SNARE dko expressing mutated v-SNARE and complexin II ko cells.

Using amperometry it was shown that lengthening the juxtamembrane region of synaptobrevin II leads to a progressive decrease in current amplitude and prolongs transmission discharge (Kesavan et al., 2007). Using our method we studied the effects of the synaptobrevin II linker mutant (12aa) on a zero genetic background. Increasing the length between the synaptobrevin transmembrane domain and its SNARE domain led to a strong decrease in the number of single exocytotic events consistent with the reduced frequency of amperometric spikes for this mutant (Kesavan, 2007). Furthermore, our data showed an increase in the number of transient fusion events and also decrease in the conductance of the fusion pores before expansion. This may indicate that more energy is needed to reach the membrane metastable transition states that lead to fusion and some vesicle cannot overcome the energy barrier of the fusion and stay intact in the cells. Our findings confirm and emphasize the importance of a short distance between vesicle and plasma membrane for proper fusion pore dilation.

We find that the complexin II ko cells has a bigger fusion pore size before rapid expansion suggesting that the complexin II is important for keeping the fusion pore

stable and is likely restricting the fusion pore dilation. Complexin binds to SNARE complex and it might be important for coordinating multiple complexes located at the bottleneck of the fusing vesicle. Consistent with that previous work suggests that complexins may operate at a post-priming step in synaptic vesicle exocytosis, either by stabilizing SNARE complexes in a highly fusogenic state (Reim et al., 2001; Xue et al., 2007) or by acting as a prefusion clamp that arrests SNARE complexes to halt membrane merger and is removed upon the activation of synaptotagmin-1 by Ca^{2+} and its concomitant binding to the SNARE complex (Huntwork et al., 2007; Giraudo et al., 2006; Tang et al., 2006).

5.4 Fusion pore: a proteinaceous structure

The molecular structure of the fusion pore and its regulatory mechanisms are currently unknown. Models for membrane fusion have generally focused on the two alternative mechanisms. First, the stalk hypothesis is a macroscopic theory that treats membranes as bendable sheets and largely ignores local fluctuations of lipids (Chernomordik and Kozlov, 2003). Hemifusion is defined as the state in which the outer membrane leaflets are already continuous, but no aqueous connection has formed. Hemifusion could be a stable intermediate in vesicle fusion process.

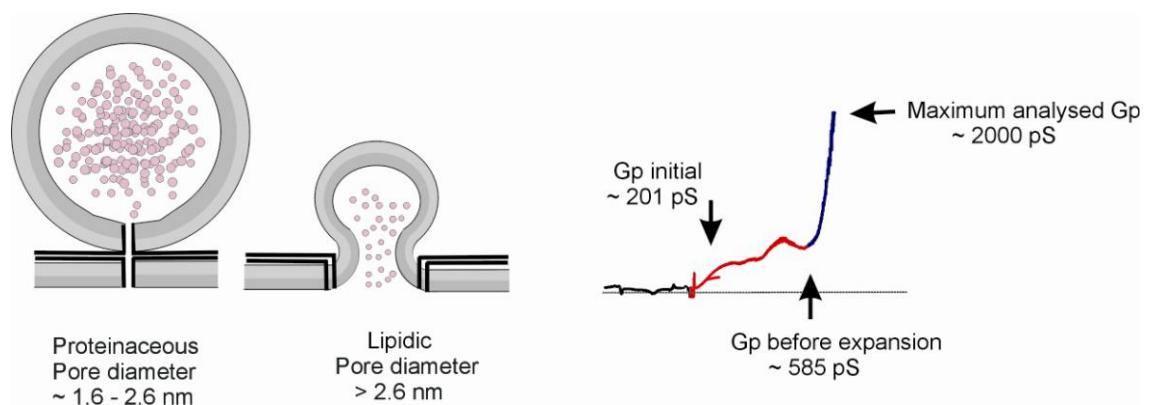


Figure 29. Schematic representation of proteinaceous fusion pores. Analysis of fusion pore conductance may support the proteinaceous model of the pore. The rigid open state is followed by structure that is more fluid.

Second, models with proteinaceous fusion pores invoke a gap junction–like channel that is formed as proteins from the vesicular and target membranes associate (Figure 29) (Lindau and Almers, 1995; Jackson, 2007; 2008). The open state of a proteinaceous fusion pore should be rigid, like an open ion channel. From the open fusion pore state, a second transition must occur in which the fusion pore dilates as lipids replace protein. After dilation has started, the incorporation of lipid would make the structure more fluid. A picture of the initial fusion pores of SNARE protein-mediated exocytosis is emerging in which SNARE protein membrane anchors form the walls of the fusion pore.

Fusion pore conductance obtained from our measurements may support that the dilation of a fusion pore is a transition from a proteinaceous gap-junction-like structure in which SNARE protein membrane anchors line the pore through the two membranes. The open state of a pore with rigid initial conductance of 201 ± 19 pS (pore diameter of 1.58 nm) which is found similar in different types of the cell, confirm formation of a rigid pore. It could expand slowly for about 59 ± 12 ms with proteinaceous structure until reaches the maximum pore conductance of 585 ± 55 pS (pore diameter of 2.6 ± 0.2 nm), then accelerates its expansion with the more fluid structure with an average rate of 310 ± 44 pS/ms. The kink can be a transition point that converts the fusion pore from protein to lipid. The idea of a proteinaceous fusion pore seems to be a more attractive scenario due to the physiological importance to control the size of the fusion pore. If the pore was solely lipidic it is hard to imagine a mechanism which would prevent the pore from rapid widening as expected from lipid leaflets trying to straighten the curvature.

Evidence has been presented suggesting that the membrane anchor of syntaxin lines the initial fusion pore of exocytosis (Han et al., 2004). These results suggested that the half of the fusion pore through the plasma membrane is composed of the membrane anchor of syntaxin. The obvious partner to syntaxin in forming the fusion pore through the vesicle membrane would be synaptobrevin, a SNARE protein anchored in the vesicle. Completing the assembly of the SNARE complex can drive a late step of membrane fusion to expand the initial proteinaceous pore and initiate a transition to a pore composed of lipid. During this transition, lipid molecules must intercalate between the protein segments that line the fusion pore. Combining multiple SNARE complexes to form a proteinaceous fusion pore can focus the energy and

provide the driving force necessary to overcome the hydrophobic energy barrier that obstructs the transition to a lipidic pore.

5.5 Success rate of simultaneous cell-attached and whole-cell recordings

It was technically challenging to make a good double patch recording because the embryonic cells were small and good signal to noise ratio was very crucial. On average, two good recording could be made per experimental day for wildtype cells. Semliki forest virus transfected cells are not as healthy as wildtype cells and therefore the chance to get a good double electrode recording was lower, which made data collection time consuming. The experiments were difficult for several reasons. The cells should be large enough for double patch configuration. Second, cell membrane should be healthy and clean for establishing a good gigaseal with big pipette in cell-attached configuration. 1 M Ω pipette was an optimal pipette size to allow formation of a gigaseal and would allow having a big enough membrane patch to be able to detect events. Since it is harder to find a healthy cell among virus transfected cells, finding them was time consuming as well. In addition, to detect small and low frequency capacitance upward-steps, stable cell-attached recording with low noise was required. The capacitance noise was reduced by using thick wall pipette heavily coated with sylgard, and by lowering the surface level of bath solution. Moreover, vesicles in chromaffin cells are not homogeneously distributed, so there was a possibility to get very few vesicles under the membrane patch in cell-attached configuration. In summary, a combination of several experimental procedures and requirements made the recording of capacitance upward-steps difficult to perform. A more gentle viral infection system like adeno virus may be helpful to improve the health of infected cells and therefore increase the success rate of good recording. Using a cell line could improve the success rate because the cell membrane is clean and seal formation is much easier. Nonetheless, the ability to monitor the kinetics of the fusion pores directly under tight control of calcium and the ability to see the effects of mutated proteins on the kinetics of the fusion pore for the first time was worth it.

5.6 Possible implications of electrical measurements of the fusion pore

While much knowledge of the fusion pore have been learned by capacitance measurements, very limited knowledge have been obtained of the fission pore (pore formed during endocytosis) (Rosenboom and Lindau, 1994; Suss-Toby et al., 1996; Lollike et al. 1998). Due to the strong calcium stimulus (20 M Ca^{2+}) used in our experiments the patched membrane favored exocytosis. By reducing the intensity of the stimulus more endocytotic events and therefore changes in fission pore can be detected. This should bring important data on the dynamics of fission pores. There is no other way to monitor fission pore kinetics at high time resolution other than admittance measurements. Amperometry cannot be used because there is no neurotransmitter to detect. Imaging techniques are too slow and cannot provide detailed information on the pore size. There are several modes of endocytosis and key molecular players like clathrin, dynamin etc. have been found (Cabeza et al., 2010). Interestingly synaptobrevin II knock-out hippocampal neurons show defects in endocytosis as indirectly shown by electron microscopy and imaging techniques (Deak et al. 2004). However, there are very few studies of the fission pore using cell-attached admittance measurements (Cabeza et al. 2010). Using the described technique endocytotic fission pores can be studied under control of intracellular components and in embryonic mouse chromaffin cells with a possibility to express a mutated protein. Basically this technique allows studying almost any kind of exocytotic or endocytotic process. It would be very interesting to study the properties of fission pores during phagocytosis.

Using our technique one could aim to probe the molecular structure of the fusion pore by changing the physical properties of the cell membrane for example changes in temperature. Temperature is a convenient means of manipulating the physical properties of membranes (Lee and Chapman, 1987). Because ion channels and other membrane transport mechanisms are affected by temperature in different and characteristic ways (Krasne et al., 1971; Boheim et al., 1980), we could design experiments to attempt to identify the nature of the early stages of the fusion pore. Oberhauser et al, has examined the participation of lipid in mast cell fusion pore by decreasing temperature. They observe a marked decline in the rate of fusion pore closure while reducing the temperature. This sudden change in temperature dependence

is reminiscent of a lipid-fluidity phase transition.

Using this technique one can monitor how changing properties of the lipid bilayer itself can affect fusion pore kinetics. For example by incorporating lipids of different structure like cones and inverted cones, which favor different curvature of the bilayer.

5.7 Future aims

The author will continue studies to elucidate the mechanism of Ca^{2+} -triggered exocytosis. Capacitance recording from PC12 and chromaffin cells, and patch clamp recording from neurons will be conducted to investigate the role of the Ca^{2+} sensor synaptotagmin. These experiments are aimed to probe the molecular composition, structure, and energetic landscape of the fusion pore as single vesicles progress through the stages of exocytosis. In addition, we plan to characterize and compare vesicle sizes, fusion pore conductances, and kiss-and-run frequency in different GFP-tracer pituitary synaptotagmin knock-out mice. These experiments will determine how the pituitary synaptotagmins influence exocytosis of each vesicle type at the single-vesicle/single-fusion-pore level.

6. References

- Abrahams et al., 1973; Abrahams, S.J. and E. Holtzman, Secretion and endocytosis in insulin-stimulated rat adrenal medulla cells. *J Cell Biol*, 1973. 56(2): p. 540-58.
- Albillos, A., G. Dernick, H. Horstmann, W. Almers, G. Alvarez de Toledo, and M. Lindau. 1997. The exocytotic event in chromaffin cells revealed by patch amperometry. *Nature*. 389:509–512.
- Ale´s E, Tabares L, Poyato JM, Valero V, Lindau M, Alvarez de Toledo G (1999) High calcium concentrations shift the mode of exocytosis to the kiss-and-run mechanism. *Nat Cell Biol* 1:40–44.
- Almers, W. and F.W. Tse, Transmitter release from synapses: does a preassembled fusion pore initiate exocytosis? 1990. *Neuron*. 4(6): p. 813-8.
- Alvarez de Toledo, G., and J. M. Fernandez. 1987. The events leading to secretory granule fusion. In *Cell Physiology of Blood*. The Rockefeller University Press, New York. 332–344.
- Alvarez de Toledo, G., and J. M. Fernandez. 1988. *Cell Physiology of Blood*. R. B. Gunn and J. C. Parker, editors. The Rockefeller University Press, New York. 333-344.
- Alvarez de Toledo, G., Fernández-Chacón, R. & Fernandez, J. M.1993. Release of secretory products during transient vesicle fusion. *Nature* 363, 554–558.
- Archer, D.A., M.E. Graham, and R.D. Burgoyne.2002. Complexin regulates the closure of the fusion pore during regulated vesicle exocytosis. *J Biol Chem*. 277(21): p. 18249-52.
- Artalejo, C.R., A. Elhamdani, and H.C. Palfrey, Sustained stimulation shifts the mechanism of endocytosis from dynamin-1-dependent rapid endocytosis to clathrin- and dynamin-2-mediated slow endocytosis in chromaffin cells. *Proc Natl Acad Sci U S A*, 2002. 99(9): p. 6358-63.
- Ashery, U., et al., 1999. An efficient method for infection of adrenal chromaffin cells using the Semliki Forest virus gene expression system. *Eur J Cell Biol*, 78(8): p. 525-32.
- Augustine, G.J., F. Santamaria, and K. Tanaka, Local calcium signaling in neurons. *Neuron*, 2003. 40(2): p. 331-46.
- Baker, P.F. and D.E. Knight. 1981. Calcium control of exocytosis and endocytosis in bovine adrenal medullary cells. *Philos Trans R Soc Lond B Biol Sci*. 296(1080): p. 83-103.
- Becherer, U. and J. Rettig, Vesicle pools, docking, priming, and release. *Cell Tissue Res*, 2006. 326(2): p. 393-407.
- Boheim, G., W. Hanke, and H. Eibl, Lipid phase transition in planar bilayer membrane and its effect on carrier- and pore-mediated ion transport. *Proc Natl Acad Sci U S A*, 1980. 77(6): p. 3403-7.
- Borisovska, M., Zhao, Y., Tsytsyura, Y., Glyvuk, N., Takamori, S., Matti, U., Rettig, J., Sudhof, T. and Bruns, D. 2005. v-SNAREs control exocytosis of vesicles from priming to fusion. *Embo J*, 24, 2114-2126.
- Braun, M., et al., Exocytotic properties of human pancreatic beta-cells. *Ann N Y Acad Sci*, 2009. 1152: p. 187-93.
- Breckenridge, L.J. and W. Almers, 1987a. Final steps in exocytosis observed in a cell with giant secretory granules. *Proc Natl Acad Sci U S A*, 1987. 84(7): p. 1945-9.

- Breckenridge, L.J. and W. Almers, 1987b. Currents through the fusion pore that forms during exocytosis of a secretory vesicle. *Nature*. 328(6133): p. 814-7.
- Bruns, D. and R. Jahn, Molecular determinants of exocytosis. *Pflugers Arch*, 2002. 443(3): p. 333-8.
- Bruns, D., 2004. Detection of transmitter release with carbon fiber electrodes. *Methods*. 33(4): p. 312-21.
- Bruns, D., and R. Jahn. 1995. Real-time measurement of transmitter release from single synaptic vesicles. *Nature*. 376:62-65.
- Burgess, T.L. and R.B. Kelly, Constitutive and regulated secretion of proteins. *Annu Rev Cell Biol*, 1987. 3: p. 243-93.
- Cabeza, J.M., J. Acosta, and E. Ales, Dynamics and regulation of endocytotic fission pores: role of calcium and dynamin. *Traffic*. 11(12): p. 1579-90.
- Cabeza, J.M., J. Acosta, and E. Ales. 2010. Dynamics and regulation of endocytotic fission pores: role of calcium and dynamin. *Traffic*. 11(12): p. 1579-90.
- Case, R.M., 1978. Synthesis, intracellular transport and discharge of exportable proteins in the pancreatic acinar cell and other cells. *Biol Rev Camb Philos Soc*. 53(2): p. 211-354.
- Chandler, D. E., and J. E. Heuser. 1980. Arrest of membrane fusion events in mast cells by quick-freezing. *J. Cell Biol* 86:666-674.
- Chandler, D. E., J. P. Bennett, and B. Gomperts. 1983. Freezefracture studies of chemotactic peptide-induced exocytosis in neutrophils: evidence for two patterns of secretory granule fusion. *J. Ultrastruct. Res*. 82:221-232.
- Chandler, D. E., M. Whitaker, and J. Zimmerberg. 1989. High molecular weight polymers block cortical granule exocytosis in sea urchin eggs at the level of granule matrix disassembly. *J. Cell Biol*. 109:1269-1278.
- Chen, P., and K. D. Gillis. 2000. The noise of membrane capacitance measurements in the whole-cell recording configuration. *Biophys. J*. 79:2162-70.
- Chen, Y.A. and R.H. Scheller, 2001. SNARE-mediated membrane fusion. *Nat Rev Mol Cell Biol*. 2(2): p. 98-106.
- Chernomordik, L.V. and M.M. Kozlov, Protein-lipid interplay in fusion and fission of biological membranes. *Annu Rev Biochem*, 2003. 72: p. 175-207.
- Chow, R.H., L. von Ruden, and E. Neher, 1992. Delay in vesicle fusion revealed by electrochemical monitoring of single secretory events in adrenal chromaffin cells. *Nature*. 356(6364): p. 60-3.
- Cohen, F. S., M. H. Akabas, and A. Finkelstein. 1982. Osmotic swelling of phospholipid vesicles causes them to fuse with a planar phospholipid bilayer membrane. *Science (Wash. DC)*. 217:458-460.
- Cohen, F.S., W.D. Niles, and M.H. Akabas, Fusion of phospholipid vesicles with a planar membrane depends on the membrane permeability of the solute used to create the osmotic pressure. *J Gen Physiol*, 1989. 93(2): p. 201-10.
- Cole, K. S. 1968. *Membranes, Ions and Impulses*. University of California Press, Berkeley, CA.
- Coulter, H.D., Vesicular localization of immunoreactive [Met⁵]enkephalin in the globus pallidus. *Proc Natl Acad Sci U S A*, 1988. 85(18): p. 7028-32.
- Curran, M.J., et al., 1993. Exocytotic fusion pores exhibit semi-stable states. *J Membr Biol*. 133(1): p. 61-75.
- De Robertis, E.D. and D.D. Sabatini. 1960. Submicroscopic analysis of the secretory process in the adrenal medulla. *Fed Proc*. 19 (Suppl 5): p. 70-8.

- Deak, F., et al., Synaptobrevin is essential for fast synaptic-vesicle endocytosis. *Nat Cell Biol*, 2004. 6(11): p. 1102-8.
- Debus, K. and Lindau, M. 2000. Resolution of Patch Capacitance Recordings and of Fusion Pore Conductances in Small Vesicles, *Biophysical Journal*, Volume 78, 2983–2997.
- Debus, K., J. Hartmann, G. Kilic, and M. Lindau. 1995. Influence of conductance changes on patch clamp capacitance measurements using a lock-in amplifier and limitations of the phase tracking technique. *Biophys. J.* 69:2808 –2822.
- Dernick, G., 1999, Simultaneous detection of fusion and secretion by patch Amperometry of exocytosis of small vesicle. Dissertation.
- Dernick, G., Alvarez De Toledo, G. & Lindau, M. 2003. Exocytosis of single chromaffin granules in cell-free inside-out membrane patches. *Nature Cell Biol.* 5, 358–362.
- Dernick, G., et al., 2005. Patch amperometry: high-resolution measurements of single-vesicle fusion and release. *Nat Methods.* 2(9): p. 699-708.
- Dreifuss, J. J., Akert, K., Sandri, C., Moor, H. 1980. Specific arrangements of membrane particles of sites of exo endocytosis in the freeze-etched neurohyphysis. *Cell Tissue Res.* 165: 3 17-25.
- Dumas, F., et al., The transmembrane protein bacterioopsin affects the polarity of the hydrophobic core of the host lipid bilayer. *Biochim Biophys Acta*, 1999. 1421(2): p. 295-305.
- Elhamdani, A., F. Azizi, and C.R. Artalejo, Double patch clamp reveals that transient fusion (kiss-and-run) is a major mechanism of secretion in calf adrenal chromaffin cells: high calcium shifts the mechanism from kiss-and-run to complete fusion. *J Neurosci*, 2006. 26(11): p. 3030-6.
- Fernandez, J. M., E. Neher, and B. D. Gomperts. 1984. Capacitance measurements reveal stepwise fusion events in degranulating mast cells. *Nature.* 312:453–455.
- Fesce, R., et al., Neurotransmitter release: fusion or 'kiss-and-run'? *Trends Cell Biol*, 1994. 4(1): p. 1-4.
- Fidler, N., and J. M. Fernandez. 1989. Phase tracking: an improved phase detection technique for cell membrane capacitance measurements. *Biophys. J.* 56:1153–1162.
- Finbow, M. E. & Harrison, M. A. 1997. The vacuolar H⁺-ATPase: a universal proton pump of eukaryotes. *Biochemical Journal* 324, 697–712.
- Finkelstein, A., J. Zimmerberg, and F. S. Cohen. 1986. Osmotic swelling of vesicles: its role in the fusion of vesicles with planar phospholipid bilayer membranes and its possible role in exocytosis. *Annu. Rev. Physiol* 48:163-174.
- Fulop, T., S. Radabaugh, and C. Smith, Activity-dependent differential transmitter release in mouse adrenal chromaffin cells. *J Neurosci*, 2005. 25(32): p. 7324-32.
- Gillis, K. D. 1995. Techniques for membrane capacitance measurements. Single channel recording, 2nd edition. Plenum Press, New York. 155-198.
- Giraudo, C.G., et al., A clamping mechanism involved in SNARE-dependent exocytosis. *Science*, 2006. 313(5787): p. 676-80.
- Graham, I.M. and P. O'Callaghan. 2002. Vitamins, homocysteine and cardiovascular risk. *Cardiovasc Drugs Ther.* 16 (5): p. 383-9.

- Hamill, O. P., Marty, E., Neher, B., Sakmann, and F. J. Sigworth. 1981. Improved patch-clamp technique for high-resolution current recording from cells and cell-free membrane patches. *Pflügers Arch. Eur. J. Physiol.* 391:85–100.
- Han, X., et al., Transmembrane segments of syntaxin line the fusion pore of Ca²⁺-triggered exocytosis. *Science*, 2004. 304(5668): p. 289-92.
- He, L., Wu, X. S., Mohan, R. & Wu, L. G. 2006. Two modes of fusion pore opening revealed by cell-attached recordings at a synapse. *Nature* 444, 102–105.
- Heuser, J.E. and T.S. Reese. 1981. Structural changes after transmitter release at the frog neuromuscular junction. *J Cell Biol.* 88(3): p. 564-80.
- Higuchi, R., B. Krummel, and R.K. Saiki, 1988. A general method of in vitro preparation and specific mutagenesis of DNA fragments: study of protein and DNA interactions. *Nucleic Acids Res.* 16(15): p. 7351-67.
- Hokfelt, T., et al., Coexistence of neuronal messengers--an overview. *Prog Brain Res*, 1986. 68: p. 33-70.
- Holz, R. W. 1986. The role of osmotic forces in exocytosis from adrenal chromaffin cells. *Annu. Rev. Physiol.* 48:175-190.
- Hua, Y. and R.H. Scheller, Three SNARE complexes cooperate to mediate membrane fusion. *Proc Natl Acad Sci U S A*, 2001. 98(14): p. 8065-70.
- Huntwork, S. and J.T. Littleton, A complexin fusion clamp regulates spontaneous neurotransmitter release and synaptic growth. *Nat Neurosci*, 2007. 10(10): p. 1235-7.
- Ishizuka, T., et al., Molecular cloning of synaphins/complexins, cytosolic proteins involved in transmitter release, in the electric organ of an electric ray (*Narke japonica*). *Neurosci Lett*, 1997. 232(2): p. 107-10.
- Ishizuka, T., et al., Synaphin: a protein associated with the docking/fusion complex in presynaptic terminals. *Biochem Biophys Res Commun*, 1995. 213(3): p. 1107-14.
- Jackson, M.B. and E.R. Chapman, Fusion pores and fusion machines in Ca²⁺-triggered exocytosis. *Annu Rev Biophys Biomol Struct*, 2006. 35: p. 135-60.
- Jackson, M.B. and E.R. Chapman, The fusion pores of Ca²⁺-triggered exocytosis. *Nat Struct Mol Biol*, 2008. 15(7): p. 684-9.
- Jackson, M.B., In search of the fusion pore of exocytosis. *Biophys Chem*, 2007. 126(1-3): p. 201-8.
- Jahn, R. and R.H. Scheller, 2006. SNAREs--engines for membrane fusion. *Nat Rev Mol Cell Biol*, 2006. 7(9): p. 631-43.
- Jahn, R. and T.C. Sudhof, 1999. Membrane fusion and exocytosis. *Annu Rev Biochem*, 1999. 68: p. 863-911.
- Jensen, M.O. and O.G. Mouritsen, Lipids do influence protein function--the hydrophobic matching hypothesis revisited. *Biochim Biophys Acta*, 2004. 1666(1-2): p. 205-26.
- Johnson, R.G. and A. Scarpa, 1984. Chemiosmotic coupling and its application to the accumulation of biological amines in secretory granules. *Soc Gen Physiol Ser.* 38: p. 71-91.
- Kandel ER, Schwartz JH, Jessell TM. *Principle of Neural Science*, 4th ed., pp.178-180. McGraw-Hill, New York (2000). ISBN 0-8385-7701-6
- Katz, B. 1969. *The Release of Neural Transmitter Substances*. Liverpool Univ. Press, Liverpool, England.
- Kesavan, J., M. Borisovska, and D. Bruns, 2007. v-SNARE actions during Ca²⁺-triggered exocytosis. *Cell*, 2007. 131(2): p. 351-63.

- Klyachko V., Zhang Z., and Jackson M., 2007, Low-Noise Recording of Single-Vesicle Capacitance Steps in Cell-Attached Patches. *Methods in Molecular Biology*, Vol.440.
- Klyachko, V.A. and M.B. Jackson, Capacitance steps and fusion pores of small and large-dense-core vesicles in nerve terminals. *Nature*, 2002. 418(6893): p. 89-92.
- Krasne, S., G. Eisenman, and G. Szabo, Freezing and melting of lipid bilayers and the mode of action of nonactin, valinomycin, and gramicidin. *Science*, 1971. 174(7): p. 412-5.
- Kreft, M. and R. Zorec, 1997. Cell-attached measurements of attofarad capacitance steps in rat melanotrophs. *Pflugers Arch.* 434(2): p. 212-4.
- Krupa, B. and G. Liu, Does the fusion pore contribute to synaptic plasticity? *Trends Neurosci*, 2004. 27(2): p. 62-6.
- Lee, D.C. and D. Chapman, The effects of temperature on biological membranes and their models. *Symp Soc Exp Biol*, 1987. 41: p. 35-52.
- Lefkowitz et al., 2009). Liming He, et al., 2006). (
- Lindau, M., and E. Neher. 1988. Patch-clamp techniques for time-resolved capacitance measurements in single cells. *Pflugers Arch. Eur. J. Physiol.* 411:137–146.
- Lindau, M., and W. Almers. 1995. Structure and function of fusion pores in exocytosis and ectoplasmic membrane fusion. *Curr. Opin. Cell Biol.* 7:509–517.
- Lindau, M., Time-resolved capacitance measurements: monitoring exocytosis in single cells. *Q Rev Biophys*, 1991. 24(1): p. 75-101.
- Lindau. M, Alvarez de Toledo, G, 2003. Review: The fusion pore. *Biochimica et Biophysica Acta.* 1641:167–173.
- Littleton, J.T., et al., synaptotagmin mutants reveal essential functions for the C2B domain in Ca²⁺-triggered fusion and recycling of synaptic vesicles in vivo. *J Neurosci*, 2001. 21(5): p. 1421-33.
- Lollike, K., Borregaard, N. & Lindau, M. 1998. Capacitance flickers and ‘pseudoflickers’ of small granules, measured in the cell attached configuration. *Biophys. J.* 75, 53–59.
- Lollike, K., N. Borregaard, and M. Lindau. 1995. The exocytotic fusion pore of small granules has a conductance similar to an ion channel. *J. Cell Biol.* 129:99 – 104.
- Lucy, J.A. and Q.F. Ahkong, 1986. An osmotic model for the fusion of biological membranes. *FEBS Lett*, 199(1): p. 1-11.
- Martens, S. and H.T. McMahon, 2008. Mechanisms of membrane fusion: disparate players and common principles. *Nat Rev Mol Cell Biol.* 9(7): p. 543-56.
- Maruyama, Y., Ca²⁺-induced excess capacitance fluctuation studied by phase-sensitive detection method in exocrine pancreatic acinar cells. *Pflugers Arch*, 1986. 407(5): p. 561-3.
- McMahon, H.T., et al., 1995. Complexins: cytosolic proteins that regulate SNAP receptor function. *Cell.* 83(1): p. 111-9.
- McNew, J.A., et al., Close is not enough: SNARE-dependent membrane fusion requires an active mechanism that transduces force to membrane anchors. *J Cell Biol*, 2000. 150(1): p. 105-17.
- Meldolesi, J. and B. Ceccarelli, Exocytosis and membrane recycling. *Philos Trans R Soc Lond B Biol Sci*, 1981. 296(1080): p. 55-65.

- Merkle, C. J., and D. E. Chandler. 1989. Hyperosmolality inhibits exocytosis in sea urchin eggs by formation of a granule-free zone and arrest of pore widening. *J. Membr. Biol.* 112:223-232.
- Momayezi, M., et al., 1987. Exocytosis induction in *Paramecium tetraurelia* cells by exogenous phosphoprotein phosphatase in vivo and in vitro: possible involvement of calcineurin in exocytotic membrane fusion. *J Cell Biol.* 105(1): p. 181-9.
- Monck JR, Fernandez JM. 1994. The exocytotic fusion pore and neurotransmitter release. *Neuron* 12:707
- Morgan, A., and R. D. Burgoyne. 1997. Common mechanisms for regulated exocytosis in the chromaffin cell and the synapse. *Semin. Cell Dev. Biol.* 8:141–149.
- Neher, E. and A. Marty. 1982. Discrete changes of cell membrane capacitance observed under conditions of enhanced secretion in bovine adrenal chromaffin cells. *Proc. Natl. Acad. Sci. U.S.A.* 79:6712– 6716.
- Nusse, O. and M. Lindau, 1989. Simultaneous capacitance and calcium measurements in degranulating neutrophils. *J Protein Chem.* 8(3): p. 441-3.
- Oberhauser, A. F., J. R. Monck, and J. M. Fernandez. 1992. Events leading to the opening and closing of the exocytotic fusion pore have markedly different temperature dependencies. *Biophys. J.* 61:800–809.
- Pabst, S., et al., 2002. Rapid and selective binding to the synaptic SNARE complex suggests a modulatory role of complexins in neuroexocytosis. *J Biol Chem.* 277(10): p. 7838-48.
- Parsons, T.D., et al., Docked granules, the exocytic burst, and the need for ATP hydrolysis in endocrine cells. *Neuron*, 1995. 15(5): p. 1085-96.
- Reim, K. et al. 2001. Complexins regulate a late step in Ca^{2+} -dependent neurotransmitter release. *Cell* 104, 71–81.
- Reim, K., et al., 2005. Structurally and functionally unique complexins at retinal ribbon synapses. *J Cell Biol*, 169(4): p. 669-80.
- Rosenboom, H. and M. Lindau, Exo-endocytosis and closing of the fission pore during endocytosis in single pituitary nerve terminals internally perfused with high calcium concentrations. *Proc Natl Acad Sci U S A*, 1994. 91(12): p. 5267-71.
- Rothman, J.E. and G. Warren, 1994. Implications of the SNARE hypothesis for intracellular membrane topology and dynamics. *Curr Biol*, 4(3): p. 220-33.
- Sabatini, B.L. and W.G. 1996. Regehr, Timing of neurotransmission at fast synapses in the mammalian brain. *Nature.* 384(6605): p. 170-2.
- Sabatini, B.L., T.G. Oertner, and K. Svoboda, The life cycle of Ca^{2+} ions in dendritic spines. *Neuron*, 2002. 33(3): p. 439-52.
- Sakmann, B. and Neher, E. In *Single-Channel Recording*, 2nd edition. Plenum Press, New York. 155–198.
- Salama, G., R.G. Johnson, and A. Scarpa, 1980. Spectrophotometric measurements of transmembrane potential and pH gradients in chromaffin granules. *J Gen Physiol*, 75(2): p. 109-40.
- Schmidt, W., et al., 1983. Membrane events in adrenal chromaffin cells during exocytosis: a freeze-etching analysis after rapid cryofixation. *Eur J Cell Biol.* 32(1): p. 31-7.
- Schoch, S., et al., 2001. SNARE function analyzed in synaptobrevin/VAMP knockout mice. *Science.* 294(5544): p. 1117-22.

- Sigworth, F. J. 1995. Electronic design of the patch clamp. In *Single Channel Recording*. Plenum Press, New York. 95–125.
- Sollner, T., S. Whiteheart, M. Brunner, H. Erdjument-Bromage, M. Geromanos, P. Tempst, and J. E. Rothman. 1993. SNAP receptors implicated in vesicle targeting and fusion. *Nature*. 362:318–323.
- Somers, L.A., et al., The effects of vesicular volume on secretion through the fusion pore in exocytotic release from PC12 cells. *J Neurosci*, 2004. 24(2): p. 303-9.
- Sorensen, J.B., et al., 2003. Examining synaptotagmin 1 function in dense core vesicle exocytosis under direct control of Ca^{2+} . *J Gen Physiol*, 122(3): p. 265-76.
- Spruce, A. E., L. J. Breckenridge, A. K. Lee, and W. Almers. 1990. Properties of the fusion pore that forms during exocytosis of a mast cell secretory vesicle. *Neuron*. 4:643–654.
- Spruce, A.E., A. Iwata, and W. Almers, 1991. The first milliseconds of the pore formed by a fusogenic viral envelope protein during membrane fusion. *Proc Natl Acad Sci U S A*. 88(9): p. 3623-7.
- Sulzer, D. and E.N. Pothos, Regulation of quantal size by presynaptic mechanisms. *Rev Neurosci*, 2000. 11(2-3): p. 159-212.
- Suss-Toby, E., J. Zimmerberg, and G.E. Ward, Toxoplasma invasion: the parasitophorous vacuole is formed from host cell plasma membrane and pinches off via a fission pore. *Proc Natl Acad Sci U S A*, 1996. 93(16): p. 8413-8.
- Sutton, R.B., et al., 1998. Crystal structure of a SNARE complex involved in synaptic exocytosis at 2.4 Å resolution. *Nature*. 395(6700): p. 347-53.
- Takahashi, S., et al., Identification of two highly homologous presynaptic proteins distinctly localized at the dendritic and somatic synapses. *FEBS Lett*, 1995. 368(3): p. 455-60.
- Tang, J., et al., A complexin/synaptotagmin 1 switch controls fast synaptic vesicle exocytosis. *Cell*, 2006. 126(6): p. 1175-87.
- Taraska, J.W. and W. Almers, Bilayers merge even when exocytosis is transient. *Proc Natl Acad Sci U S A*, 2004. 101(23): p. 8780-5.
- Taraska, J.W. and W. Almers, Bilayers merge even when exocytosis is transient. *Proc Natl Acad Sci U S A*, 2004. 101(23): p. 8780-5.
- Tokumaru, H., et al., 2001. SNARE complex oligomerization by synaphin/complexin is essential for synaptic vesicle exocytosis. *Cell*. 104(3): p. 421-32.
- Towbin, H., T. Staehelin, and J. Gordon, Electrophoretic transfer of proteins from polyacrylamide gels to nitrocellulose sheets: procedure and some applications. 1979. *Biotechnology*, 1992. 24: p. 145-9.
- Trifaro, J.M., 1977. Common mechanisms of hormone secretion. *Annu Rev Pharmacol Toxicol*. 17: p. 27-47.
- Valtorta, F., J. Meldolesi, and R. Fesce, Synaptic vesicles: is kissing a matter of competence? *Trends Cell Biol*, 2001. 11(8): p. 324-8.
- Voets, T., E. Neher, and T. Moser, Mechanisms underlying phasic and sustained secretion in chromaffin cells from mouse adrenal slices. *Neuron*, 1999. 23(3): p. 607-15.
- Wang, C.T., et al., Different domains of synaptotagmin control the choice between kiss-and-run and full fusion. *Nature*, 2003. 424(6951): p. 943-7.

References

- Wang, C.T., et al., Synaptotagmin- Ca^{2+} triggers two sequential steps in regulated exocytosis in rat PC12 cells: fusion pore opening and fusion pore dilation. *J Physiol*, 2006. 570(Pt 2): p. 295-307.
- Weber, T., et al., 1998. SNARE pins: minimal machinery for membrane fusion. *Cell*. 92(6): p. 759-72.
- Wightman, R.M., et al., 1991. Temporally resolved catecholamine spikes correspond to single vesicle release from individual chromaffin cells. *Proc Natl Acad Sci U S A*. 88(23): p. 10754-8.
- Xue, M., et al., Distinct domains of complexin I differentially regulate neurotransmitter release. *Nat Struct Mol Biol*, 2007. 14(10): p. 949-58.
- Zimmerberg, J., 1987. Molecular mechanisms of membrane fusion: steps during phospholipid and exocytotic membrane fusion. *Biosci Rep*, 1987. 7(4): p. 251-68.
- Zimmerberg, J., M. Curran, F. S. Cohen, and M. Brodwick. 1987. Simultaneous electrical and optical measurements show that membrane fusion precedes secretory granule swelling during exocytosis of beige mouse mast cells. *Proc. Natl. Acad. Sci. USA*. 84:1585-1589.

Curriculum Vitae

Personal information

Paanteha, Kamalimoghadam
May 07, 1977, Tehran, Iran
Family status: Married, one child

Educational background

University of Saarland medical school Ph.D. Biophysics	Homburg, Germany 2011
Institute of physics and Technology, "KPI" M.S. Applied Physics (Neuroscience)	Kiev, Ukraine 2005
Institute of advanced studies in basic science Master student (Condense Matter Physics)	Zanjan, Gavezang, Iran 2001
Azzahra University B. S. Applied Physics (Atomic, Molecular Physics)	Tehran, Iran 2000

Research experience

04/2006- 02/2010
University of Saarland, Germany
Ph.D. student. Supervisor: Prof. Dr. Dieter Bruns

10/2005- 03/2006
Institute of Biophysics and Biochemistry, Iran
Research assistant. Supervisor: Assistant Prof. Dr. Hamid Mobasheri

1/2004- 6/2005
Bogomoletz Institute of Physiology, Ukraine
Master student. Supervisor: Prof. Dr. Nikolay Veselovsky

Language/Skills

Persian Mother Tongue
English Fluent
Russian Intermediate
German Intermediate

Computer Skills: Clampex, Clampfit, Pulse, IGOR Pro, Sigma plot, Corel Draw, office, Internet. Programming to create analysis routines.

Laboratory Techniques

- Patch clamp techniques (single and paired recording, voltage and current clamp mode)
- Membrane capacitance measurements (on-cell and whole-cell configuration)
- Preparation and culturing of chromaffin cells, hippocampal neurons, bone marrow mast cells, aortic endothelium cells, spinal cord neurons
- Mammalian cell transfection
- Intercellular Ca^{2+} measurement using ratiometric indicators Fura-2 and Fura-2/AM
- DNA extraction, Genotyping
- Experience in electron microscopy and confocal microscopy
- Field stimulation

Scientific activities

Poster Neuroscience Washington D.C. USA, November.2008
Poster Network meeting, Kaiserslautern, June 2008
Poster/Talk Joint PhD-student symposium Obergurgl, Austria, April 2008
Poster Neuro-dowo 19th Saarbrücken, April 2008

Honors and awards

July 2006 – July 2009 GK1326 scholarship, Saarland University
July 2005 Diploma of Honor 'KPI' university

Publications

- Paanteha Kamalimoghadam, Dieter Bruns. **Electrical fusion pore measurements in mouse chromaffin cells: A high-resolution analysis to study the molecular mechanisms of exocytosis.** (In preparation)
- Maria Borisovska, Paanteha Kamalimoghadam, Chad Grabner, Dieter Bruns. **Short-chain alcohol facilitates priming in chromaffin cells.** (In preparation)